COMPUTATIONAL FLUID DYNAMICAL STUDIES OF STRUCTURED DISTILLATION PACKINGS

Jennifer Hodson

Doctor of Philosophy

THE UNIVERSITY OF ASTON IN BIRMINGHAM

April 1997

The University of Aston in Birmingham

COMPUTATIONAL FLUID DYNAMICAL STUDIES OF STRUCTURED DISTILLATION PACKING

Jennifer Hodson
A Thesis submitted for the degree of Doctor of Philosophy
April 1997

In recent years structured packings have become more widely used in the process industries because of their improved volumetric efficiency. Most structured packings consist of corrugated sheets placed in the vertical plane. The corrugations provide a regular network of channels for vapour liquid contact.

Until recently it has been necessary to develop new packings by trial and error, testing new shapes in the laboratory. The orderly repetitive nature of the channel network produced by a structured packing suggests it may be possible to develop improved structured packings by the application of computational fluid dynamics (CFD) to calculate the packing performance and evaluate changes in shape so as to reduce the need for laboratory testing.

In this work the CFD package PHOENICS has been used to predict the flow patterns produced in the vapour phase as it passes through the channel network. A particular novelty of the approach is to set up a method of solving the Navier Stokes equations for any particular intersection of channels. The flow pattern of the streams leaving the intersection is then made the input to the downstream intersection. In this way the flow pattern within a section of packing can be calculated. The resulting heat or mass transfer performance can be calculated by other standard CFD procedures.

The CFD predictions revealed a circulation developing within the channels which produce a loss in mass transfer efficiency. The calculations explained and predicted a change in mass transfer efficiency with depth of the sheets. This effect was also shown experimentally.

New shapes of packing were proposed to remove the circulation and these were evaluated using CFD. A new shape was chosen and manufactured. This was tested experimentally and found to have a higher mass transfer efficiency than the standard packing.

KEYWORDS: Computational Fluid Dynamics, Distillation, Structured Packings, Heat Transfer, Mass Transfer

ACKNOWLEDGEMENTS

I wish to thank the following people for their help during the course of my PhD studies.

Professor K.E. Porter, who supervised me for the first two years of the project and who continued to offer advice after his retirement.

Dr J.P. Fletcher for taking over and supervising during the final year.

Dr Jenkins and Paul Russell for hands on assistance with experimental work.

BOC Process Plants and the EPSRC for sponsoring the work.

The technical and support staff in the department.

The other members of the research group for their friendship.

My family and friends for all their moral support.

Mike, my husband, without whose constant support and encouragement the project would not have been possible.

CONTENTS

TITLE **1**

Summary 2

Acknowledgements 3

Contents 4

List of Figures 9

List of Tables 12

1. INTRODUCTION **13**

2. LITERATURE REVIEW **17**

2.1 Structured Packings - Historical Perspective 17

2.2 Description of Modern Structured Packings 20

2.2.1 Packing Geometry 21

Channel Shape 21

Channel Inclination Angle 22

Block Height 23

2.2.2 Surface Treatment 23

Surface Texture 24

Perforations 25

2.3 Summary 26

2.4 Models of Structured Packings 27

2.4.1 Pressure Drop 28

2.4.2 Liquid Hold-Up 32

2.4.3 Area 35

2.4.4 Flooding and Capacity 37

2.4.5 Mass Transfer Efficiency 40

2.5 Block Models 44

2.6 CFD Models 44

2.7 Other Models 45

2.8 Approaches to Modelling 45

2.9 Summary 47

2.10 Introduction to Computational Fluid Dynamics 48

2.11 Theory 49

2.12 Description of a Typical CFD Package 50

2.12.1 Pre-processor 51

Meshes 52
Commercial Mesh Generation Software 54
2.12.2 User Defined Subroutines 54
2.12.3 Main Analysis Program or Solver 55
2.12.4 Post-processor 55
2.13 Capabilities and Limitations 56
2.14 Choice of Package 57
2.15 CFD in the Chemical Industry 58
2.16 Summary 60
2.17 Chapter Summary 60

3. PHOENICS - AN INTRODUCTION 62
3.1 The Structure and Basic Concepts of Phoenics 62
3.1.1 The Q1 File 63
3.1.2 RESULT and PHI Files 64
3.1.3 Ground Subroutines 65
3.1.4 Variables 65
3.1.5 Meshes 66
3.1.7 Solver 67
3.2 The Equations Applied 68
3.3 Solution Method 70
3.4 Boundary Conditions as Sources 71
3.4.1 Fixed Value Boundary Conditions 72
3.4.2 Fixed Flux Boundary Conditions 72
3.4.3 Mass Flow and Pressure Boundary Conditions 73
Fixed Mass Boundary Conditions 73
Fixed Pressure Boundary Conditions 74
3.5 Turbulence Models 74
3.5.1 The k-ε Turbulence Model in PHOENICS 75
3.5.2 Application of k-ε Model in Triangular Ducts 76
3.6 Summary 77

4. CFD MODEL 78
4.1 Model Geometry and Specifications 78
4.2 The Model Q1 File 80
Groups 1-6 ---------- 80
Groups 7-9 ---------- 80

Group 13 ---------- 81
Groups 15-24 ---------- 81
4.3 Junction Numbering 82
4.4 Ground Coding 83
4.5 Consistency of Results 86
4.5.1 Introduction 86
4.5.2 Grid Independence 86
4.5.3 Solver Independence 87
4.6 Fluid Flow Model 96
4.6.1 Laminar Flow Model 96
4.6.2 Turbulent Flow Model 97
4.6.3 Validation of Method 98
4.6.4 Mixing Between Channels 98
4.6.5 Pressure Drop 99
4.6.6 Throughput and Channel Inclination Angle 100
4.7 Heat Transfer Model 101
4.7.1 Energy Equation 101
4.7.2 Boundary Conditions 102
4.7.3 Wall Heat Transfer 102
4.7.4 Number of Transfer Units 102
4.8 Results 103
4.8.1 Heat Transfer Rates 103
4.8.2 Number of Transfer Units 105
4.9 Effect of Sheet Width 107
4.9.1 Edge Junctions 107
4.9.2 Model Assumptions 108
4.9.3 Number of Transfer Units 108
4.10 Results 109
4.10.1 Number of Transfer Units 109
4.11 Summary 109

5. PACKING DEVELOPMENT 111
5.1 The New Shape 111
5.2 CFD Model 112
5.2.1 Model Geometry 112
5.2.2 Fluid Flow Path 113
5.2.3 Boundary conditions 115

5.2.4 Ground Coding 117
5.2.5 Limitations of Present Model 117
5.3 Results 118
5.3.1 Fluid Flow Patterns 120
5.4 Heat Transfer Modelling 122
5.4.1 Junction Heat Transfer 122
5.4.2 Overall Average Heat Transfer 123
5.4.3 Wall Heat Transfer 125
5.4.4 Number of Transfer Units 127
5.4.5 Pressure Drop 128
5.5 Summary 129

6. EXPERIMENTAL WORK 130
6.1 Aim of Experimental Work 130
6.2 The Large Scale Test Rig and Experiments Carried Out 130
6.2.1 Description of large scale rig 130
6.2.2 Operation of Test Rig 131
6.2.3 Recording and Processing of Experimental data 131
6.2.4 Recommissioning the Rig 132
6.2.5 Packings Tested 133
6.2.6 Results 133
6.3 Manufacturing the New Packing 135
6.3.1 The design specifications 135
6.3.2 Manufacturing Method 137
6.4 The Small Scale Test Rig and Experiments Carried Out 139
6.4.1 Description of small scale rig 139
6.4.2 Operation of the test rig 140
6.4.3 recording and processing of experimental data 141
6.4.4 Packings tested 141
6.4.5 Results 142
6.5 Summary 145

7. DISCUSSIONS AND CONCLUSIONS 146
7.1 Simplifications 147
7.2 Problems and Limitations 148
7.3 Current State of Structured Packing Models 149
7.4 Current State of Structured Packings 150

7.5 Results and Predictions 150
7.6 Packing Development 152
7.7 Final Conclusions 152
7.8 Suggestions For Further Work 154

Nomenclature 155
References 158
Appendix 1 - Summary of CFD Companies and Produces 164
Appendix 2 - Summary of Capabilities of Commercially Available CFD packages 168
Appendix 3 - Q1 File for flow in a Triangular Duct 174
Appendix 4 - Q1 File for Plain Junction, Turbulent Flow 178
Appendix 5 - GROUND Coding for Basic Model 182
Appendix 6 - Q1 File for Plain Junction, CCM Solver 194
Appendix 7 - Additional GROUND Coding for Slots 200

List of Figures

CHAPTER 2

Figure 2-1 Configuration of structured packing.

Figure 2-2 Typical plot of dry and irrigated pressure drop.

Figure 2-3 Various mesh types.

Figure 2-4 Multiblock and fine grid embedded meshes.

CHAPTER 3

Figure 3-1 The structure of Phoenics and the files.

Figure 3-2 Cartesian mesh showing axes directions.

Figure 3-3 Cell nomenclature.

Figure 3-4 Location of scalar and vector quantities.

Figure 3-5 Distribution of longitudanal velocity.

Figure 3-6 Secondary flow field at $\theta = 11.4^0$ and Re = 10000.

CHAPTER 4

Figure 4-1 Tianjin Mellapak Structured packing.

Figure 4-2 Geometry outline showing inlet, outlet and wall boundary conditions.

Figure 4-3 Junction Numbering

Figure 4-4 Ground coding concept.

Figure 4-5(a) Velocity vectors and pressure contours at inlets using the staggered grid solution method.

Figure 4-5(b) Pressure contours at inlets using the staggered grid solution method.

Figure 4-6(a) Velocity vectors and pressure contours at inlets using the CCM solution method.

Figure 4-6(b) Pressure contours at inlets using the CCM solution method.

Figure 4-7 Temperature contours at outlets of third junction using the staggered grid solution method.

Figure 4-8 Temperature contours at outlets of third junction using the CCM solution method.

Figure 4-9 Junction 22 velocity vectors.

Figure 4-10 Junction 88 velocity vectors.

Figure 4-11 Junction 33 velocity vectors.

Figure 4-12 Contours of A - Laminar flow model.

Figure 4-13 Contours of A - Turbulent flow model.

Figure 4-14 Comparison of dry pressure drop predictions.

Figure 4-15 Comparison of pressure drop predictions.

Figure 4-16 Variation of Junction Heat Transfer.

Figure 4-17 Variation of heat transfer for each wall of junction.

Figure 4-18 Contour plots of temperature at centre of fifth junction.

Figure 4-19 Variation of NTU with junction number.

Figure 4-20 Overall NTU/N against block height.

Figure 4-21 Numbering of edge junctions.

Figure 4-22 Increase in number of transfer units with column width.

CHAPTER 5

Figure 5-1 Profile of new shape of packing.

Figure 5-2 Geometry of original junction.

Figure 5-3 Geometry of opposite junction.

Figure 5-4 Slot and bulk fluid flows at a 2-D plane through packing.

Figure 5-5 Flow path through slots.

Figure 5-6 2-D representations of new packing models.

Figure 5-7 Horizontal tabs - Junction 33.

Figure 5-8 Horizontal tabs - Junction 55.

Figure 5-9 Vertical tabs - Junction 33.

Figure 5-10 Vertical tabs - Junction 55.

Figure 5-11 Variation of junction heat transfer.

Figure 5-12 Variation of total heat transfer/N.

Figure 5-13 Variation of heat transfer at each wall - horizontal tabs.

Figure 5-14 Variation of heat transfer at each wall - vertical tabs.

Figure 5-15 Temperature contours centre of 5th junction - slot only model.

Figure 5-16 Pressure drop predictions for new shaped packing.

CHAPTER 6

Figure 6-1 Comparison of column pressure gradient against F-factor for two block heights of Tianjin Mellapak 350 m^2/m^3.

Figure 6-2 Comparison of NTP/m against F-factor for two block heights of Tianjin Mellapak 350 m^2/m^3.

Figure 6-3 Details of new packing design.

Figure 6-4 A sheet of the new packing.

Figure 6-5 Flowsheet of the small scale test rig.

Figure 6-5 Column pressure drop for packings tested in small rig.

Figure 6-6 Number of Theoretical Stages per metre for packings tested in small rig.

Figure 6-7 Comparison of NTP/m for Tianjin Mellapak tested in two rigs.

List of Tables

CHAPTER 2

Table 2-1 Number of commercial CFD companies.

CHAPTER 3

Table 3-1 Description of Phoenics programs and files.

CHAPTER 5

Table 5-1 Summary of model simulations.

Table 5-2 Average wall heat transfer rates.

1. INTRODUCTION

'From small beginnings in the mists of history, when it originated as a technique to produce liquors from plant and animal substrates, distillation has developed into a workhorse of the chemical and process industries' (Darton ,1992). Clearly, the use of distillation for the separation and purification of volatile mixtures is not new. As a result of it being such a mature technology a frequently held view is that it can not benefit from further research. However, distillation is a major consumer of energy - estimated to amount to at least US$ 524 billion/annum (Porter, 1995) - so any improvements in efficiency, however minor, can have considerable economic and environmental advantages.

Within distillation columns there are a number of different methods used to bring about the contact of vapour and liquid. Most of the contacting devices can be classified as either trays or packings. Trays bring about contact of vapour and liquid in a stagewise manner whereas packings give continuous contact. In general, columns with small diameters, less than 0.6m, are filled with packing. Many shapes have been used for packings, varying from the randomness of stones through to sophisticated shapes, designed specifically to maximise mass transfer whilst reducing pressure drop. Alternatively the contact may be brought about in a stagewise manner by horizontal plates as is often favoured in large scale commercial columns. In tray devices liquid flows across the plate as vapour is bubbled up through it. Tray efficiencies are usually of the order of 70% compared to an ideal equilibrium stage. However, it is not uncommon to have lower efficiencies. Tray designs also have relatively large pressure drops compared to packings.

Packings can be classified as random or structured. As the names imply random packings are usually dumped inside the column whereas structured packings have an ordered arrangement. Both packings can be made from a variety of materials of which the most common are metal, ceramic and plastic. The first structured packings were made from gauze but as these are very expensive they are now usually confined to applications where sheet metal varieties would not be suitable, for example,

vacuum distillation with pressures in the order of 20 mmHg. In terms of mass transfer efficiency and pressure drop per theoretical stage the packings can be ranked in descending order of performance as, gauze structured packing, sheet metal structured packing then random packings (Billet and Mackowiak, 1988).

Both random and structured packings have been used successfully in small scale and laboratory columns for some years and have been shown to have a higher volumetric efficiency and a lower pressure drop than traditional tray type contacting devices (Huber, 1969). The initial reluctance in using these packings in large scale columns was due to the lack of success that was often experienced when scaling up. This has been shown to be due largely to maldistribution of the phases within the packing (Meier and Huber, 1969). Since then considerable effort has been put into designing efficient liquid distributors so that liquid is distributed uniformly over the top of the packed section.

With the increased usage of structured packings has come the wish to understand and model the processes taking place within the packing. Several groups of workers, most notably Fair et al. at the University of Texas (Fair and Bravo, 1990), and Billet at Ruhr University, have devised and developed models, which attempt to predict important parameters such as the pressure drop, capacity and mass transfer efficiency of various packings. However, although varying in the exact formulation, these models are mainly based on fitting experimental results to semi-empirical expressions. Such empirical data fits are only suitable for predicting the performance of existing packings. These models will be discussed in detail in chapter 2.

There is a continual desire to design new shapes of structured packings that will produce a better mass transfer efficiency with the minimum of pressure loss, in order to reduce both capital and operating costs. However, this design process is more of an art than a science with new shapes being developed by trial and error. This is both expensive and time consuming as a new manufacturing tool is needed to make each new shaped packing, before it can be tested experimentally. Previous models of structured packings have not tried to predict the shape effects on the micro scale -

rather they have concentrated on the column as a whole, or the macro scale. This work approaches the problem from the micro scale, examining the flow initially within single channels.

Most of the commercially available structured packings are made from corrugated sheets of metal, stacked side by side, such that channels of neighbouring sheets cross at right angles to one another. Various geometrical quantities, such as crimp height etc. can be varied. All such packings have a very regular structure which can be exploited to develop other approaches to modelling the packings. The work described in this thesis approaches the modelling of structured packings by means of the fundamental equations of fluid flow applied to the channels in structured packing. One method of solving such equations would be to write a computer program for the specific problem. The approach adopted here is to use instead one of the fairly sophisticated Computational Fluid Dynamics (CFD) software packages that are now available on the market. This will allow different shapes to be investigated easily in developing new packings.

During the last decade rapid development of very powerful computers at an economic price has taken place and this has allowed mathematical modelling techniques to be applied to many problems of engineering importance. Since 1981, when PHOENICS appeared as one of the first generation of CFD packages, a great many more have appeared on the market. Some have been targeted at very specialised applications e.g. the flow of air around computer chips, whereas others have been of very wide and general application. As the software codes vie for a place in the market they have been developed from rather unfriendly codes into sophisticated packages, which are easier for the user to interact with. All such programs calculate solutions at a set of discrete points rather than providing a continuous solution function. Such a set of points is usually described by the nodes of a grid or mesh. The scope of the calculations has widened from solution of the equations, to include automatic generation of the mesh and graphical presentation of the results in a range of ways to assist visualisation. Many of these features have been used in the work described in this thesis.

The research aims of this project were as follows:

* To study flows and processes occurring within structured packings using a commercially available CFD package

* To determine which aspects of existing packings should be modified to produce a packing having improved mass transfer efficiency at an acceptable pressure drop and throughput.

* To investigate and optimise the design of any new packing using the CFD method.

* To manufacture and experimentally compare any new packing developed with existing ones in order to determine whether it has the desired properties and to assess the viability of using CFD to design new structured packings.

The remainder of this thesis describes the work carried out to satisfy these aims. A brief literature review, giving the background of both CFD and the previous work on the modelling of structured packings, is given. Chapter 3 explains the basic concepts of the CFD code PHOENICS, the code chosen for this work, such that the remaining chapters can be read and understood. Chapters 4 and 5 describe the CFD model and development of a new packing shape, before manufacturing techniques and experimental testing are discussed in chapter 6. Final discussions and conclusions are given in chapter 7.

Within the scope and time limit of this project it has been possible to review the CFD codes on the market and to study previous models used for predicting the performance of structured packings. A method for modelling the flows within the channels of structured packings has been implemented within the CFD code PHOENICS and various new shapes have been assessed using the method. A manufacturing technique for producing the new shaped packing was devised but as this was a lengthy process it could not be manufactured in large enough quantities to allow tests to be carried out in the test facility available. A smaller scale distillation rig was built and the new packing tested.

2. LITERATURE REVIEW

In this literature survey two topics will be covered: firstly structured packings and secondly computational fluid dynamics (CFD). When considering structured packings, it will be seen how they have evolved from the first randomly dumped packings into the sheet metal packings that are becoming widely used in distillation today. Approaches that have been used in an attempt to increase the efficiency of packings will be looked at and the considerable previous work that has been done in the area of modelling structured packings will also be discussed. General background will be given on the nature of CFD technology, its availability, and the sort of problems it is claimed to simulate.

2.1 Structured Packings - Historical Perspective

In a packed column contact between gas and liquid is continuous, rather than stagewise, as in a plate column. Liquid, flowing downwards over the surface of the packing is contacted with vapour, usually flowing counter-currently upwards. The purpose of any packing is to provide a large surface area over which the gas and liquid can be contacted. To perform successfully it needs to promote an even distribution of liquid over the surface. It is also desirable that the packing should have a low pressure drop.

A clear motive behind developing any new contacting device for the separation or purification of a mixture is to do the same job more efficiently and hence more cheaply. Structured packings have been shown to exhibit desirable properties that reduce the overall costs of an operation. Although structured packings are more expensive than trays they have a higher separation efficiency and hence a smaller volume is required, reducing the capital cost of the column. Compared to trays they have a lower pressure drop, which leads to reduced operating costs. Structured packings also have a lower liquid hold-up compared to trays which is advantageous in batch processes.

Most early packings were tested in small scale columns and good separation efficiency was obtained. However, when using the packing in large diameter columns unexpectedly low separation efficiency was obtained. This problem may have led to reluctance on the part of commercial companies to invest in the technology. The main reason given for such failures in scale-up was maldistribution of the liquid. As long ago as 1969 Meier and Huber used Sulzer's gauze packings to investigate effects of poor initial distribution of the liquid. They concluded that the separation efficiency reached its usual value after 1m height of packing. Kouri and Sohlo (1987) showed experimentally that liquid distribution in a plastic Sulzer packing was good and that an initial maldistribution of the reflux was corrected within four to six blocks of packing. This is in contrast to Olujic et al. (1992) who showed that in a large diameter bad initial maldistribution was not corrected within the 4.2m height of packing. They also say that maldistribution can occur due to discontinuities between the blocks of packing making up one layer. However, with careful design and installation of liquid distributors and the blocks of packing these problems should not occur. Findings of many authors conclude that vapour maldistribution is not a problem.

Wall flow can also be a problem that can significantly reduce the separation efficiency of a structured packing. Experimental work carried out by Higginbotham (1992) showed that in the worst case over 70% of the liquid was flowing down the walls. At low flowrates the efficiency could be increased by approximately 25% by installing suitable wallwipers around the packing blocks.

The development of structured packings will now be charted briefly.

1930s - The first structured packing to be described in the literature appears to be that of Stedman (1937). The Stedman packing, as it became known, was fabricated from fine mesh gauze. This was stamped to form truncated cones, and punched to provide vapour outlets. The sheets were stacked horizontally with successive layers being offset such that a point would lie vertically above a hole. This provided an arrangement of cells which were claimed to split and recombine the phases in a regular manner and prevent maldistribution.

1940s - The work of Stedman was followed up in the latter half of the decade, after the war. One of the motives behind developing a low pressure drop packing was for a light weight air separation column, which could be used on mobile units or on board aircraft or ships. Weedman and Dodge (1947) tested a variety of packings. These included a Stedman packing, a regenerator packing of coiled, corrugated aluminium strips and a knitted metal cloth rolled into cylinders: basic ideas that would become familiar in later packings. Watson (1949) also tested various structured packings. His was probably the first to be made from corrugated metal sheets. Again they were stacked horizontally.

1950s - Hayter (1952) followed up the work of Watson and tested corrugated gauze packings. Sheets were stacked horizontally and segments were cut out on opposite sides of the sheets to allow vapour flow. Each element was rotated through 90^0 with respect to the previous one.

Scofield (1950) developed a somewhat different packing manufactured from expanded metal lath. Trays were made from several layers of the corrugated metal material and stacked such that the apexes of adjacent layers were in contact. It was reported that this had been used successfully in commercial columns with diameters up to 4".

The Goodloe column packing described by Bragg (1957) has the basic features of modern structured packings. Double thickness, knitted, wire strips were corrugated at a angle of 60^0 and two such strips were placed together with the corrugations in opposite directions. This was then wound up to form a cylindrical roll, which was inserted vertically into the column.

1960s - The introduction of a new generation of packings was made with Sulzer's gauze BX packing. It formed the basis of many of the later packings.

1970s - Meier et al. (1977) reported the performance of the Sulzer packing, Mellapak, based on the shape of the gauze BX packing but made from perforated sheet metal or

plastic. Alternative channel shapes were also investigated, for example the packing described by Regehr (1975).

1980s - This was the decade in which most of the commercially successful packings were introduced. Many claims of improved efficiency were made based on channel shape and surface treatments. Montzpak, from Montz, was an early competitor of Sulzer's Mellapak, introduced around 1983. In addition there was Glitsch Gempak, Raschig Ralu-Pak, Norton Intalox and Jaeger Max-Pak, which were all based on the channel type packing. The only one that differed fundamentally from the rest was Kuehni Rombopak, which was introduced in 1982. It was manufactured from expanded metal sheets arranged next to one another.

1990s - Variations on the theme of channel type packings are still being reported. However, such packings have not become serious competitors to the well established ones since the improvement in separation efficiency is usually small. The latest packing to be introduced is Sulzer's Optiflow.

2.2 Description of Modern Structured Packings

It has been seen briefly how the design of structured packing has evolved from the first packings. The modern structured packings in use today will now be discussed in more detail. Many such designs have been described in the literature, often showing minimal differences in their overall performance. Inevitably there are a few which are most widely used - these being the ones supplied by the largest packing companies. For example, Mellapak from Sulzer, also licensed to Koch as Flexipac in the USA, and Intalox Structured Tower Packing from Norton. It is important to investigate which features of the packings have developed and for what reasons in order to gain further insight into the processes occurring within the structure. From the description of the features of modern structured packings it will be seen how complex any process occurring within the channels of a structured packing is and hence the difficulties that will be involved in attempting to model such processes.

2.2.1 Packing Geometry

In general a block of packing is constructed from several vertically orientated corrugated sheets. The sheets are positioned such that the channels criss-cross one another. Figure 2-1 shows detail of the corrugation and sheet. Each block is rotated with respect to the previous block, usually by 90^0, when they are stacked vertically inside the column.

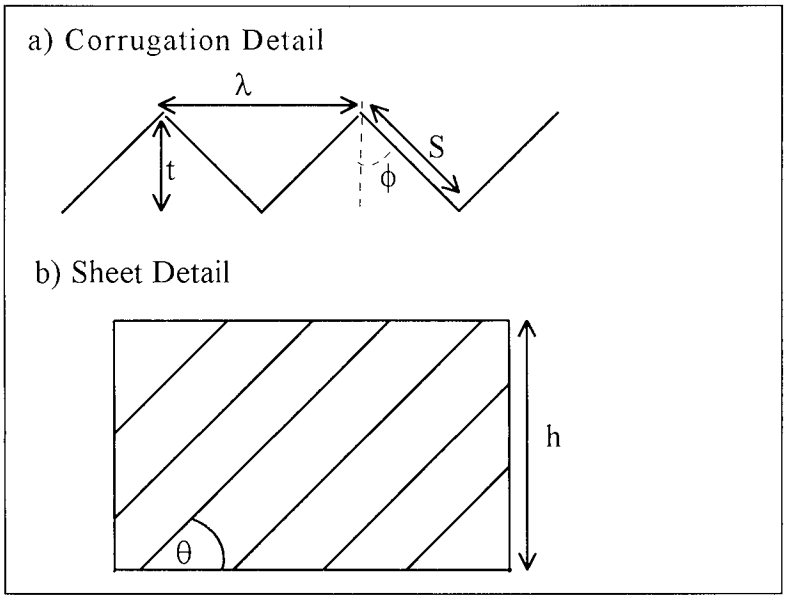

Figure 2-1 Configuration of structured packing.

Channel Shape

Most modern packings are based on the first gauze packing from Sulzer. This had a zig-zag corrugation and is the shape of their Mellapak packing. Montzpak from Montz has basically the same structure except that the channel corrugations are sinusoidal rather than sharp. This is supposed to prevent channelling of liquid in the sharp corners and reduce vapour pressure drop by reducing the form drag (Nutter Engineering Bulletin, 1987). Norton employs a slightly different channel shape to create a successful packing. This has the same basic shape as Mellapak, although the corrugations are less sharp and the crimp angle larger. The difference in the design is that peaks switch over to become troughs and vice versa, within the length of a sheet.

This has the effect of reducing the liquid and gas flow path length and creating mixing in a similar manner to that achieved by rotating the blocks. Hsia (1987) describes the improvement in efficiency as being due to liquid drops forming and falling as they reach the peak/trough switch over point.

Other modifications of the basic zig-zag shape have been proposed. For example, the peaks may be truncated to form a honeycomb type structure. Regher (1975) describes a shape in which the corrugation peaks and troughs are truncated at regular intervals. This reduces the number of contact points between adjacent sheets and is claimed to reduce pressure drop. Kolev and Nokov (1993) also describe a honeycomb type shape. However, the two flat surfaces together will tend to lead to a reduction in the total surface area available for gas/liquid contact. Another variation on the basic zigzag corrugation is given by Meier (1984). This has steep sections between the corrugations which are said to accelerate the descending liquid and also offer less resistance to gas flow, hence reducing pressure drop.

Channel Inclination Angle

The inclination angle of the channels may range from anything above horizontal up to vertical; generally between 15 and 60^0. As vertical channels may lead to a poor performance, particularly if the initial distribution of the phases is not good, the majority of packings have inclined channels; often 45^0. Kolev and Nokov (1993), describe a honeycomb packing having vertical channels and claim that vertical walled designs are more efficient than other packings. Gaiser and Kottke (1989) show how channel inclination angle effects the flow pattern and hence the local distribution of heat and mass transfer coefficients. They found that at high inclination angles and short wave lengths, defined as λ/t, the major part of the flow follows the valleys, is reflected at the wall and returns along the valley of the neighbouring sheet. Whereas, at low inclination angles and large wavelengths a greater part of the flow is in the main flow direction, between the contact points of adjacent sheets. These different flow patterns led to a wide distribution of local heat and mass transfer coefficients. With the channel angle at 45^0 a more homogeneous distribution of transfer

coefficients was displayed. It was also found that the channel angle had a greater effect on pressure drop - increasing the channel angle reduced the pressure drop.

Block Height

If the structured packing is to be inserted into a large scale industrial column the block height is limited by the size of the man-way through which it has to be inserted. Hence, the block height is usually of the order of 200-300mm. Each layer of blocks are rotated with respect to the previous layer, usually by 90^0. This has the effect of mixing the phases before they are redirected into the channels of the next block. There is little reference to the importance of block height in the literature. However, it would appear that a shorter block height may lead to greater efficiency. Billet and Mackowiak (1988) and Bauermann and Benhamou (1983) both report results of tests on Montzpak. Bauermann and Benhamou state that the block height is 125mm whereas Nutter (Nutter Engineering Bulletin, 1987) give the block height as 8" (203.5mm). Comparison of the results show a 5-10% lower efficiency and a 15% higher capacity for the taller blocks. This increased efficiency might be expected due to the fact that in the entrance region of channels the boundary layers are developing and are therefore thinner. Hence, higher heat and mass transfer coefficients will be achieved than in fully developed flow.

2.2.2 Surface Treatment

Surface treatment of the metal also influences the overall performance of a packing. It can affect both the surface area available for mass transfer and the liquid film turbulence. Major vendors of basically similar sheet metal structured packing employ different surfaces.

Surface Texture

Early structured packings were made of gauze due to its good wettability since difficulties were encountered in getting a uniform liquid film to form on sheet metal. However many different surfaces have now been described, all claiming improved liquid spreading etc. and hence improved mass transfer.

The surface texture may be described in several ways. Fluting describes the small ripples rolled onto the surface, often perpendicular to the axis of the sheet. Alternatively the surface may be lanced, which describes the process of piercing the surface with tiny slits. Finally the surface may be embossed. This involves punching some pattern onto the metal surface, which may or may not be pierced through to form holes at the dimple. Sulzer's Mellapak has a fluted surface whilst Norton's Intalox has a deeply embossed surface. Huber (1980) describes a packing surface with alternating horizontal fluted and smooth section. The fluted surface is said to promote liquid spreading by capillary action while the smooth surface allows rivulets to form. Meier (1981) describes a similar surface having flutes at an opposite angle to the main corrugations such that capillarity is aided by gravity.

McGlamery (1988) tested eight stainless steel textured surfaces using five systems and ranked the surfaces in terms of mass transfer. He concluded that the greatest improvement in mass transfer can be obtained by inducing turbulence in the liquid film. This relates to a deeply embossed surface texture. Liquid spreading is also important in increasing mass transfer area and hence the fluted surface also performed well. Kolev and Nokov (1993) describe a similar device to create liquid film turbulence in their vertical channelled honeycomb packing. A semi-circular ridge punched into the surface, normal to the channel axis is said to induce liquid film turbulence and increase liquid hold-up, hence increasing separation efficiency.

Perforations

The performance of structured packings is not usually attributed to the channel shape or surface texture alone. Many also employ a pattern of perforations in addition to the texture. It appears that the presence of perforations, allowing communication between the two sides of the sheet, is important, although it is not understood why.

Chen and Chuang (1989) describe tests carried out on three different surfaces, all having holes. They showed that different combinations of texture and hole size performed well at different liquid flow rates. Smaller holes appeared more effective at low liquid loads when the hole had the effect of splitting the liquid film. Larger holes gave better results at high liquid rates where smaller holes became blanked over.

The arrangement as well as size of holes may also be important. Chen and Acerra (1987) suggest that the holes should be arranged on a square rather than triangular pitch and that burrs left as a result of the manufacturing process are beneficial. This leads to an embossed type surface, which has been shown to be efficient.

McGlamery (1988) also concluded that perforations were important. Bravo et al. (1991) postulate that the effect of holes may be to promote lateral spreading due to surface tension effects or to give better gas/liquid distribution between the two sides of the sheet. They also conclude that perforations which direct the flow positively across the sheet are better than mere perforations.

One such packing is Jaeger's Max-Pak. This is described by Seah (1987) and has W and V tabs and slots located at specific points in relation to the main corrugations. The benefit is described as being due to the openings promoting a zigzag flow path of fluid from one side of the sheet to another. The tabs are pushed out in such a way as to provide drip points for the liquid. The separation efficiency appears to be similar to that of the Norton Intalox packing (Jaeger Products, 1988).

Specifically positioned holes have also been used by Yeoman (1994) to produce a nested structured packing. Holes along the channel corrugations allow sheets to sit closer together, hence increasing the surface area in a given volume. Liquid flow in the apex can also be disrupted by the apex of a neighbouring sheet corrugation protruding through the hole.

Sulzer's new packing, Optiflow (Sulzer Chemtech, 1994) also used holes to produce a rather different kind of structure. Rhomboid shaped holes, cut such that when the metal is folded they lie along the corrugation walls, lead to a very open structure. The formation of fan-like vane elements is said to provide for improved distribution of the liquid phase and allow for more than one preferred direction for gas flow (Wilhelm, 1989 and 1992). However, this does result in a considerable reduction in available surface area and must reduce the mechanical strength of the packing. Manufacturing may also be more complex since the placement of sheets will be crucial to form the desired structure of four propeller-like blades.

2.3 Summary

The development of structured packings that has taken place over the last half century has been briefly charted. The features of modern structured packings have been described and the benefit attributed to the particular features discussed. From this it can been seen that producing models, based on fundamental principles, for predicting the performance characteristics of such packings will be a difficult task.

2.4 Models of Structured Packings

With the increasing use of structured packings there has been considerable effort put into attempting to develop models to predict their performance. Some models have been developed as extensions of empirical correlations originally devised to predict the performance of random packings. Other models have a more theoretical basis with differences between actual and predicted results accounted for by a constant, which may be applicable to a family of packings or may only apply to one particular size and design.

Many empirical models have been proposed for predicting the performance of structured packings. However, as these models are based on fitting expressions to experimental data they can only be used in the design of new columns or revamps of old ones using existing structured packings. They can not give predictions of the way in which new packings will perform. Also, as shown by Porter and Jenkins (1979) '... all the physical properties, as well as the economic design flow rates, may be approximately correlated against the flow parameter, and thus in effect against each other'. So, a correlation may indeed predict the experimental results whilst being based on an incorrect theory.

When designing a column the important factors that need to be considered are the pressure drop across the bed, the maximum capacity, and the mass transfer efficiency, since this determines the size of the column. The liquid hold-up and wetted surface area are also important, as they influence both the pressure drop and mass transfer rate. In the following sections some of the models proposed for these parameters will be looked at.

Since several variables are closely dependent on one another, for example pressure drop and liquid hold-up, the model proposed by a given author usually contains expressions for several variables, not just one. The complete model is composed of expressions for each variable and is solved simultaneously. Discussion of the models will be on a variable by variable basis rather than on complete models by a particular

author. References will be made to other parts of the model discussed in previous or following sections, where necessary. Such an arrangement allows for easier comparison of the various expressions for a given variable. Contrasts and comparisons between the approaches of the various authors will then drawn. The suitability of the models in predicting the performance of new structured packings will also be discussed.

2.4.1 Pressure Drop

Several methods of predicting pressure drop have been proposed. Some involve the use of a friction factor that can be measured and correlated from experimental data of pressure drop through the bed in the absence of liquid flow. Pressure drop is also related to liquid hold-up as this reduces the available space in the column for vapour flow. Hence the expressions for hold-up and pressure drop often have to be solved simultaneously. An alternative method for predicting the pressure drop is the use of correlation charts, which is a fairly well established method for random packings that has been modified to be applicable to structured packings.

On a log-log plot of pressure drop versus gas rate for a given liquid rate several distinct regions can be seen, see Figure 2-2. At relatively low vapour rates the effect of gas rate on the liquid is negligible. The line of wet pressure drop is higher but parallel to that of the dry pressure drop. As the gas rate is increased it starts to influence the structure of the liquid film and liquid begins to hold up. This is seen as a divergence of the wet pressure drop line from the dry pressure drop line and is termed the loading point. Finally, as the gas rate is increased further liquid can no longer flow downwards; the column is said to be flooded, and pressure drop increases rapidly. Some models for irrigated pressure drop modify the dry pressure drop expression, while others calculate it directly, in a similar way to dry pressure drop.

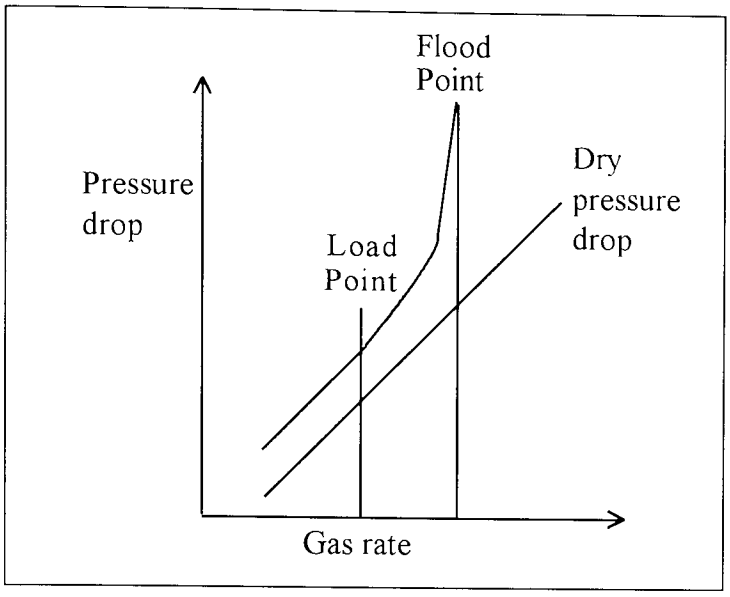

Figure 2-2 Typical plot of dry and irrigated pressure drop.

One of the earliest models proposed for predicting pressure drop was that of Bravo et al. (1986). Their model was originally applied to gauze packings although they thought it should equally apply to corrugated sheet metal packings. The derivation of the equations was based on previous work on random packings. Their equation for irrigated pressure drop, which is a modification of the dry pressure drop is of the form:

$$\left(\frac{dp}{dz}\right)_{irr} = \left(\frac{dp}{dz}\right)_{dry}\left[\frac{1}{(1-K\,h_l)}\right]^5$$

The relationship only applied below the loading point where liquid hold-up, h_l, was correlated with the Froude number. The constant K was found from experimental data for each packing.

Rocha et al. (1993) present a more rigorous model that applies to all regions of gas loading, up to the flood point. Model equations for the liquid hold-up (see section 2.4.2) are developed by considering the forces acting on the falling liquid film. The wet pressure drop is again a correction of the dry pressure drop and is of the form given above. In this model the value of K is correlated with S, the corrugation side length, or characteristic packing dimension.

The final model equation of Stichlmair et al. (1989) is similar and applies to any operational regime up to flooding. The model is a particle, rather than channel type model, and is based on an analogy with fluidised beds in that the bed porosity changes due to liquid loading. The equation is given below.

$$\left(\frac{dp}{dz}\right)_{irr} = \left(\frac{dp}{dz}\right)_{dry} \left\{\frac{[1-\varepsilon\,(1-h_l/\varepsilon)]}{(1-\varepsilon)}\right\}^{(2+c)/3} (1-h_l/\varepsilon)^{-4.65}$$

The dry pressure drop is expressed in terms of a single particle friction factor and the void fraction of the bed. A total of three packing specific constants are required in the correlations given for the single particle friction factor and the constant, c.

The model of Billet and Schultes (1992) is similar in form to those proposed by Bravo et al., except that irrigated pressure drop is not calculated from the dry pressure drop. However, a similar form of equation is used which accounts for the reduction in void fraction due to the presence of liquid. An expression for the friction factor is found from evaluation of experimental data, and is correlated against the liquid and vapour Reynolds numbers and liquid hold-up. A constant to correct for each packing is also required.

Hughmark (1980) also determines friction factors for various packings from pressure drop data. A relative vapour velocity based on the void fraction and the liquid velocity is used. The model of Hughmark (1986) extends the earlier one and applies into the loading region. It correlates friction factors against the ratio of film thickness to hydraulic diameter. The pressure drop is split, such that a fraction, α, represents the shear drag.

An alternative method for predicting pressure drop is the use of Generalised Pressure Drop Correlations or GPDC.

Robbins (1991) proposed a new pressure drop correlation presented in a generalised pressure drop correlation of pressure drop versus G_f with L_f/G_f as the parameter. The variables G_f and L_f, the gas and liquid loading factors, were correlated against the gas

or liquid rate respectively, density and a dry bed packing factor. The dry bed packing factors were correlated with gas rates for many packings, most of them random.

Kister and Gill (1992) also give a new GPDC chart, but specifically for structured packings. They give data on a Souders type diagram plotting the flow parameter, X against the capacity parameter Y, where:

$$X = \frac{L}{G}\left(\frac{\rho_g}{\rho_l}\right)^{0.5} \quad \text{and} \quad Y = U_s\left(\frac{\rho_g}{\rho_l - \rho_g}\right)^{0.5} F_p^{0.5}\,\nu^{0.05}$$

Again the model is dependent on an empirical factor, F_p, characteristic of the packing size and shape. The method is not fully satisfactory since experimental data are required to give what they term a GPDC interpolation chart. Interpolation between the new GPDC curves and experimental data is then used to calculate pressure drop. Use of the curves is not recommended in regions where experimental data is not available.

Spiegel and Meier (1987) and (1992) also present models relying heavily on experimental data. The loading range is divided into distinct regions with different approaches applied in each. At low loads, in 1987 this was below 50% capacity and in 1992 below 45% capacity, dry pressure drop data is used. The 1987 model simply used the dry pressure drop whereas the 1992 model modified this by several factors to account for liquid hold up (f_1) and the relative velocities of the two phases (f_2). A third factor (f_3) was required at high liquid loads and allows for different liquid viscosities and surface tensions.

$$\left(\frac{dp}{dz}\right)_{irr} = f_1 f_2 f_3 \left(\frac{dp}{dz}\right)_{dry}$$

A polynomial curve fit is used to represent pressure drop in the region between low loading and the capacity limit. The capacity limit was taken as a fixed pressure drop point.

Several alternative methods have been proposed for prediction of pressure drop. These may require an understanding of liquid hold-up and are therefore dependent on the ability to predict this accurately.

2.4.2 Liquid Hold-Up

It has already been seen that liquid hold-up within a column is closely related to vapour rate and pressure gradient. Liquid hold-up can be split into two parts - static hold-up i.e. liquid that remains in the packing in the absence of gas flow, and dynamic hold-up i.e. liquid hold-up resulting from vapour flow. Since dynamic hold-up is usually much larger than static hold-up, the latter is ignored in all models.

Hold-up is also related to the liquid film flow so many models incorporate some model for film thickness. This is often Nusselt's laminar film theory for flow of liquids on smooth surfaces. Although this is one of the simplest methods it may be inappropriate for a number of reasons: For example the packing surface is usually textured and the resulting film may not be laminar.

The various models, which can be classified broadly as either correlations or laminar film theory, will now be discussed.

The early model of Bravo et al. (1986), which only applies below the loading region, empirically correlates hold-up with the liquid Froude number.

$$h_o = C_3 \, Fr^{0.5}$$

Values of C_3 were found to vary with size and type of packing and are presumably also dependent on the type of surface.

Their later model, Bravo et al. (1992), is more rigorous and extends into the loading region. It therefore accounts for the liquid film thickness, which is calculated from a modification of the Nusselt laminar falling film equation. Wetted area is incorporated

by use of the Shi and Mersmann (1985) model (see section 2.4.3). The final model equation validated against experimental data is given as:

$$h_l = \left(4\frac{F_t}{S}\right)^{2/3} \left(\frac{3\,\mu_l\,u_{ls}}{\rho_l\,\varepsilon\,g_{eff}\,\sin\theta}\right)^{1/3}$$

The empirical coefficient F_t, which is a correction factor for experimental hold-up is correlated by:

$$F_t = \frac{29.21\,(We_l\,Fr_l)^{0.15}\,S^{0.359}}{Re_l^{0.2}\,\varepsilon^{0.6}\,(1-0.93\cos\gamma)(\sin\theta)^{0.3}}$$

and g_{eff}, which is the effective gravity, is correlated by:

$$g_{eff} = g\left[\left(\frac{\rho_l-\rho_g}{\rho_l}\right)\left(1-\frac{(dp/dz)_{irr}}{(dp/dz)_{flood}}\right)\right]$$

The model is limited by the fact that a value of the flooding pressure drop is required. In the absence of experimental data this then relies on some method to predict it. Bravo et al. used a constant value for this pressure drop.

The model presented by Stichlmair et al. (1989) is similar to that of Bravo et al.. Hold-up below loading is correlated by a modified Froude number:

$$h_o = 0.555\left(\frac{u_{ls}^2\,a}{g\,\varepsilon^{4.65}}\right)^{1/3}$$

Above the load point hold-up is modified to account for the vapour rate and is given by the following expression:

$$h_l = h_o\left[1+20\left(\frac{(dp/dz)_{irr}}{\rho_l\,g}\right)^2\right]$$

Henriques de Brito et al. (1992) also give a correlation for hold-up in terms of liquid rate. However, it is not clear how this would be affected by different types of packing as the only two they used were Sulzer Mellapak 250Y and 500Y. Their expression is:

$$h_l = C_3 \, B^{C_4}$$

where B is the specific liquid load (m^3/m^2h) and C_3 and C_4 are constants for different sizes of packing. For both those tested C_4 was found to be 0.397.

Spiegel and Meier (1992) plot hold-up as a function of liquid load for various sizes of Mellapak. Two different liquid load regions can be seen with the dependence of hold up in each being approximately:
low liquid loads: $h_l \propto u_l^{0.4}$; high liquid loads: $h_l \propto u_l^{0.6}$

Billet (1987) and Billet and Schultes (1987) use laminar film theory with differences for things such as turbulent flow accounted for by a flow factor function, ξ. The resulting expression is:

$$h_l = \left[\frac{a^2 \, \mu_l \, u_{ls}}{\frac{1}{3} g \, \rho_l - \frac{1}{4} \xi \frac{a}{h_l (\varepsilon - h_l)^2} F_v^2} \right]^n$$

For laminar liquid films n=1/3, but for structured packings it was found that n=2/3. The resistance coefficient is correlated empirically by an equation of the form:

$$\xi = \frac{g}{C^2 \left[\frac{L}{V} \sqrt{\frac{\rho_g}{\rho_l}} \left(\frac{\mu_l}{\mu_g} \right)^m \right]^n}$$

Values of m and n were found to be constant whereas C was dependent on the packing.

Billet and Schultes (1992) also use a laminar film model below loading but include an empirical correction for wetted area to account for differences in predicted and experimental hold-up results.

$$h_o = \left(12 \frac{\mu_l a^2 u_{ls}}{\rho_l g} \right)^{1/3} \left(\frac{a_h}{a} \right)^{1/3}$$

Above the loading point hold-up is correlated empirically with vapour rate.

$$h_l = h_o + (h_{l,fl} - h_o) \left(\frac{u_g}{u_{g,fl}} \right)^{13}$$

Hold-up at the flood point is calculated as 2.2 times the hold-up below loading.

Hughmark (1986) gives an empirical correlation for the dimensionless film thickness in terms of the Reynolds number and states that for structured packings the interfacial area should equal the surface area of the dry packing.

2.4.3 Area

The simplest method of incorporating area into the equations is to use the dry surface area of the packing. This method was originally adopted for models of gauze packing where good surface wettability even at low liquid rates probably made the assumption true. The same approach was adopted by some of the earlier models for sheet metal packing e.g. Bravo et al. (1985), Billet (1987).

Several different surface areas can be defined. For instance, the wetted surface area is the area between the liquid and packing surface. This however may contain dead zones of liquid. The effective interfacial area between gas and liquid includes additional surface area created by liquid flows which are not in contact with the packing surface e.g. bubbles and droplets. Shi and Mersmann (1985) propose a model for wetted surface area based on considerations of static and flowing films.

$$\frac{a_h}{a} = 0.76 \frac{(We_l\, Fr_l)^{0.15}}{Re_l^{0.2}\, \varepsilon^{0.6}\, (1 - 0.93\, \cos\gamma)}$$

Bravo et al. (1992) employ this expression correlated with hydraulic diameter. An empirical constant and exponent on the equivalent diameter account for differences in predicted and recorded liquid hold-ups. Their mass transfer model uses the same expression for effective interfacial area with a correction factor for different packings. For gauze packings they propose their own correlation:

$$\frac{a_h}{a} = 1 - 1.203 \left(\frac{u_{ls}^2}{S\, g}\right)^{0.111}$$

In an earlier paper, Fair and Bravo (1990) suggest reducing the packing surface area to allow for areas which are not wetted.

$$\beta = 0.5 + 0.0058\ (\%\, flood)$$

Where β = fraction of surface wetted, and above 85% flood β = 1.

Billet and Schultes (1992) give two different expressions for area. The first allows for differences in experimental and calculated hold-up values. It is given as the wetted surface area where C_h is a packing dependent constant.

$$\frac{a_h}{a} = C_h\, Re_l^{0.15}\, Fr_l^{0.1} \qquad Re_l < 5$$

$$\frac{a_h}{a} = 0.85\, C_h\, Re_l^{0.25}\, Fr_l^{0.1} \qquad Re_l > 5$$

The second correlation, from mass transfer data, gives an expression for interfacial area which shows a similar dependence on liquid velocity.

$$\frac{a_e}{a} = 1.5\, (a\, d_h)^{-0.5} \left(\frac{\rho_l\, u_l\, d_h}{\mu_l}\right)^{-0.2} \left(\frac{u_l^2\, \rho_l\, d_h}{\sigma_l}\right)^{0.75} \left(\frac{u_l^2}{g\, d_h}\right)^{-0.45}$$

Experimental mass transfer results of Spiegel and Meier (1987) for four sizes of Mellapak led to the expression:

$$a_e = C\,(\rho_l\, u_{ls})^{0.2}$$

However, Henriques de Brito et. al. (1994), who also carried out experiments using various sizes of Mellapak gave the following expression:

$$\frac{a_e}{a} = 0.465\, Re_l^{0.3}$$

An expression for area is incorporated into many of the models as a method of reconciling experimental and predicted results. All the expressions, be they correlations of experimental results or theoretically based models, show a similar dependence on superficial liquid velocity with exponent values in the range 0.2-0.45.

2.4.4 Flooding and Capacity

The flood point may be defined in several ways. The most theoretical is in terms of hydraulic capacity and is defined as the maximum vapour rate for a given liquid rate. At this point liquid can be seen backed up on top of the packing and pressure drop increases rapidly. An alternative definition can be given in terms of mass transfer efficiency which decreases at flooding. A flood point definition can be given as where the separation falls to a certain fraction of the normal operational efficiency. Three different approaches to modelling the flood point have been adopted in the literature.

The simplest method is to choose a constant value of pressure drop. This has been used by several workers. However, it has the disadvantage that the value chosen may not accurately represent the flood point for all shapes and sizes of packings and with all systems. Various values of flooding pressure drop have been used:

Spiegel and Meier (1987)	10 mbar/m
Spiegel and Meier (1992)	12 mbar/m
Bravo et al. (1992)	10.25 mbar/m

Another method is to correlate experimental data. One of the earliest correlations for predicting the flood point was given by Alekseev et al. (1972) who used data for various corrugated packings and various systems. The final expression was simplified to:

$$K = 0.32\, Fr^{-0.22}\, We^{-0.26}$$

where:

$$K = \frac{u_{g,fl}\, \rho_g^{0.5}}{g^{0.25}\, \sigma^{0.25}\, (\rho_l - \rho_g)^{0.25}}$$

$$Fr = \frac{Q_m\, g^{0.25}\, (\rho_l - \rho_g)^{0.75}}{\sigma^{0.75}}$$

$$We = \frac{\sigma}{g\, (\rho_l - \rho_g)\, d_e^2}$$

and Q_m = bulk flowrate of liquid relative to wetted perimeter (m^3/ms)

Experimental flooding data can be plotted in a number of ways, following methods developed for random packings. A Wallis diagram, plotting $c_G^{1/2}$ against $c_L^{1/2}$, gas and liquid capacity factors gives straight lines that can be represented by:
$c_G^{1/2} + m\, c_L^{1/2} = C$, where m and C are adjustable constants. Alternatively, data can be represented on a Souders diagram plotting the capacity factor c_G against the flow parameter. Spiegel and Meier (1987) show data for four sizes of Mellapak on both types of diagram. Data is represented by two straight lines of different slopes on both diagrams. This indicates distinct hydraulic regimes at different liquid loads.

Kister and Gill (1992) give data for several types of structured packings plotted on a generalised pressure drop correlation chart. From experimental data they give an expression for the flooding pressure drop (inches water per foot of packing) in terms of the packing factor (ft^{-1}):

$$\left(\frac{dp}{dz}\right)_{flood} = 0.115\ (F_p)^{0.7}$$

Flooding velocities can then be found from the chart.

The third method for modelling the flood point is to extend the model for irrigated pressure drop into the flooding region. Various different theoretical definitions of the flood point have been proposed. These conditions are then incorporated with the model for pressure drop in the region below flooding.

Bravo et al. (1992) define an effective gravity acting on the liquid film which will equal zero when flooding is reached. The flooding vapour velocity is calculated as the theoretical flooding pressure drop is approached. Hughmark (1986) makes a similar assumption, that flooding will occur when the shear stress on the liquid film is zero.

Billet (1987) gives the flood point in terms of the velocity and hold-up. Flooding is defined by the following definitions:

$$\frac{du_{ls}}{dh_l} = 0 \text{ and } \frac{du_{gs}}{dh_l} = 0$$

From the initial part of the model the following flooding velocities result:

$$u_{v,fl} = \sqrt{\frac{2\,g}{\xi_{fl}}}\ \frac{(\varepsilon - h_{l,fl})^{3/2}}{\varepsilon^{1/2}}\ \sqrt{\frac{h_{l,fl}}{a}}\ \sqrt{\frac{\rho_l}{\rho_g}}$$

$$u_{l,fl} = \frac{g}{3}\ \frac{1}{a^2}\ \frac{\rho_l}{\mu_l}\ (h_{l,fl})^3 \left(1 - \frac{3}{2}\ \frac{(\varepsilon - h_{l,fl})}{\varepsilon}\right)$$

where: $(h_{l,fl})^3 (3\ h_{l,fl} - \varepsilon) = \frac{6}{g}\ \frac{L}{V}\ \frac{\rho_g}{\rho_l}\ a^2\ \varepsilon\ \frac{\mu_l}{\rho_l}\ u_{v,fl}$

The resistance flow factor is correlated by:

$$\xi_{fl} = \frac{g}{C_{fl}^2 \left[\frac{L}{V} \sqrt{\frac{\rho_g}{\rho_l}} \left(\frac{\mu_l}{\mu_g} \right)^{0.2} \right]^{-0.388}}$$

where C_{fl} depends on the packing. Iterative solution of the above equations yields the flooding velocities and liquid hold-up at the flood point. Billet and Schultes (1992) correlate liquid hold-up at the flood point with hold-up in the region below loading, with a correction for the system properties referenced to those of water.

Stichlmair et al. (1989) also define a flood point in terms of the gas flow and liquid hold-up. By using $(dp/dz)_{dry}$ as a measure of gas flow, and $(dp/dz)_{irr}$ as a measure of hold-up flooding is related to the earlier part of the model. The flood condition is given as:

$$\frac{d(dp/dz)_{dry}}{d(dp/dz)_{irr}} = 0$$

Substitution of the relevant model equations and differentiation gives a complicated expression. Solution by iteration for a given liquid rate gives a value of pressure drop at the flood point.

2.4.5 Mass Transfer Efficiency

The mass transfer efficiency of a packing is an important design parameter since it will determine the size of the column. The efficiency may be expressed in a number of ways. The most common are as mass transfer coefficients or as a Height Equivalent to a Theoretical Plate (HETP). The roots of models to predict efficiency in structured packing can be traced back to earlier work on random packings and on wetted wall columns. The approach taken by many workers is a correlation of experimental results by dimensionless groups. An alternative, but little used approach, is a theoretically based model. Correlations of liquid phase mass transfer coefficients are frequently based on penetration theory.

Bravo et al. (1985) and (1992) give the gas phase mass transfer coefficient in a correlation of dimensionless groups. The more recent model, which is applicable to sheet metal packings is given by:

$$Sh = 0.054\, Re_g^{0.8}\, Sc_g^{0.33}$$

Effective velocities allow for liquid hold-up and are used in calculating the dimensionless groups. The simplified equivalent diameter, being the side length of a corrugation is used.

The liquid phase mass transfer model is based on penetration theory. The contact time is calculated as the time taken for liquid to flow across a corrugation side. The 1992 model has a modified contact time in order that predicted results agree better with those observed experimentally. This is explained as accounting for areas where surface renewal is slow. Hence:

$$k_l = \sqrt{\frac{D_L\, C_E\, u_{le}}{\pi\, S}}$$

The value of C_E was found to be approximately 0.9 for all packings.

Billet and Schultes use similar correlations to those of Bravo et al., assuming a penetration model for each phase. Their correlation is fitted to experimental data and requires constants for each type and size of packing. Contact times are determined from liquid hold-up, contact length and phase loading. The final equations in terms of the volumetric coefficients are:

$$k_g\, a_e = C_g\, \frac{1}{(\varepsilon - h_l')^{1/2}}\, \frac{a^{3/2}}{d_h^{1/2}}\, D_g \left(\frac{\rho_g\, u_{gs}}{a\, \mu_g}\right)^{3/4} \left(\frac{\mu_g}{\rho_g\, D_g}\right)^{1/3} \left(\frac{a_e}{a}\right)$$

$$k_l\, a_e = C_l \left(\frac{\rho_l\, g}{\mu_l}\right) \left(\frac{D_l}{d_h}\right)^{1/2} a^{2/3}\, u_{ls}^{1/3} \left(\frac{a_e}{a}\right)$$

A correlation is given for interfacial area available for mass transfer (given in section 2.4.3).

Spiegel and Meier (1987) also correlate the gas phase mass transfer coefficient in the same way. Exponents on the Reynolds and Schmidt numbers are 0.8 and 1/3 respectively. Their model ignores k_l on the assumption that it is often much larger than k_g and since diffusivity is hard to measure.

Henriques de Brito et al. (1992) and Laso et al. (1995) give a semi-empirical correlation for the liquid phase mass transfer coefficient. It is based on Higbie's penetration theory and uses an empirical model for contact time and liquid hold-up.

Hughmark (1980) and (1986) is the only worker to present a theoretical model of mass transfer, based on analogy to momentum transfer. The model assumes turbulent flow of vapour and gives dimensionless mass transfer coefficients for the turbulent core and transition region. The viscous sublayer is ignored. The model can be represented as:

$$k_g = \frac{u_g^*}{1/k_t^+ + 1/k_c^+}$$

Since only a fraction of the pressure drop is due to shear the vapour shear velocity is given by:

$$u_g^* = u_g \, \alpha \, (f/2)^{1/2}$$

The effective velocity relative to the liquid is given by:

$$u_g = \frac{u_{gs}}{\varepsilon} + u_l$$

and the dimensionless mass transfer coefficients are given as:

$$k_t^+ = \frac{0.097}{Sc_g} \left\{ a \tan\left[34.6 \, (0.0094 \, Sc_g)^{1/2} \right] - a \tan\left[5.5 \, (0.0094 \, Sc_g)^{1/2} \right] \right\}^{-1}$$

$$k_c^+ = 2\,\alpha\,(f/2)^{1/2}$$

The liquid phase mass transfer is correlated by:

$$k^+\,Sc^{1/2} = 0.012\,Re^{1/3}$$

The shear velocity is calculated from a characteristic shear stress, τ_c which is approximated by:

$$\tau_c = 2/3\;\tau_{wall} + \tau_{int}$$

The shear stress at the wall and interface are calculated from equations for vertical, annular gas/liquid flow, modified for the packing situation. Although the model is more fundamentally based it still requires the friction factor and the fraction of the pressure drop due to shear. However, these can be determined from hydraulic tests on the dry and irrigated packing.

Strigle (1994) gives a simpler correlation, developed by the Norton company which may be used to predict HETP values. The value of n is given for three sizes of the Intalox structured packing.

$$\ln HETP = n - 0.187\ln\sigma + 0.213\ln\mu$$

where σ = surface tension in dyne/cm, and μ = liquid viscosity in centipoise.

None of the models allow for variation in the transfer coefficients at different positions within the packed bed. Kaiser and Gottke (1989) showed such local variations do occur; this will also be backed up by findings in this work.

2.5 Block Models

All the models discussed to date have considered the packed bed in its entirety. This approach restricts the model to predicting overall average values rather than local values. A somewhat different approach has been taken by Stoter et al. (1992) and (1993). They divide the packing into sections, the size of which varies on the model being used.

The large scale model (Stoter et al., 1992) considers blocks having size similar to the height of a packed section and has been used to predict distribution of gas and liquid and separation efficiency in large scale columns. The model uses splitting factors to divide the flow at intersections of blocks. Various splitting factors are used to represent different sections of the bed i.e. bulk of packing, near wall. These factors were determined experimentally.

The small scale model is divided into cells of a size similar to the hydraulic diameter of the packing and has been used to predict distribution of the gas phase. A model of such a scale should enable the fundamental processes occurring within the corrugated channels to be studied. The basic unit cell of the model represents the intersection between two channels of neighbouring sheets. The equations are formulated from balances of mass, momentum and energy. Three distinct zones in the packing sheet are included: bulk zone, wall zone, either with or without wall wiper bands, and the inlet zone at the lower edge. Again, friction factors are required which are deduced from experimental results and this does mean the model still has a degree of empiricism. A similar model whose unit block allowed for the shape of the packing could be of use in developing new packing designs.

2.6 CFD Models

It appears that no workers have used a CFD approach to the modelling of structured packings due to the lack of published work. Sulzer's brochure for their new packing,

Optiflow, hints at the use of CFD but there are no papers in the literature to back this up. Modification of the work of Stoter et al. (1993) has the makings of a CFD based model.

2.7 Other Models

The models presented by Hanley et al. (1994) are the only ones to be based on a completely alternative theory. They develop models for pressure drop, flooding, liquid hold-up, separation efficiency and mass transfer area based on an analogy with electrical percolation on a conductor/insulator lattice. The passages within the packing are either "conducting", when vapour flow can occur, or "insulating" when the passage is blocked by liquid. The occurrence of such an "insulated" channel gives rise to localised flooding. The flood point is defined as the range of gas and liquid velocities which cause the liquid cluster to form in voids spanning the entire column. This means the model accounts for both localised and macroscopic flooding whereas others cannot. The pressure drop model can be recast in a form reminiscent of models based on completely different arguments, and is a correction of the wetted and drained pressure drop. This is in contrast to many other models which use dry pressure drop - here static hold-up is included. Flooding predictions are given in the form of a Wallis equation, and requires two constants for a specific packing.

The model, which may indeed be soundly based, will be hard to use since empirical constants are required and it is hard to understand.

2.8 Approaches to Modelling

Different approaches have been taken to model the important parameters involved in the design of distillation columns containing structured packings. Clearly the processes of mass, momentum and heat transfer taking place within the channels of structured packings are very complex. Due to this fact the models are generally of an empirical nature and rely on experimental data to provide model constants that may

apply to a group of packings or just a single size and shape of packing. The constant incorporates, or bulks together, many unknown or unmeasured effects of the packing. For instance, although some models do include a characteristic size for the packing, and the channel inclination angle, the effect of surface texture or block height is not modelled. Alternatively, correlation charts have been used but again these are not universally applicable. This means that the models are only able to predict the performance of existing packings and can give no information on how a new, differently designed packing will behave. Any new packing developed would have to be manufactured and tested experimentally in order to determine whether the correlation was applicable or to find the packing specific constants. It may also be that many correlations, supplemented by suitable constants would predict the experimental results satisfactorily.

A somewhat different approach has been taken by Stoter et al. in the form of a block model. This represents a more fundamental method of modelling since the packing is considered more on the micro scale and the equations solved are balance equations for momentum, mass and energy, around a unit cell of the packing channels. The unit cell, comprises of an intersection between channels of neighbouring sheets. However, these predictions are also corrected by a friction factor that is deduced from experimental data. A model with a similar basis, but considering the packing on a smaller scale, to the extent of modelling what is happening inside the unit cell, rather than modelling it overall, would have great implications in that the packing shape and possibly other features could be included.

An approach such as this would require the writing of complex computer programs to solve the balance equations for each shape of unit cell. However, a simpler method would be to use a computational fluid dynamics (CFD) code. These have the benefit that a pre-processor is usually a standard front end to the package. This can be used to create meshes of grid points to fit any desired shape, and to specify physical properties of materials. Since the equations are solved at discrete locations within the unit cell this would also provide data on local variations in predicted variables. The equations that must be solved to model the full distillation process, which involves

heat, mass and momentum transfer and two phase fluid flow are extremely complex and may indeed themselves be models that are not universally valid. It is impossible to remove all empirical assumptions as for example, in turbulent flow some turbulence model must be chosen to represent the phenomenon.

The potential of using CFD, if a suitably validated approach can be developed, is that the shape of the packing can be included in the modelling. The performance of new shaped packings could be 'tested' on a computer instead of having to manufacture the packing and test it experimentally. The empirical basis of the existing models means that they are not able to give information on new packings. New designs have to be manufactured and tested and then modified and tested again. This is a costly process in terms of tool making and time. A far greater number of shapes could be investigated by a CFD method, and those found to be good optimised by further runs of the computer code.

2.9 Summary

The models that have been proposed to predict the performance of structured packing have been described. These are generally correlations of experimental data and must be supplemented with constants for each packing and so can give no indication of the way in which new packings will perform. A model developed using a CFD package to solve fundamental equations on the small scale within the packing may have enormous potential by allowing new shaped packings to be 'tested' on a computer.

2.10 Introduction to Computational Fluid Dynamics

The technology of CFD as it is today results from an amalgamation of advances made in the areas of computer science, mathematics and engineering. It is no longer exclusively the realm of academics in universities but is being used by engineers in industry as a design tool. CFD can be used for a wide range of applications, from the design of aerofoils in the aeronautical industry, to the flow of blood to the heart in biological applications, to the mixing occurring in vessels in the process industries.

A large number of CFD codes are available commercially. These are becoming more accessible to the engineering world in general since the majority of engineers now have access to relatively powerful computers, with graphical operating systems, capable of running large programs. In addition to the companies supplying complete CFD codes there are those who supply pre- and post-processor packages for the generation of the meshes of grid points for calculation and for displaying simulation results. At a CFD event in February 1994, hosted by IBM, Dr Boysen from Fluent Europe gave information on the number of commercial CFD companies world-wide. This is shown in Table 2-1. The numbers have probably increased since then.

Package Type	Number of Companies
Pre-processor	13
Post-processor	22
Flow solver	19
Complete CFD	18

Table 2-1 Number of commercial CFD companies.

Appendix 1 lists some of the CFD codes available and the companies producing them. Some companies market packages to be used for very specific problems. For example, Flowmerics produce two codes, Flotherm, for predicting air flow and heat transfer around electronic components and Flovent for predicting ventilation within buildings. Other packages, such as CFX4 (formerly Flow3D) and PHOENICS can be

used for a much wider range of situations. Details of all the codes mentioned are given in appendix 2.

In the following sections the basic theory behind the CFD codes will be discussed. This will be a brief review of the various codes and the theory behind their application, with no bias to any one code in particular. Their capabilities and limitations will be assessed, with particular reference to the chemical process industries.

2.11 Theory

The task of any CFD code is to solve the equations governing the conservation of mass, momentum, energy or chemical species, given various boundary and initial conditions. Solution of such a set of differential equations is not simple as they are often coupled and non-linear.

The differential equations can be written in a general form as shown, where the meaning of each term is indicated.

$$\underset{UNSTEADY}{\frac{\partial}{\partial t}(\rho\,\phi)} + \underset{CONVECTION}{div\,(\rho\,\mathbf{u}\,\phi)} = \underset{DIFFUSION}{div\,(\Gamma_\phi\,grad\,\phi)} + \underset{SOURCE}{S_\phi}$$

The general variable, ϕ can represent a number of different quantities, for example, enthalpy or temperature, a velocity component, or a mass fraction of a chemical species. To generate a particular equation the appropriate meanings are then given to Γ_Φ and S_ϕ. For example, if ϕ represents u, the velocity component in the x direction; the diffusion coefficient Γ_Φ represents the dynamic viscosity, μ, and S_ϕ may contain pressure gradients and body forces. The x direction momentum equation for flow with constant density and viscosity would then be written as:

$$\rho\frac{\partial u}{\partial t} + \rho\,u\frac{\partial u}{\partial x} + \rho\,v\frac{\partial u}{\partial y} + \rho\,w\frac{\partial u}{\partial z} = \mu\left(\frac{\partial^2 u}{\partial x^2} + \frac{\partial^2 u}{\partial y^2} + \frac{\partial^2 u}{\partial z^2}\right) - \frac{\partial p}{\partial x} + \rho f_x$$

and the continuity equation as:

$$\frac{\partial u}{\partial x} + \frac{\partial v}{\partial y} + \frac{\partial w}{\partial z} = 0$$

In order to solve such a set of equations some numerical technique is applied. Such techniques provide the solution at discrete points rather than providing a continuous solution function. The points, or nodes are formed by a mesh which divides the domain over which the equations are to be solved. The general differential equations are then replaced by algebraic equations in terms of the grid point in question and values at neighbouring grid points and the solution task is that of solving the algebraic equations at all locations simultaneously, in conjunction with the boundary conditions.

Several different methods, known generally as discretization methods, exist for deriving the algebraic equations from the governing differential equations. The three most common techniques are the finite difference, finite volume and finite element methods. The finite difference method is based on a truncated Taylor series. In the finite volume method the differential equations are integrated over the control volumes formed around each grid point. Some profile for the variation of the variable in question is then assumed, so that each term in the integrated equation can be written in terms of the grid point values of the variable. The technique is described fully by Patankar (1980). The finite element method developed primarily from structural engineering where it was used to predict stresses and strains within solid structures. It has now been applied to fluid mechanic situations.

These methods, in various combinations and formulations, are used by most of the CFD codes. The solution method is usually iterative, rather than direct, since the number of equations is often large and they may be strongly coupled. An initial guess is refined by successive iterations until some convergence criterion is reached, when the solution is sufficiently close to the correct solution of the algebraic equations.

2.12 Description of a Typical CFD Package

The first CFD packages to emerge on the market were developed in universities and were written in Fortran 77. They concentrated primarily on solving the fundamental

equations of fluid flow without placing much emphasis on the ease of use or presentation of results. By today's standards they were deemed to be user-unfriendly. However, once the idea was taken from the university environment and launched as a commercially attractive venture the emphasis inevitably had to change. Most CFD packages are now directed towards the engineer who has an understanding of fluid flow but can use the package relatively easily without any prior CFD knowledge. Graphical presentation has also advanced so that complex geometries can be viewed easily from all directions and useful hard copies obtained. The graphical capabilities may be limited by the types of specific computer hardware used but there have been even greater advances in this area, which has helped to make the CFD revolution possible.

The majority of CFD packages are built around three core program parts. These are the pre- and post-processor and the main computational code. A brief description of each follows.

2.12.1 Pre-Processor

The pre-processor is used for setting up the problem to be solved. The major task at the pre-processing stage is that of constructing a suitable grid over the region of interest, or domain. When complex geometries are involved this may take a large proportion of the total simulation time - up to 75% of the man-hours spent on the project (Foumeny, 1996).

The equations to be solved and hence the variables calculated are specified. If, for example, the problem involves heat transfer, temperature or enthalpy will be calculated. Boundary conditions and, in time dependent problems, initial conditions must be specified. This is done by grouping together all the grid cells over which a certain condition, e.g. inlet, wall, applies. Physical properties pertaining to the problem are also supplied.

Additional settings for control of the solution procedure may also be made. For example, relaxation factors may be applied to certain variables. This alters the speed with which the variable changes from one iteration to the next and can make an important contribution to the ultimate success of the simulation.

Meshes

The early CFD packages used fairly simple Cartesian and cylindrical polar co-ordinates, Fig 2-3 (a) and (b). Meshing facilities are now becoming very much more advanced and therefore codes can accommodate the complex geometries which are often encountered. The problem of mesh generation is a separate area of research and is aimed at developing methods which can create suitable grids with the minimum of user input and as quickly as possible.

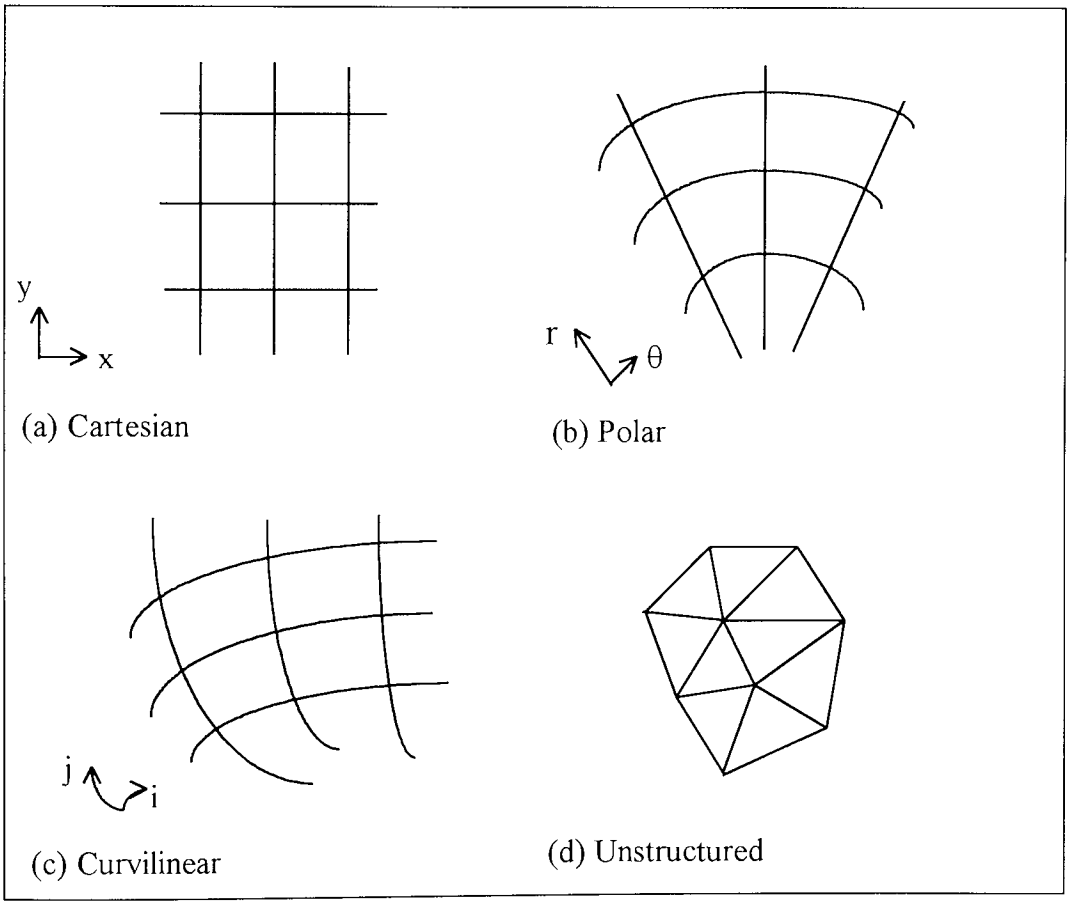

Figure 2-3 Various mesh types.

The mesh may be either structured, having a well defined topology which is 'stretched' from a Cartesian grid, Fig 2-3 (a) - (c), or unstructured, the points filling the space but not connected in such a regular manner, Fig 2-3 (d).

In earlier CFD times it was probably true to say that finite difference or volume programs required regular structured meshes whereas finite element codes used irregular unstructured meshes. The advantage of the regular mesh was that the solver ran faster since data was found more easily but this was weighed against the disadvantage that complex geometries could not be modelled as well as with an unstructured grid and therefore finite element program. However with the development of new methods this is no longer true. Finite volume methods can now be implemented on unstructured meshes with arbitrary cell shape (Patel, 1994), hence allowing complex geometry to be modelled as accurately as with a finite element code.

Finite volume codes using structured grids can use several methods to mesh complex shapes. Body fitted co-ordinates, Fig 2-3 (c), where a basic Cartesian grid is 'stretched' to fit the required shape and mapped on to local grid directions are often used. However this may still be limited by the solver's preference for rectangular or cuboid cells.

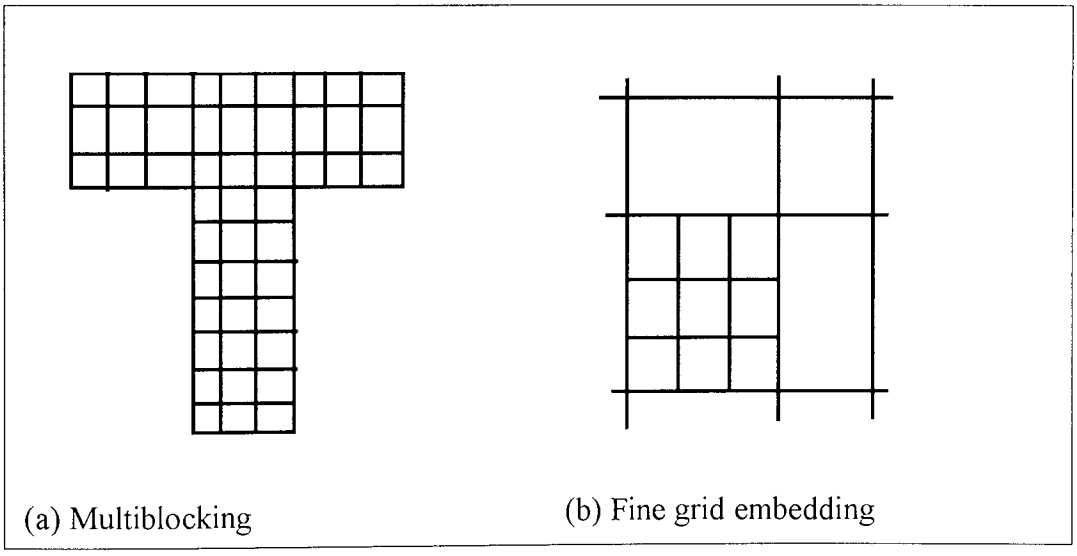

Figure 2-4 Multiblock and fine grid embedded meshes.

Another type of grid that may be encountered is the multiblock type, Fig 2-4 (a). This is an attempt to combine the flexibility of modelling complex geometries with the speed advantage of using regular grids. The overall grid is made up by patching together several blocks of grid enabling the domain to be specified without having to define large areas as solid and therefore wasting computer time and memory. Fine grid embedding, Fig 2-4 (b), enables areas of particular interest to be studied in greater detail without requiring large numbers of grid points throughout the whole domain. Previously finite element codes had the advantage in this respect.

Commercial Mesh Generation Software

These packages have been around for some time and are mainly directed at finite element structural analysis. As such they are very general and therefore when using one it is necessary to keep in mind the CFD solver program. However the huge benefits that can be achieved with their use are now being realised. Many mesh generator and CFD packages now have suitable interfaces so that easy or invisible translation of files is possible. In fact the new FLUENT pre-processor has been developed in collaboration with ICEM, a company specialising in the use of CAD and grid generation technology (CFD News, May 1994). Such developments can only be of benefit to the CFD user.

2.12.2 User Defined Subroutines

In addition to the main parts of the CFD package most include a user defined subroutine facility. This enables the user to define non-standard information, for example non-Newtonian models. Some packages may even allow users to add numerical features such as their own solution methods. This means that the program maintains a large degree of flexibility. The required coding is written in a Fortran subroutine which is then linked to the solver program. This is not usually an easy process and to do this the user must have considerable knowledge of the way in which the solver has been written.

2.12.3 Main Analysis Program or Solver

The main analysis program, or the solver, solves the algebraic equations representing the fundamental equations for the conservation of mass, momentum, energy and chemical species for each grid point in the domain using one of a number of mathematical techniques. Since the solution procedure is an iterative one an initial guess is supplied. The equations are then solved to find a better approximation to the solution and iterations continue until the residuals, the measure of error, are sufficiently small. Residuals are used to check if the solution is converging (residuals decreasing) or diverging (residuals increasing).

The solver is controlled through inputs to the pre-processor and information on the number of iterations, limits of residuals, data to be stored etc. can be specified.

The general types of flow phenomena that can be solved by most of the commercially available CFD packages include the following:

Steady or transient
Laminar or turbulent
Newtonian or non-Newtonian
Compressible or incompressible
Heat transfer
Mass transfer and chemical reaction
Buoyancy and rotation

2.12.4 Post-Processor

Often, due to the vast amount of data generated by the solver, the only way to make sense of it is to view the results graphically. This is done using the post-processor. It is also possible to view the results in other post-processing packages. The boundary or mesh can be viewed from any direction and vector or contour plots of velocity and scalar quantities viewed. These are usually in colour but this depends on the computer hardware.

2.13 Capabilities and Limitations

Although CFD can give insight into an ever increasing range of situations involving fluid flow the user must be aware of its limitations. The simulation results depend on the model supplied by the user and can therefore only be as accurate as that model. The assumptions of any models implemented through the choices made using the pre-processor must be understood by the user.

An example of this is the simulation of turbulent flows. Turbulence adds a randomness to the flow that is so complex it cannot yet be described by a set of equations. Assumptions must be made in an attempt to model the flow using a relatively simple set of equations to account for the different flow patterns produced in turbulent flow regimes compared to laminar ones. The κ–ε model of Launder and Spalding (1974) is the most widely used turbulence model but its limits of validity may be seriously exceeded in some situations. Various other models such as the Reynolds Stress Model (RSM) and the Renormalisation Group Theory (RNG) (Versteeg and Malalasekara, 1995) which use more equations to model the extra turbulence terms have been developed and may be more appropriate in some situations. It is worthy of note that in benchmark tests carried out using several commercial CFD packages, test cases for turbulent simulations showed a much greater deviation from experimental results than in the laminar test cases (Freitas, 1995). In addition it was demonstrated just how different the results can be using various turbulence models. This is clearly an area in need of further research to expand the theoretical knowledge of the phenomenon.

As already noted the mesh is very important and generating a mesh having the optimum number of points is a trial and error process. Obviously complex phenomena cannot be simulated accurately using a coarse mesh but conversely using an extremely fine grid can be wasteful of computer time (and could result in rounding errors due to loss of precision).

Code robustness is another area identified as needing further research by Douglass and Ramshaw (1994). Their description of codes that are often "touchy and temperamental" and can only be used successfully by experienced staff is probably a feeling shared by many CFD users. Such problems can be due to the strong coupling of the equations. Newer, more stable methods of solution are usually more complicated which may lead to a reluctance on the part of CFD developers to implement them. Douglass and Ramshaw (1994) also feel that the modelling of complex fluids within complex domains has yet to reach its full potential, for example flows involving not only turbulence but also compressibility, multiple phases and chemical reactions.

2.14 Choice of Package

It would be impossible to say which package is the best one to choose and in many instances one of several may be perfectly adequate for the job. The potential user needs to think carefully about the requirements needed for the modelling to be pursued, and then match these up with the advertised capabilities of the various packages. Points to consider might include which turbulence models have been shown to be most appropriate for the given flow simulation. It is also important to consider the geometry of the problem and ensure that suitable meshing facilities will be available.

Appendix 1 gives a table of some of the CFD vendors and their products which were available in June 1994. Inevitably many changes will have occurred since then and the capabilities of the packages will have developed considerably. Similar, less extensive tables have been compiled by Dombrowski, Foumeny and Riza (1993) and Bschorer and Schierholz (1993), who give particular emphasis to packages capable of modelling rheologically complex flows. Other useful sources of up to date information can be found on the World Wide Web.

User friendliness is another important feature of any CFD package and something a prospective user should consider. Obviously this is very subjective and will depend on

personal preferences. Some packages have a text based interface, whereas others have a Graphical User Interface (GUI) to assist the process of data entry to the pre-processor. This is often easier for the new user to understand but experienced users often find text input faster. Similar thought should be given to the level of user support a company is willing to offer since it is likely that the user will at some time require assistance, especially in using the more advanced facilities of the package.

2.15 CFD in the Chemical Industry

It has been seen in this review of CFD and the codes that their development, coupled with the major advances in computing technology over the same period, has made the technique more accessible to the engineer. CFD has been used for many years as a tool for engineering design where fluid flow characteristics are of interest. It has been widely used in both the aero and automotive industries. However, it would seem, due to the lack of available literature that CFD has not been so widely used in the chemical industry. It has also been noted recently by Bode (1994) that the potential of CFD has been slow to be realised in chemical engineering. It would appear that one of the main reasons for this is the problem of dealing with the complex geometries that are often encountered; however this can now often be successfully overcome with the use of CAD to generate the mesh. Another problem that may hinder the use of CFD in some instances arises from the difficulties involved in modelling of turbulence and other phenomena, such as two phase flow. Until the validity of models of such complex physical phenomena has been established, there will still be a constraint to verify results experimentally. For example, different turbulence models may be more applicable to certain situations and it may not be known a priori which one should be used. This means that results from CFD models cannot be used with confidence until some experimental verification has been carried out, which may not always be feasible. The κ–ε turbulence model is well developed and generally the most accessible for use but was not developed specifically for the many flow problems to which is has been applied. Other models are being developed for different applications but so far are not as widely accessible.

No literature on the use of CFD to model flows within the channels of structured distillation packings has been found, although Sulzer do claim that their latest packing, Optiflow has been optimised with the aid of CFD (Sulzer Chemtech Ltd, 1994). The method has been adopted by Adderly et al. (1995) to model flows within the channels of compact heat exchangers. They use the finite element code FIDAP to investigate the effects of Reynolds number and the corrugation angle of the channel on the 'thermal effectiveness' with a view to obtaining reliable results for the performance of various geometries.

Another field where CFD is finding some use is in mixing; from relatively simple simulations of pipeline tee mixers to more complex simulations of the flow in mixing vessels. Both Bode (1994) and Monclova and Forney (1995) show that results of mixing quality within a pipeline tee from numerical simulations fall within the range of available experimental results. A far more complex mixing situation that has been modelled is the flow of one or more fluid phases in a mixing vessel with baffles and impellers. Bakker and van den Akker (1994) use a combination of CFD (FLUENT) to calculate the kinetic energy dissipation rate, with micromixing models to predict the yield of a reactor involving chemical reaction. The impeller is modelled as a moving wall with empirical boundary conditions obtained from experimental results. A similar geometry is simulated using Flow3D by Fokema et al. (1994), who present results for different empirical boundary conditions at the impeller. Bode (1994), using STAR and a specially developed subroutine to allow the mesh to move as a function of time avoided the use of any experimentally based input.

Flow3D has also been used by Oakley (1994) to model spray dryers. Again it is stated that without better models for complex phenomena, turbulence in this particular case, CFD is limited in its use as an innovative design tool. He is restricted to the use of established designs of chamber so that various turbulence models can be assessed as to their suitability for the given geometry and design. In a similar way in which this work aims to move away from the empiricism used in predicting the performance of structured packing so Oakley wishes to devise an accurate CFD

method that could be used in place of the current empirical correlations used by vendors.

A somewhat different approach to the fundamental modelling of flow phenomena can be taken. Overall predictions can be simulated by combining the equations of motion with experimentally determined empirical expressions. Parsons (1991) uses PHOENICS to model the velocity distribution of gas above a shallow packed bed by incorporating the Ergun equation into the equations solved by the program.

2.16 Summary

The theory of CFD has been introduced briefly and some of the issues involved in the use of a typical package have also been discussed.

The technology of CFD is being used in an increasingly wide range of situations involving fluid flows and this includes the chemical process industries.

The CFD packing PHOENICS is chosen for this work to model the flows occurring within structured packings. It is a finite volume code built around the three core program parts. Structured meshes are used and these may be body-fitted. One of the main advantages of the package is the flexible user-defined subroutine section, which is standard rather than an added extra. The post-processor allows geometry to be viewed in three dimensions.

2.17 Chapter Summary

Three main topics have been covered in this literature review: the development and current state of structured packings, the models that have been presented to predict the performance of such packings, and finally CFD.

The sections on structured packing give background to what is aimed to be modelled and the methods so far adopted. The introduction to CFD shows the current capabilities and limitations of this rapidly developing technique. In chapter 4 these two topics will be combined in the presentation of a novel method of modelling structured packings using CFD.

3. PHOENICS - AN INTRODUCTION

It has been seen in the review of CFD packages that PHOENICS (CHAM, London, UK), standing for Parabolic Hyperbolic Or Elliptic Numerical Integration Code Series, was one of the early players on the commercial market, being first released well over a decade ago. During the intervening years many developments and improvements have been made to enhance the features available within the code and to improve the user-friendliness of the package. The package was chosen for this work as it is believed to have one of the most flexible user subroutine sections. It was installed on the university mainframe computer, a Sun computer running Solaris 2 and the departmental Silicon Graphics Indy workstation running IRIX 5.3. This chapter explains the method of usage of PHOENICS and also many of the terms used by its authors to describe its components.

3.1 The Structure and Basic Concepts of Phoenics

PHOENICS has the same basic structure as the majority of CFD packages and comprises three core parts; the pre-processor, solver, and post-processor. In PHOENICS these are known respectively as SATELLITE, EARTH, and PHOTON. In addition to PHOTON a graph plotting facility, AUTOPLOT is also provided. A subroutine called GROUND allows users to customise the code to their own requirements. Table 3-1 lists the main program parts of PHOENICS and the files that it generates. The way in which these are interconnected is illustrated in Fig 3-1.

PROGRAMS	Description
Satellite	Pre-processor, for set-up of problem to be solved
Earth	Equation solver
Photon	PHoenics OuTput OptioN, pictures of velocity vectors, contour plots
Autoplot	Graph plotting facility
Ground	Subroutine for users non-standard coding; interacts with Earth
FILES	
Q1	Containing problem specification, written in Phoenics Input Language (PIL)
Eardat	Produced by Satellite from Q1 file; used by Earth
xyz	Produced by Satellite; contains geometry information
Phi	Produced by Earth; contains results of simulation and used by Photon and Autoplot for viewing results
Result	Tabulated results of simulation to be read by user

Table 3-1 Description of Phoenics programs and files.

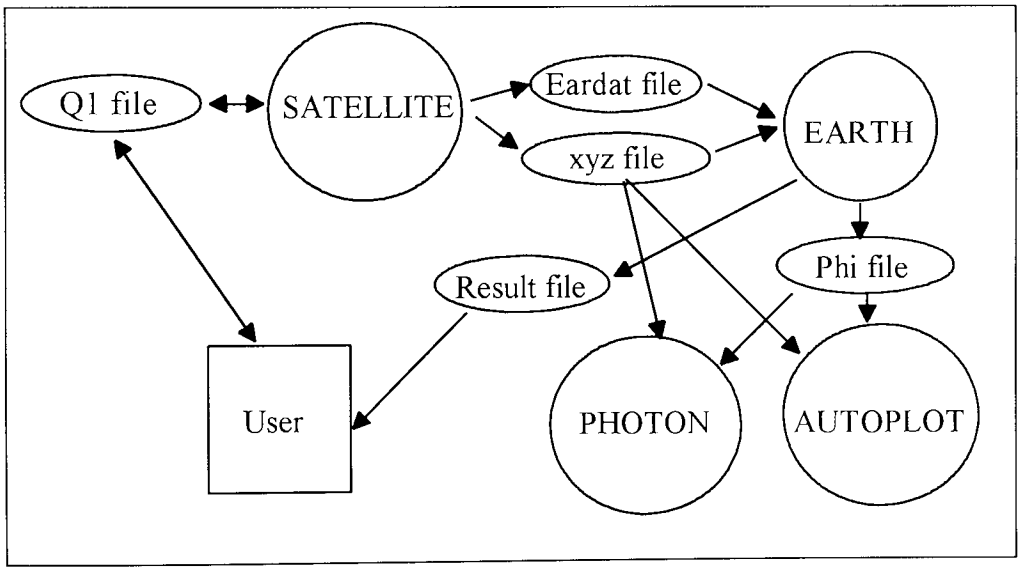

Figure 3-1 The structure of Phoenics and the files.

3.1.1 The Q1 File

The main user input file is called the Q1 file. It is divided into twenty four separate groups containing the Phoenics Input Language (PIL) commands which define the problem to be solved. Not all of these are needed in any particular case. The group

structure of the Q1 file with the headings of each section as defined by CHAM is as follows.

Group 1. Run Title
Group 2. Transience
Groups 3, 4, 5. Grid Information
Group 6. Body-Fitted Co-ordinates
Group 7. Variables: STOREd, SOLVEd, NAMEd
Group 8. Terms & Devices
Group 9. Properties
Group 10. Inter-Phase Transfer Processes
Group 11. Initialise Var/Porosity Fields
Group 12. Convection and Diffusion Adjustments
Group 13. Boundary & Special Sources
Group 14. Downstream Pressure For PARAB
Group 15. Terminate Sweeps
Group 16. Terminate Iterations
Group 17. Relaxation
Group 18. Limits
Group 19. EARTH Calls To GROUND Station
Group 20. Preliminary Printout
Group 21. Print-out of Variables
Group 22. Monitor Print-Out
Group 23. Field Print-Out & Plot Control
Group 24. Dumps For Restarts

This file can be created in two ways, either using a Menu system within Satellite or by typing the PIL commands directly into a file. The Menu system involves clicking on a series of buttons on the computer screen to generate the appropriate PIL, and is the easiest option for the new user. When greater familiarity with the package is gained, typing PIL directly becomes the quicker option.

Once the Q1 file is created by some means, the Satellite program is run. Satellite reads the PIL commands and generates the eardat file, a file that is read by EARTH. A geometry file, XYZ, is also generated for cases using body fitted co-ordinates (BFCs).

3.1.2 Result and Phi Files

The solver program, EARTH, reads the eardat and xyz files and produces two files at the end of the solution process, PHI and RESULT. The PHI file contains all the data

relating to the solution of the problem e.g. velocities at each grid point. The choice of output to the RESULT file is controlled by the user and it may contain values of any chosen variable. It can also contain details of the case run, the convergence reached and the mass and heat balance.

To view the results of the simulation the program PHOTON reads the PHI file and if necessary the XYZ file. Using PHOTON pictures of velocity vectors and contour plots of variables can be viewed and hard copies made if required.

3.1.3 Ground Subroutines

There are many options available within PHOENICS. An even greater degree of flexibility is introduced by the provision of the subroutine GROUND. This subroutine is arranged in groups in a similar fashion to the Q1 file and is called at certain points from within the program EARTH. Each user may implement their own coding (in FORTRAN 77) to introduce any special requirements and this is called when needed by EARTH. This subroutine is combined with EARTH to produce a new version specific to that problem, usually termed a private version of EARTH.

PHOENICS also has a range of other add-on modules which are specific GROUND subroutines to perform various tasks. For example, GENTRA is used for particle tracking.

3.1.4 Variables

The dependent variables that may be solved for are the three velocity components, U1, V1, W1, the pressure P1, enthalpy H1 or temperature TEM1, and any other auxiliary variable C1...C35 the user cares to solve for. The independent variables are the three spatial directions x, y and z and the time dimension, t.

3.1.5 Meshes

Meshes generated by PHOENICS can either be Cartesian, polar or body fitted. The mesh must be structured and in the case of body fitted grids must also be topologically Cartesian i.e. all cells must have four sides in 2-D or six faces in 3-D. In some cases the real problem has to be distorted to get a solution at all since severely non-orthogonal grids are likely to cause divergence rather than produce a converged solution.

PHOENICS version 2.1 onwards also has a multiblocking and fine grid embedding technique. Multiblocking allows separate pieces of grid to be joined together to fit into the desired shape and can eliminate the need to grid unwanted areas. Fine grid embedding allows different scales of grid to be used so that some areas can be studied in greater detail without needing large numbers of grid points throughout the whole domain. These two techniques were shown diagramatically in Figure 2-4.

A compass point notation is used for the mesh and cell. Figure 3-2 shows the naming convention on a typical Cartesian grid.

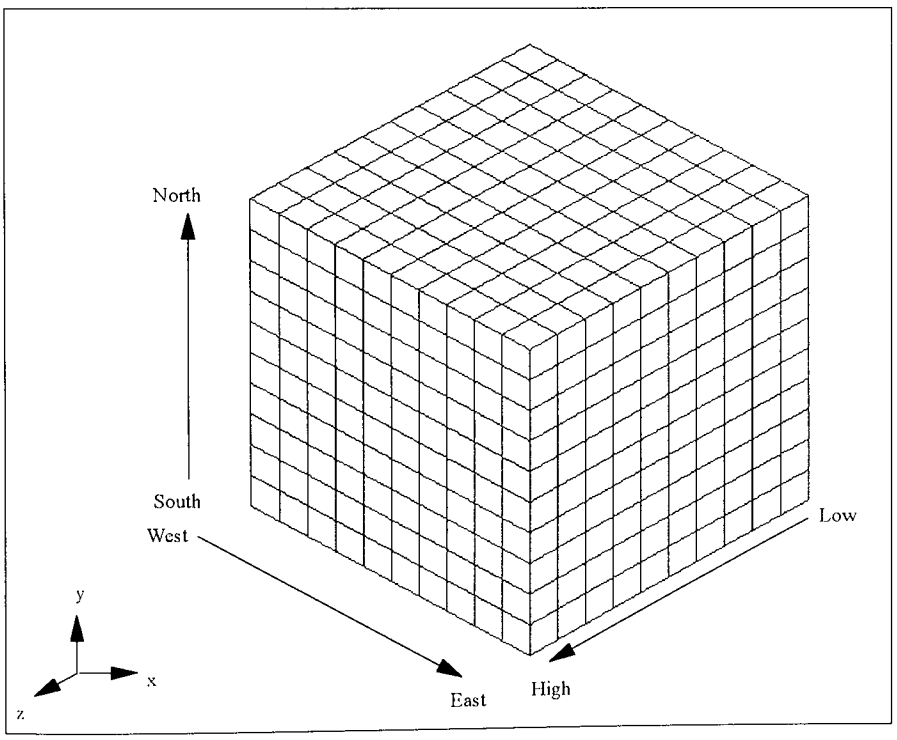

Figure 3-2 Cartesian mesh showing axes directions.

3.1.6 Cell Geometry and Nomenclature

Each cell in the grid follows a similar convention. A single cell with the nomenclature used is shown in Fig 3-3.

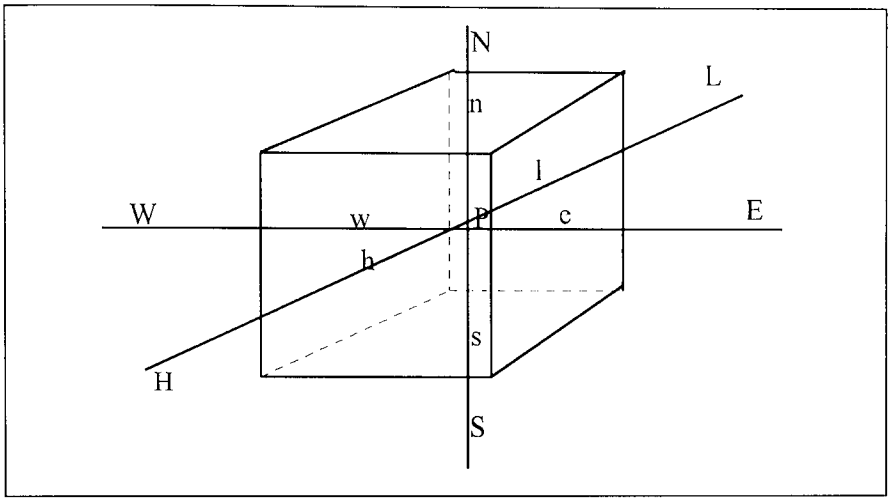

Figure 3-3 Cell nomenclature.

P = cell centre
N, S, E, W, L, H = neighbouring cell centres
n, s, e, w, l, h = cell face centres

3.1.7 Solver

The standard Phoenics solver uses a staggered grid in order to overcome the problem of 'wavy fields' which are physically unrealistic but which do obey continuity. This means that vector quantities are not located in the same positions as scalars. Figure 3-4 shows the position of the scalar, at point P, and the two velocities U1 and V1. Mathematically this means that the velocity is driven by two pressures, one on either side.

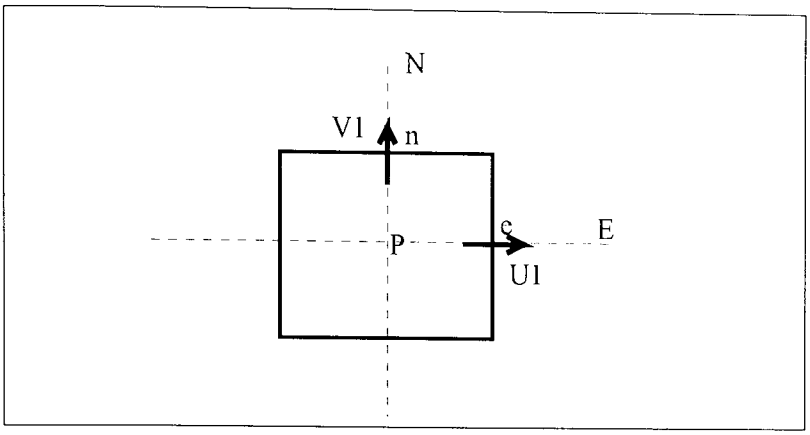

Figure 3-4 Location of scalar and vector quantities.

An alternative solver, known as CCM is now available. This was developed in conjunction with the multiblocking and fine grid embedding capabilities of which it is an essential part. It can also be used as an alternative solver for problems having only one domain. It employs a colocated grid where the cell-centred velocities, UC1, VC1, WC1 are solved for, and the face centred velocity components U1, V1, W1 are calculated. This has produced better results in some cases where the grid is non-orthogonal.

3.2 The Equations Applied

The basic balance equation that PHOENICS solves is:

Accumulation + Flow out of cell - Flow into cell = Source within cell

This can be written as follows, for the general variable, ϕ

$$\frac{\partial \rho \phi}{\partial t} + div\,(\rho u \phi - \Gamma_\phi grad \phi) = S_\phi$$

To formulate a particular equation the appropriate values must be given to ϕ, Γ_ϕ, and S_ϕ.

These are given below with the equation formed.

Momentum

$\phi = u, v, w$

$\Gamma_\phi = \rho(\nu_t + \nu_l)$ (laminar, turbulent viscosity)
$S_\phi = -gradP + gravity + friction + ...$

x direction:

$$\frac{\partial u}{\partial t} + u\frac{\partial u}{\partial x} + v\frac{\partial u}{\partial y} + w\frac{\partial u}{\partial z} = -\frac{1}{\rho}\frac{\partial P}{\partial x} + f_x$$

where f_x is some viscosity term, usually; $\frac{\mu}{\rho}\left(\frac{\partial^2 u}{\partial x^2} + \frac{\partial^2 u}{\partial y^2} + \frac{\partial^2 u}{\partial z^2}\right)$
and similarly for the y and z direction.

Continuity
$\phi = 1, \quad \Gamma_\phi = 0; \quad S_\phi = 0 + boundary\ sources$

$$\frac{\partial \rho}{\partial t} + \frac{\partial(\rho u)}{\partial x} + \frac{\partial(\rho v)}{\partial y} + \frac{\partial(\rho w)}{\partial z} = 0$$

For incompressible fluids this can be reduced to:

$$\frac{\partial u}{\partial x} + \frac{\partial v}{\partial y} + \frac{\partial w}{\partial z} = 0$$

Enthalpy
$\phi = T$
$\Gamma_\phi = \rho(\nu_t + \nu_l)$ ie. diffusion coefficient
$S_\phi = -\frac{DP}{Dt} + heat\ sources$

The equation for heat transfer within the fluid is obtained by applying the equation of motion in its most basic form to derive the mechanical energy balance for a fluid with viscous stresses. The first law of thermodynamics is then applied to a moving fluid. After many simplifications the equation can be written as follows:

$$\frac{\partial T}{\partial t} + u\frac{\partial T}{\partial x} + v\frac{\partial T}{\partial y} + w\frac{\partial T}{\partial z} = \frac{k}{\rho c_p}\left(\frac{\partial^2 T}{\partial x^2} + \frac{\partial^2 T}{\partial y^2} + \frac{\partial^2 T}{\partial z^2}\right)$$

The following assumptions are made in writing the energy equation as above:
The enthalpy, h, can be expressed in terms of temperature, T, by $dh = c_p dT$ and the specific heat is effectively constant.
The flow is steady.
Kinetic energy changes and shear work are neglected
The effects of potential energy are ignored.

The differential equations are valid for a particular instant in time, and are therefore the equations that are solved when laminar flow is being considered. If however the case involves turbulent flow then time-averaged equations are solved, and it is presumed that the length of time over which the average was made is long compared with the time scale of the turbulent motion.

3.3 Solution Method

PHOENICS solves finite volume equations which are obtained by integrating the differential equations over each control volume and assuming some profile for the variation of ϕ between grid points. Different variations of ϕ may be used, for example, linear piecewise profile. These are known generally as interpolation schemes. By default PHOENICS uses the fully implicit upwind scheme, due to its reliability. This means that in formulating the convection term the value of ϕ at an interface between two control volumes is equal to the value at the grid point on the upwind side of the interface. Implicit means that in time dependent problems, updated values of ϕ are not only related to known values prevailing at the old time step, but to unknown values at the new time step. This necessitates the solution of simultaneous equations.

The finite volume equations are written in the following form, where a's are the links with neighbouring cells.

$$a_p \phi_p = a_N \phi_N + a_S \phi_S + a_E \phi_E + a_W \phi_W + a_H \phi_H + a_L \phi_L + a_T \phi_T + Sources$$

and $a_p = a_N + a_S + a_E + a_W + a_H + a_L + a_T$

It can be seen that a highly non-linear set of equations have been written in a linear form, and standard mathematical techniques can then be used in their solution. The total number of equations will be large since for each dependent variable the number of equations is equal to the total number of cells in the domain. Since the above equations are linked in various ways they need to be solved simultaneously, and in

order to make the equation set soluble it is necessary to supply additional equations giving information about auxiliary variables, e.g. C1 (which may depend on other auxiliary variables, e.g. C2, C3, and dependent variables e.g. P1, U1), and boundary conditions.

The solution procedure is an iterative process involving an initial guess and subsequent refinement of the guess. During the iteration coefficients and sources are assumed to be temporarily constant so that the equation sets may be solved using linear equation solvers. The coefficients and sources are then updated at the next iteration from the latest values of the dependent variables and the linear equations reformed and the procedure repeated until the imbalance in the equations is small enough to be negligible. The solution is often said to be 'slab-wise'; a slab being an x-y array of cells having the same value of z. Fluid properties, finite volume equation coefficients and velocities are always calculated slab by slab and several iterations over a single slab may be performed before the next slab is considered. The complete domain is covered by what is termed a 'sweep' - a set of slabwise operations performed from low z slab to high z slab. In order to achieve the convergence criteria many sweeps must usually be made.

Another solution technique that can be employed for any variable except velocities is the 'whole field' procedure. This requires more computer storage but reduces the number of sweeps that need to be made. Pressure is often solved in this manner. Patankar (1980) gives a full explanation of the solution method. When using the CCM solver everything is solved by the whole field method. This can lead to convergence problems since values of all variables may be changing quickly.

3.4 Boundary Conditions as Sources

In PHOENICS all boundary conditions are inserted as linearised sources for the cells adjacent to the boundary. Since source terms are inserted at cell centres, rather than cell walls, boundary conditions are not strictly inserted at boundaries. However, the

difference in location can be made negligible by making cells in the region of the boundary small. The linear source term is of the form:

$$S_{BC} = a_{BC} (\phi_{BC} - \phi_p)$$

or Source = Coefficient $(Value - \phi_p)$

The source term is added to the finite volume equation (see section 3.3 above) and the equation rearranged to arrive at an equation for the variable phi:

$$\phi_p(a_p + a_{BC}) = a_N\phi_N + a_S\phi_S + ... + a_T\phi_T + a_{BC}\phi_{BC}$$

$$\phi_p = \frac{(\Sigma a_i\phi_i + a_{BC}\phi_{BC})}{(a_p + a_{BC})}$$

The coefficient (Coeff) and value (Val) are entered in the PIL command COVAL(patchname, variable, Coeff, Val), to achieve the desired boundary condition.

3.4.1 Fixed Value Boundary Conditions

In this case it is wished to set the value of $\phi_p = \phi_{BC}$. Therefore the Coeff (or a_{BC}) is set to a large number so that it becomes the dominant term in the denominator. This is done by using the PIL variable FIXVAL which has a suitably large value. This has the effect of making the first term of the equation $((\Sigma a_i \phi_i + a_{BC} \phi_{BC})/(a_p + a_{BC}))$ small and hence:

$$\phi_p \sim \phi_{BC}.$$

3.4.2 Fixed Flux Boundary Conditions

To achieve a fixed flux boundary condition the Coeff (or a_{BC}) is set to a small number and $a_{BC} \times \phi_{BC}$ is set to the desired flux. Therefore:

$$\phi_p = \frac{\Sigma a_i \phi_i}{a_p} + \frac{a_{BC} \phi_{BC}}{a_p}$$

This is achieved by setting the coefficient to FIXFLU which has a small value, and the value to the desired flux.

3.4.3 Mass Flow and Pressure Boundary Conditions

In order to solve the differential equations boundary conditions must also be supplied giving information on where and how much flow enters or leaves the domain for fluid flow problems. The boundaries of the domain are assumed to be non-porous walls and no flow through them is allowed.

Pressure is the "driving force" for mass flow and therefore mass boundary conditions are introduced as linearised source terms in the continuity equation.

i.e. $$\frac{\partial \rho}{\partial t} + \frac{\partial(\rho u)}{\partial x} + \frac{\partial(\rho v)}{\partial y} + \frac{\partial(\rho w)}{\partial z} = \Sigma (S_{BC})_{all\ patches}$$

The source term is written in a similar way as before,

$$S_{BC} = T C_m (V_m - P_p)$$

where C_m and V_m are the coefficient and value for pressure and T is a multiplier to get the correct units e.g. area, volume. In this case Coeff and Val are set to give either a fixed mass or fixed pressure boundary condition.

Fixed Mass Boundary Conditions

This is achieved by setting the value to the desired mass flux, (kg/m^2s) and coefficient to FIXFLU, which has a numerical value of 2e-10. The mass flux is fixed irrespective of the internal cell pressure.

Fixed Pressure Boundary Conditions

Fixed pressure boundary conditions are often used at the domain outlet. Setting the coefficient to a large number (1e3 is usually satisfactory) the internal pressure of cells adjoining the outlet become close to the external pressure, which is the value given to Value.

3.5 Turbulence Models

Turbulent flow, which occurs at high values of Reynolds number is often encountered in problems of engineering interest. The flow is characterised by intermittent and random small scale motions in the fluid. Generally, turbulent flow can be described by the Navier-Stokes equations and it is convenient to express the instantaneous velocity components as a sum of the main velocity and the random fluctuating turbulent velocity. The random velocity fluctuations transport momentum which changes the mean motion of the fluid in comparison to laminar flow and this effectively introduces some additional stresses into the equations of motion. These represent the transport of momentum due to turbulence and are known as Reynolds stresses. It is not possible to model turbulence by a direct numerical method since a vast number of grid points would be needed to represent the widely varied length and time scales of the eddy motion. Hence turbulence models define some equations to mathematically model these additional stresses. Many models have been proposed and different numbers of equations are used to model the stress terms. Some of the oldest and simplest models have used the concept of eddy viscosity and mixing length and use either one or no additional differential equations. Other widely used models solve two additional transport equations, for the turbulent kinetic energy and its rate of dissipation. Newer models solve more equations but are more costly on computer time.

The [illegible]odel, which is a two equation model, has been widely used and is the most [illegible] CFD codes. The model coded into PHOENICS is that proposed by [illegible]ling (1974).

3.5.1 The k–ε Turbulence Model in Phoenics

Additional PIL commands relate to the implementation of the model. The PHOENICS variables for k and ε respectively are KE and EP. The turbulence quantities for the standard k–ε are given below in the terms used by PHOENICS.

EL1 = GRND4; calculates the mixing length scale from $L = C_D \times \frac{KE^{1.5}}{EP}$

ENUT = GRND3; calculates the turbulent (or eddy) viscosity using the Prandtl-Kolmogorov formula, $ENUT = C_\mu \times EL1 \times KE^{0.5}$

PRT(EP) = 1.314; sets the effective Prandtl number (a constant in the modelling of EP).

The following lines set sources for the production and dissipation of KE and EP.

PATCH(KESOURCE, PHASEM, ixf, ixl, iyf, iyl, izf, izl, itf, itl)

COVAL(KESOURCE, KE , GRND4, GRND4)

COVAL(KESOURCE, EP , GRND4, GRND4)

In the region of walls, where the local Reynolds number becomes small the standard model, which assumes a high Re must be modified. This can be done by applying wall functions, which are used to bridge the laminar sublayer so that very fine grids in the region of the walls are not necessary. This assumes that the first grid node lies within the fully turbulent region and empirical formulae are used to relate the wall shear stress to the dependent variables at the near wall node. Three wall functions are available:

1) Blasius Power Law (GRND1)
2) Logarithmic equilibrium wall function (GRND2)
3) Generalised non-equilibrium wall function (GRND3)

Specifying l[illegible]v wall functions is done by inserting the following lines of PIL,

'AL(' [illegible]e, KE , GRND2, GRND2)

AI [illegible]ne, EP , GRND2, GRND2)

3.5.2 Application of k–ε Model in Triangular Ducts

The k–ε model has been widely used even in situations in which the assumptions on which the model are based may not hold. Many structured packings have a basic triangular shaped channel and Chapters 4 and 5 describe work based on such a shape. Therefore it is important to firstly assess the accuracy of the model in triangular ducts. Usui et al. (1983) compute the fully developed turbulent flow at Re = 10,000 in a duct having an apex angle of 11.4^0. A similar geometry was set up in PHOENICS and the κ–ε model used; the Q1 file is shown in Appendix 3. A long duct was used (approximately 150 equivalent diameters) to ensure that the flow was fully developed. This was verified by viewing velocity profiles in the AUTOPLOT facility of PHOENICS. These remained constant as the plotting plane was increased. Figure 3-5 shows the distribution of longitudinal velocity at the centre of the duct. The best results of Usui et al. (1983) and experimental results of Tung and Irvine are shown for comparison. PHOENICS predicts well the experimental results.

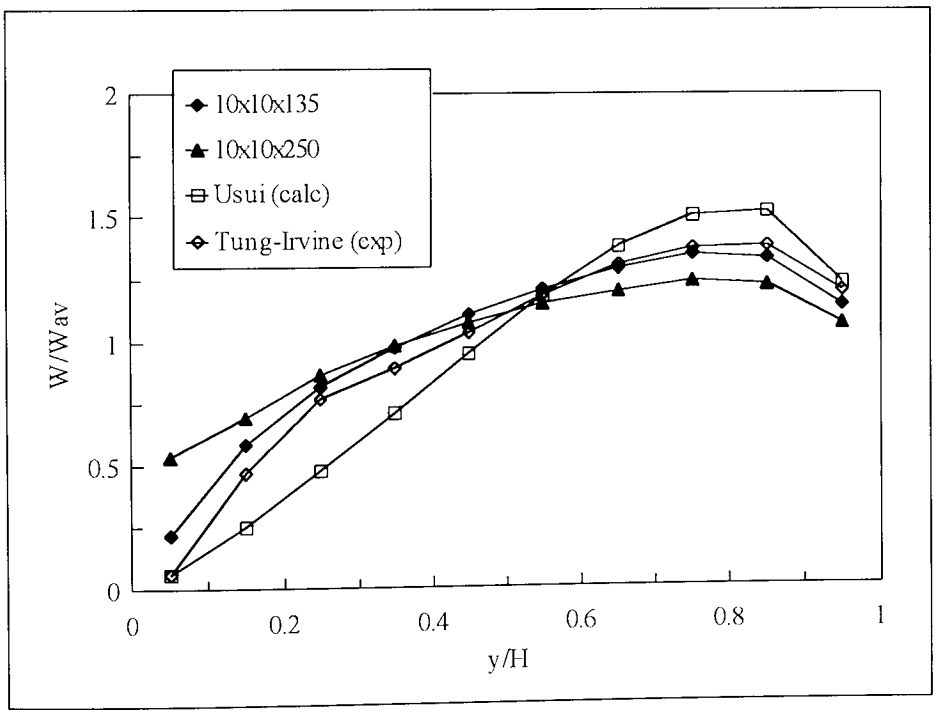

Figure 3-5 Distribution of longitudinal velocity.

Usui et al. also report a secondary flow, which in the narrow apex case consisted of two counter-rotating flows in each symmetrical half of the duct. Such a pattern was not predicted by the PHOENICS simulation. However, Usui et al. also state that

several other workers do not observe the secondary flow when using both experimental and computational techniques. Figure 3-6 shows the secondary flow pattern that was produced by PHOENICS.

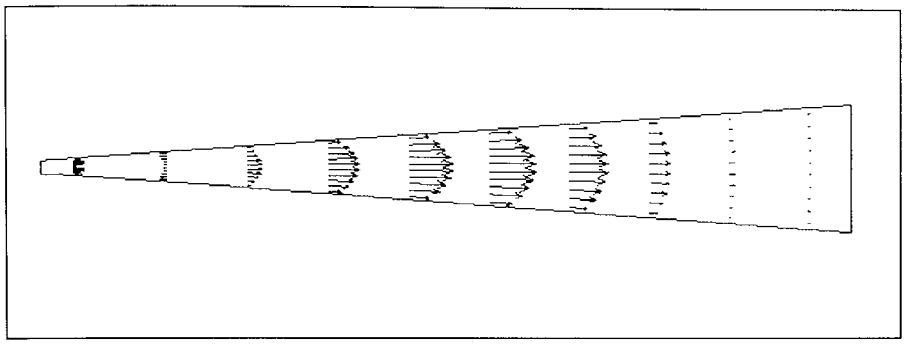

Figure 3-6 Secondary flow field at $\theta = 11.4^0$ and Re = 10000.

3.6 Summary

The basic concepts of the CFD code PHOENICS have been introduced such that chapters 4 and 5 can be understood without the need for lengthy explanations.

4. CFD MODEL

Structured packing has a very regular repeating pattern, and this property has been used as the basis of the CFD model. The modelling work has concentrated on the intersections (or junctions) between adjacent sheets of packing, as a block of packing is simply composed of a large number of similar junctions. The method used is to model a single junction and simulate the flow within it. This model is then replicated to model an entire sheet of packing. Each junction model has inputs derived from the outputs of previous junctions in the direction of gas flow. A set of flow simulations of junctions simulate a section of packing. Modelling of the entire block in one go is not possible since the grid would require a large number of nodes, and although this is possible to grid, it becomes very irregular in the PHOENICS mesh generator and convergence can not then be attained. In this chapter the CFD modelling process is explained using the Q1 data file developed for this model.

4.1 Model Geometry and Specifications

The dimensions for the model, which considered flow of the vapour phase only, were taken from Tianjin Mellapak 350 m^2/m^3. This packing is very similar to the Sulzer Mellapak packing and is manufactured at the Tianjin Packing Factory in PR of China. A sheet of the packing is pictured in Figure 4-1. It has the standard geometry which was shown in Figure 2-1 and the channels are inclined at 45^0 to the horizontal. The outline of the geometry used in the model is shown in Figure 4-2. The arrows indicate the direction of vapour flow up the column. The positions and names of the inlet, outlet and wall boundaries are indicated. It will be noted that the apexes of the triangular channels are squared off. This was necessary due to the requirement of the EARTH program to have a topologically Cartesian grid, i.e. in three dimensions all cells must have six faces. Meshes for two different junctions were also used, corresponding to channels inclined at 30^0 and 60^0 to the horizontal. The flow conditions and fluid properties were taken from typical values obtained experimentally from the test facility described by Higginbotham (1993), who recorded the vapour

flow as being in the turbulent regime at all vapour flowrates. The Reynolds number, based on an equivalent diameter of the triangular channel ranged from approximately 4000, at low flows, to 10000 at high vapour flowrates. Three inlet velocities, of 3.6m/s, 2.5m/s and 1m/s, were used to model a range of flowrates. The kinematic viscosity and density, averaged from properties recorded at the top and bottom of the column, were taken as 2.76e-06m^2/s and 3.4kg/m^3 respectively.

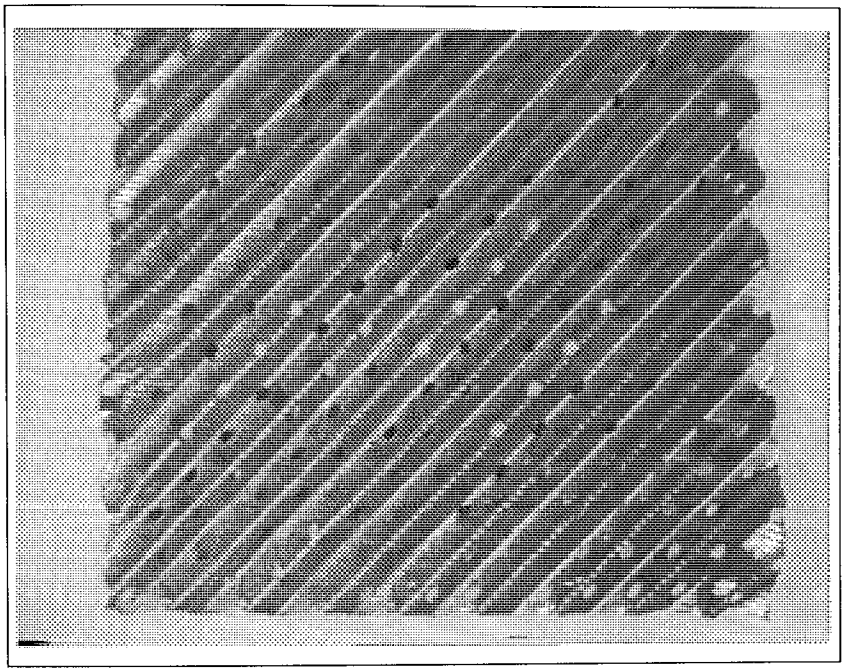

Figure 4-1 Tianjin Mellapak Structured packing.

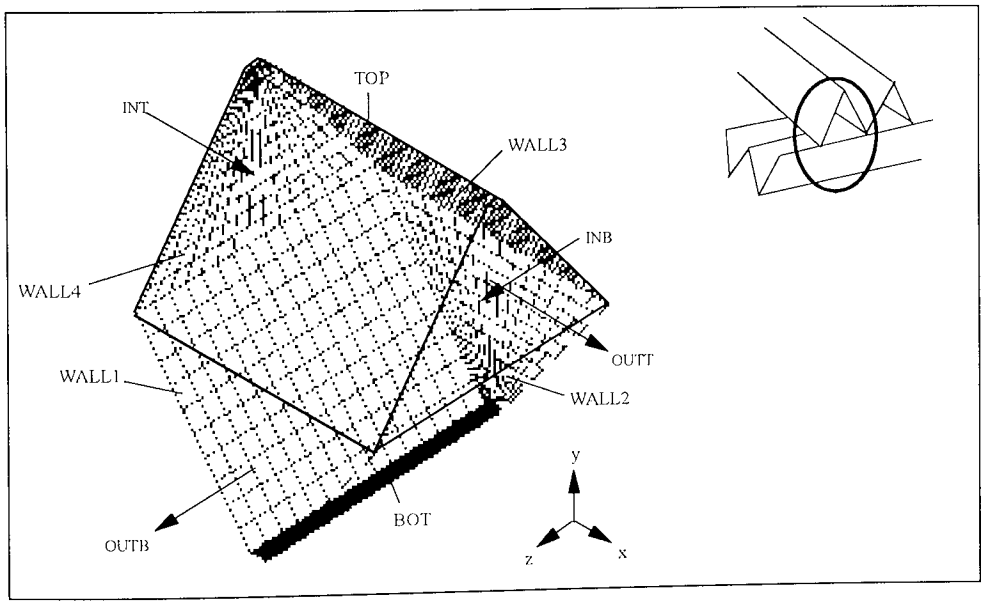

Figure 4-2 Geometry outline showing inlet, outlet and wall boundary conditions.

A Q1 file for a typical case, generated through the SATELLITE menu system is shown in Appendix 4. The particular case shown uses the k–ε model of turbulence and flat velocity profiles are specified as the inlet boundary condition. A constant pressure boundary condition is used at the outlet. Wall functions are specified at each wall to provide near wall boundary conditions by using empirical formulae to bridge the viscous sublayer.

4.2 The Model Q1 File

This section describes how the model was developed in terms of a Q1 file and relates to the file given in Appendix 4.

Groups 1-6

The first groups of the Q1 file set the run title and define the grid to be used. The size of the domain and the total number of cells are defined via XULAST, YVLAST, ZWLAST and NX, NY, NZ respectively in groups 3, 4, 5. Group 6 defines the choice of a body fitted grid and contains the information on the co-ordinates used to construct the mesh, the lines joining which points and the number of cells required on each line. The mesh is then created by setting frames, matching these to the grid mesh and then copying the grid in the appropriate direction to give the 3-D mesh. At this stage the boundaries of the mesh will be defined as regions to which boundary conditions can later be applied.

Groups 7-9

In these groups the variables to be solved and stored are specified along with any additional information on the solution procedure. The physical properties of the fluid and parameters relating to the turbulence model are set in group 9.

Group 13

In this group the boundary conditions are set. When using a body fitted grid, the patch, or area, over which a boundary condition will apply is set in terms of regions; these will have been created by the grid generation process and can be individually identified by labels.

Inlets are either set using user supplied values over the entire face, or values of velocity components are derived from output from a previous calculation. PHOENICS supplies a subroutine called GXBFC for setting a constant velocity profile over a face of a body fitted grid. This is called when the name given to the patch over which the boundary condition applies starts with the letters BFC. This subroutine has been used to set the flat velocity profiles assumed in the model at the inlets to the packed section.

The outlet boundary conditions are set using a constant value for pressure. This is achieved by setting the coefficient for the variable P1 to a high value; a value of 1000 is often suitable and has been used in this case. This type of boundary condition has been described in section 3.4.3.

The boundary conditions at the walls are assumed to be no slip and equilibrium log-law wall functions are specified. These are the default options inserted by the SATELLITE program when the k-ε turbulence model is chosen using the menu system. These are assumed to be appropriate in this case since in reality the boundary region of the gas will be in contact with a liquid film flowing countercurrently. This will retard the gas flow and lead to the development of a boundary layer in a similar way in which a stationary wall would.

Groups 15-24

The remaining groups of the Q1 file are concerned with the solution of the problem. The number of sweeps, the convergence criteria, the relaxation parameters and the

output to the result file are all controlled by inserting appropriate PIL commands in these groups. Fairly strong relaxation is applied in order to avoid possible divergence as the solution proceeds. The parameter KELIN is also used to overcome problems of divergence. The value of KELIN determines which linearization scheme is used for the source terms of KE and EP. Setting KELIN=1 obtained convergence for this problem. This option aims to anticipate the effects of walls, where production of turbulence is approximately equal to its rate of dissipation.

4.3 Junction Numbering

In order to apply PHOENICS to this particular problem a Q1 file was assembled to model one junction of the packing. The same model can describe geometrically any junction as they are all considered to be the same. The main difference is the inlet condition to each junction. The column is considered to be infinitely wide such that any effects of the column walls can be ignored. With this assumption the junctions modelled were numbered as shown in Figure 4-3. The first number refers to the channel in the z-direction and the second to the channel in the x-direction and relates to the number of cross overs through which the fluid has passed. Each junction with the same number is represented by the same model and calculation.

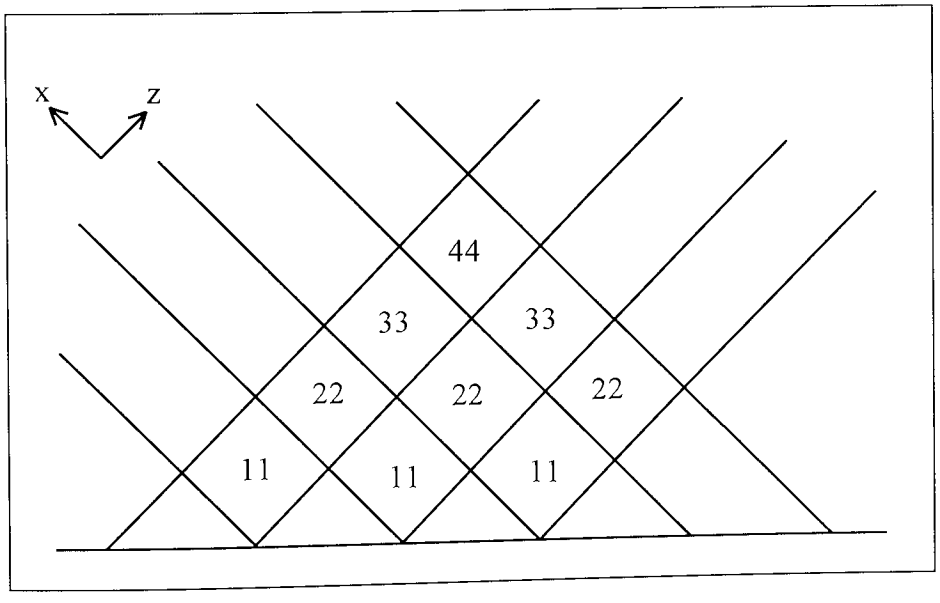

Figure 4-3 Junction Numbering

The present model takes no account of the bottom edge of the packing element where the vapour changes direction from vertical, or some other angle, to the direction of the channel flow. It is assumed that the uniform inlet flow is normal to the inlet. Tianjin Mellapak 350m^2/m^3 in 100mm blocks has approximately nine junctions, i.e. up to junction 99, before the vapour changes direction upon entering the next block of packing. The more usual block height is 200mm so vapour will pass through twice as many channel intersections before being redirected when it enters the next packing block.

4.4 Ground Coding

To build up a sheet of packing from a single junction calculation it was necessary to be able to store velocity data from junction outlets for one run and then to read this data back in as the inlet boundary condition for subsequent simulations. Figure 4-4 explains this diagramatically, using a square junction for ease of explanation.

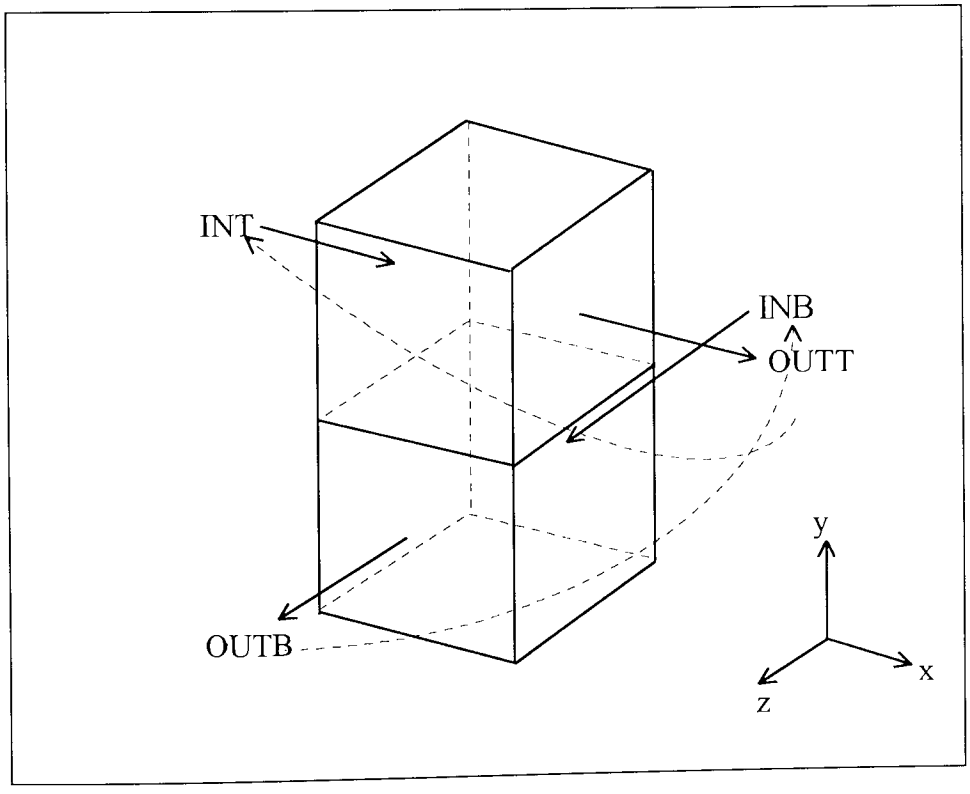

Figure 4-4 Ground coding concept.

The process was started by using a flat velocity profile as the inlet boundary condition for junction 11. In subsequent runs a user-defined boundary condition was specified at the inlet such that GROUND would be called to supply the appropriate data. These calculations must be done in sequence i.e. 11, 22, 33 etc.. In PHOENICS the real numbers used in calculations are stored in a single real-value array known as the F-array. Data in the array are stored in an orderly arrangement so that the location-index, i.e. position within the array, of a particular variable at a particular cell can easily be determined. This provides a means of obtaining data for output or placing data on input.

The easiest way of accessing data within the F-array is by use of the L0F(LB) function subroutine. L0F is termed the "zero F-location index" and is the location just before the data positions of interest. The argument of the L0F function can be of various forms. The argument used here is ANYZ(INDVAR, IZZ), which yields the L0F of the dependent variable specified and at the slab where IZ equals IZZ. An indicial expression is then used to count from the starting location to the position in the array for the cell in question. With this expression in a DO loop a range of locations can be accessed.

In this way data relating to the outlets can be retrieved from the array, stored in user-defined arrays and then set as the value of the incoming flow.

Various program sections were developed to facilitate the reading and writing of data for various combinations of dependent variables. A brief description of the sections of GROUND used follows and relevant extracts, commented with explanations, can be found in Appendix 5.

i) Group 19, Section 8, End of Time Step

Data at outlets is retrieved from the F-array and written to files.

ii) Group 19, Section 1, Start of Time Step

Data is read from files into user-defined arrays.

iii) Group 13, Section 12, Value=GRND

For the inlet patches the values of each variable specified are given by inlet data from a user-defined array which is put into the F-array.

Mass flowrate is calculated by one of two methods:

a) Mass flow = Velocity * Density

b) Mass flow = P1 * Coeff

where P1 is the value of pressure from the outlet of the previous junction.

Using the first method the mass flowrate at an inlet is calculated from the product of the velocity vector and the fluid density. This is explained in the PHOENICS Encyclopedia and forms the basis of the PHOENICS subroutine called GXBFC. Using the second method the mass flowrate is calculated from the product of P1, stored from the outlet of the previous calculation, and the coefficient used for the variable P1. To model a section of packing from calculations on one junction model it was necessary to convey the output values from previous calculations to the input values of the next one. The mass flowrate at an outlet is calculated from the in-cell value of P1 and the coefficient used for P1. Storing the outlet data of P1, in the same way as was done for the velocity components and all other variables, and using this to calculate the inlet mass flowrate into the next junction gave an exact mass balance on transferring from one junction to the next. In some instances, when the outlet boundary was parallel to the main direction of flow, the mass flowrate obtained from the first method did not equal that from the second method. Therefore the second method of using the P1 data to calculate the inlet mass flowrate was adopted since it was found to give correct answers in all cases encountered during this work.

Coding in Group 19 of GROUND was written such that a series of junctions could be run successively without any input from the user. Files containing the outlet data were named uniquely by sending character strings from Q1 to GROUND to distinguish the particular junction being simulated. Separate PHI files were saved by use of the NSAVE command to rename the PHI file. An extended Q1 file was made by appending individual junction Q1s one after the other. The IRUNN and RUN(1,N) PIL commands were then used to detail the runs to be carried out.

4.5 Consistency of Results

4.5.1 Introduction

It is necessary to carry out various consistency checks in order to assess how much confidence can be placed on the results of a CFD simulation. This section deals with the issues that were investigated in checking the consistency of the results. The solution should be independent of the number of grid points that form the mesh and the numerical method by which the solution is obtained. The computational code should also be internally consistent such that the same result is predicted every time a given problem is run.

Two inconsistencies were discovered from preliminary runs. Firstly it was noticed that the results did not show the same symmetry as possessed by the problem. Secondly, different results were predicted by altering the orientation of the mesh with respect to the axes. Two alternative solution methods are available in PHOENICS and these have both been used in resolving these inconsistencies. Comparisons between the results from the two methods are discussed to highlight the similarities and differences and to give credence to results that follow.

4.5.2 Grid Independence

It is important that the solution to any problem solved by CFD is independent of the number of grid points used to create the mesh. Figure 4-2 shows the outline of the mesh used to model the junction. The size of the mesh is 15x20x15 cells in the xyz directions respectively. For a laminar case of junction 11 the grid size was doubled to 30x40x30 cells in order to assess the effects of grid size on the solution. As no significant difference in the results was seen, it was felt that the slight increase in detail, shown on vector plots, did not merit the greatly increased time required for each simulation. Hence the smaller number of grid points was used for all following work. Also, since the emphasis of the work being carried out was comparative the

importance of ensuring that the solution was grid independent was reduced since absolute values were not needed.

4.5.3 Solver Independence

It is reasonable to expect that in most circumstances the results of a simulation should possess the same symmetry as the model. Results from the simulations using the junction shown in Figure 4-2 with an inlet flowrate of 3.6m/s and using the k-ε model showed that the mass balance was non-symmetrical. Although equal mass flowrates entered both inlets of the first junction the outlets were not identical and after the first eight junctions 60% of the total mass flow was through the bottom (z direction) channel and only 40% through the top (x direction) channel. This may be due to the way in which the PHOENICS staggered grid algorithm stores variables at certain sides of cells (N, H, and E sides). This may give a bias when the residual errors are calculated, which accumulated on moving through the series of junctions. A possible solution may have been to alter the sweep direction but this is not an option in PHOENICS. It may have been possible to achieve the same effect by rotating the grid through 90^0 every so many sweeps using coding in GROUND. This was not done.

It would also be expected that the results predicted should be the same regardless of the orientation of the model grid with respect to the xyz co-ordinate axes. Investigations showed that the results predicted for pressure, and hence mass flow, were dependent upon the orientation of the junction mesh.

The first junction was simulated for laminar flow and no slip wall boundary conditions using an alternative CFD code, POLYFLOW. This is a finite element package, developed primarily for non-Newtonian flows. Identical pressure profiles on both channels were predicted. This was the expected result since both channels were exposed to exactly the same boundary conditions.

After discussions with CHAM, the suppliers of PHOENICS, the problem was simulated again using the CCM solver as an alternative CFD solver. This method, which is available with PHOENICS version 2.1 onwards, uses a cell centred method and did predict symmetrical results. It was possible to re-run some simulations using the cell centred CCM solution technique once the new version of PHOENICS was installed.

Differences between the staggered grid method and the CCM method are illustrated in Figures 4-5 (a) and (b) and 4-6 (a) and (b). They show the pressure contours and velocity vectors at the two inlets to the first junction where the boundary condition specified is a flat velocity profile of 3.6m/s. It is clear that the staggered grid method does not produce a symmetrical solution of the variable P1 (Fig 4-5 (b)). A negative region of pressure is predicted in the inlet boundary, INB. This is lower than the outlet pressure where the boundary condition specifies a zero pressure level. However, despite the negative value of pressure, flow is still into the domain.

Figure 4-6 (b) shows that the CCM solution of P1 is symmetrical and does not predict any negative values. Comparison of the velocity vectors shows them to be very similar for both methods so results of velocity from the staggered grid method can be used in greater confidence. However, pressure results from the staggered grid method must be treated with caution.

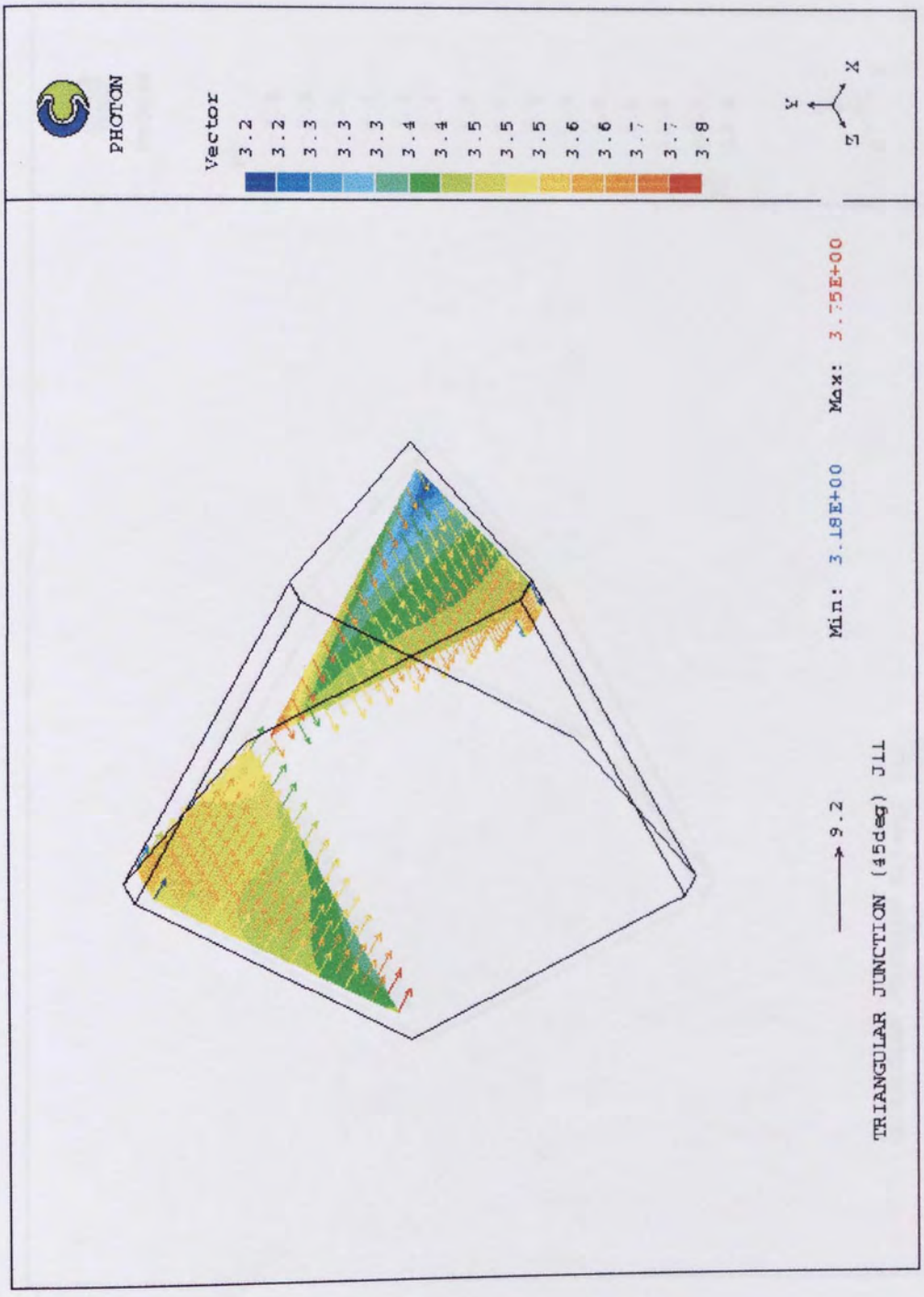

Figure 4-5(a) Velocity vectors and pressure contours at inlets using the staggered grid solution method.

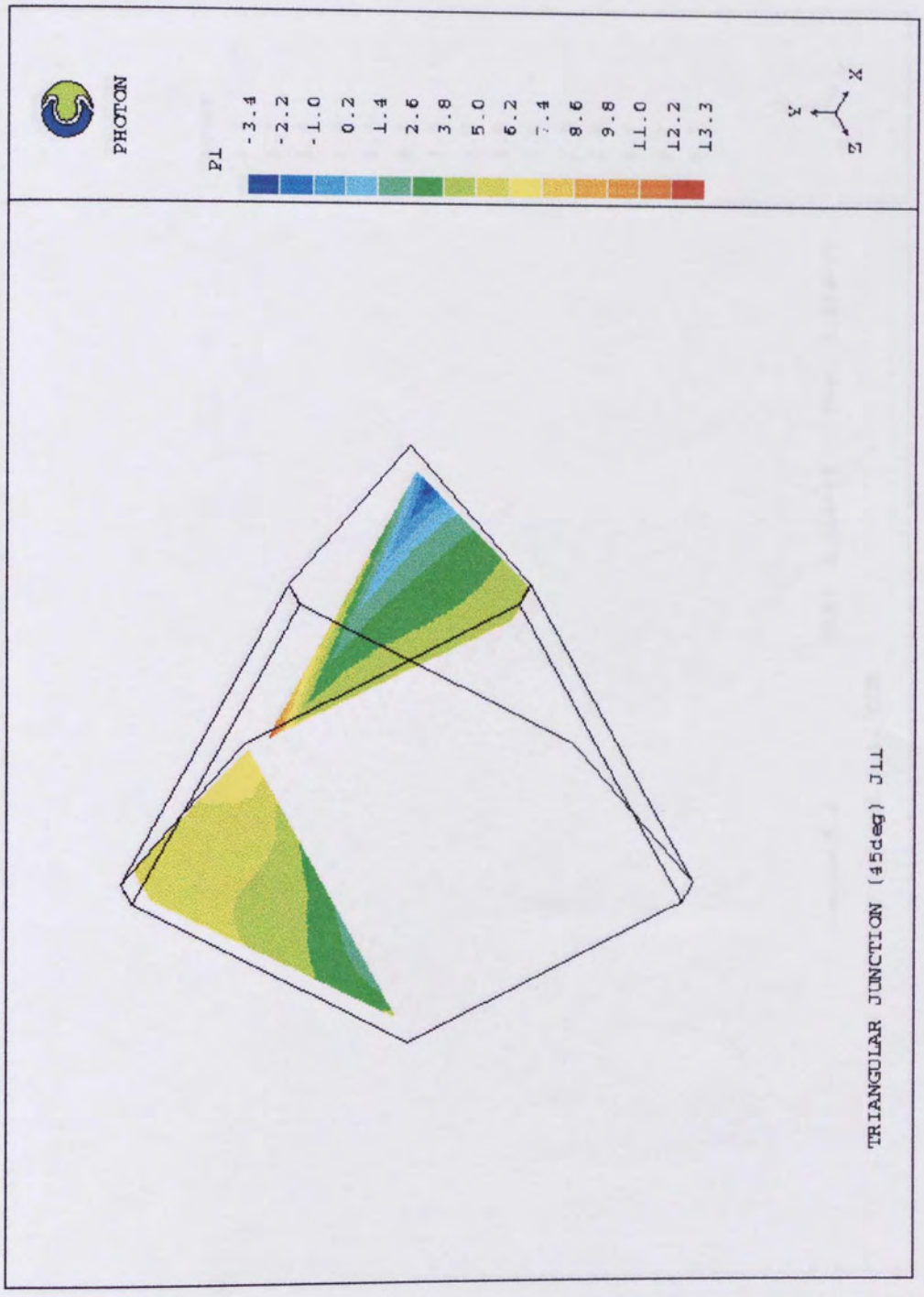

Figure 4-5(b) Pressure contours at inlets using the staggered grid solution method.

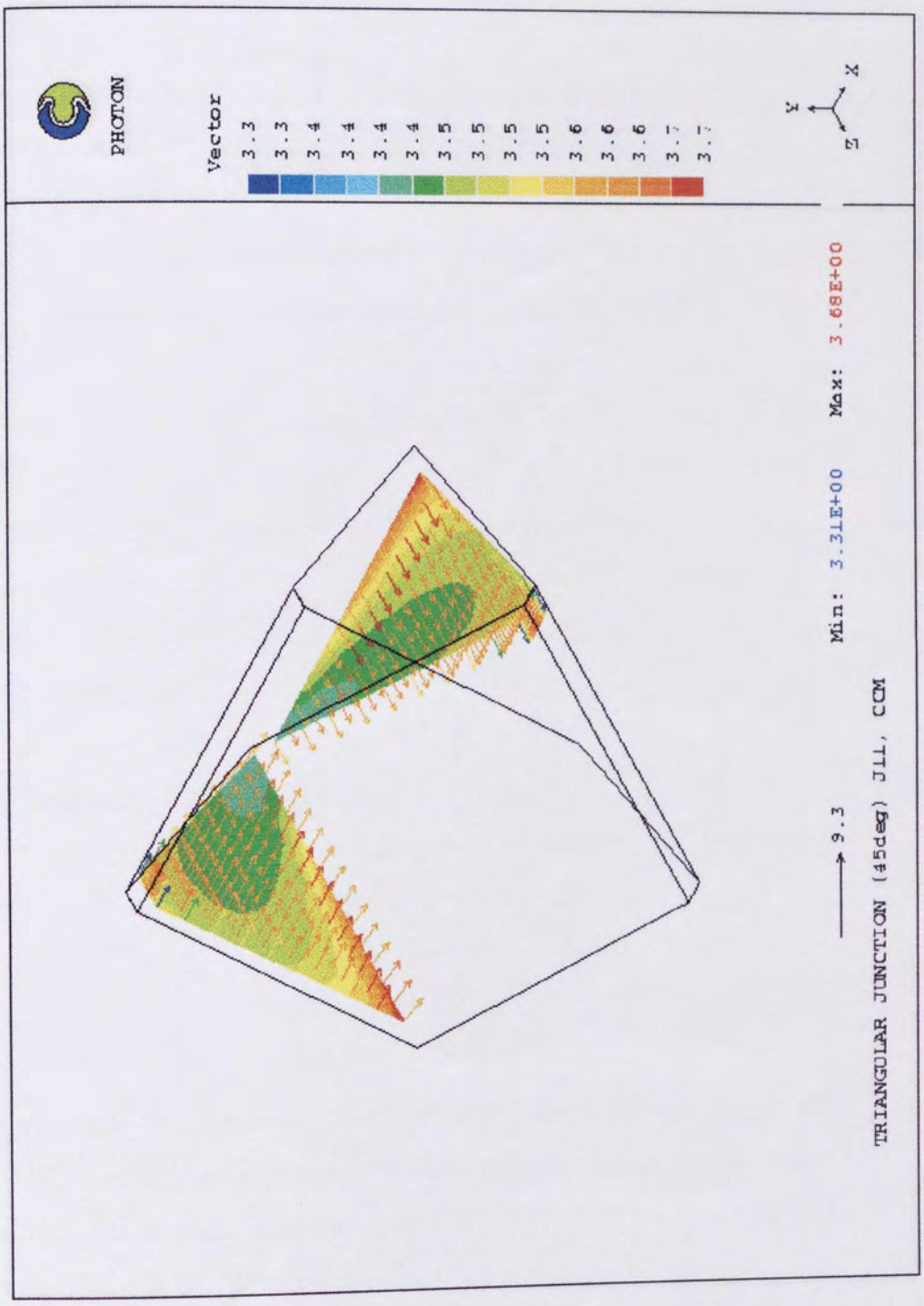

Figure 4-6(a) Velocity vectors and pressure contours at inlets using the CCM solution method.

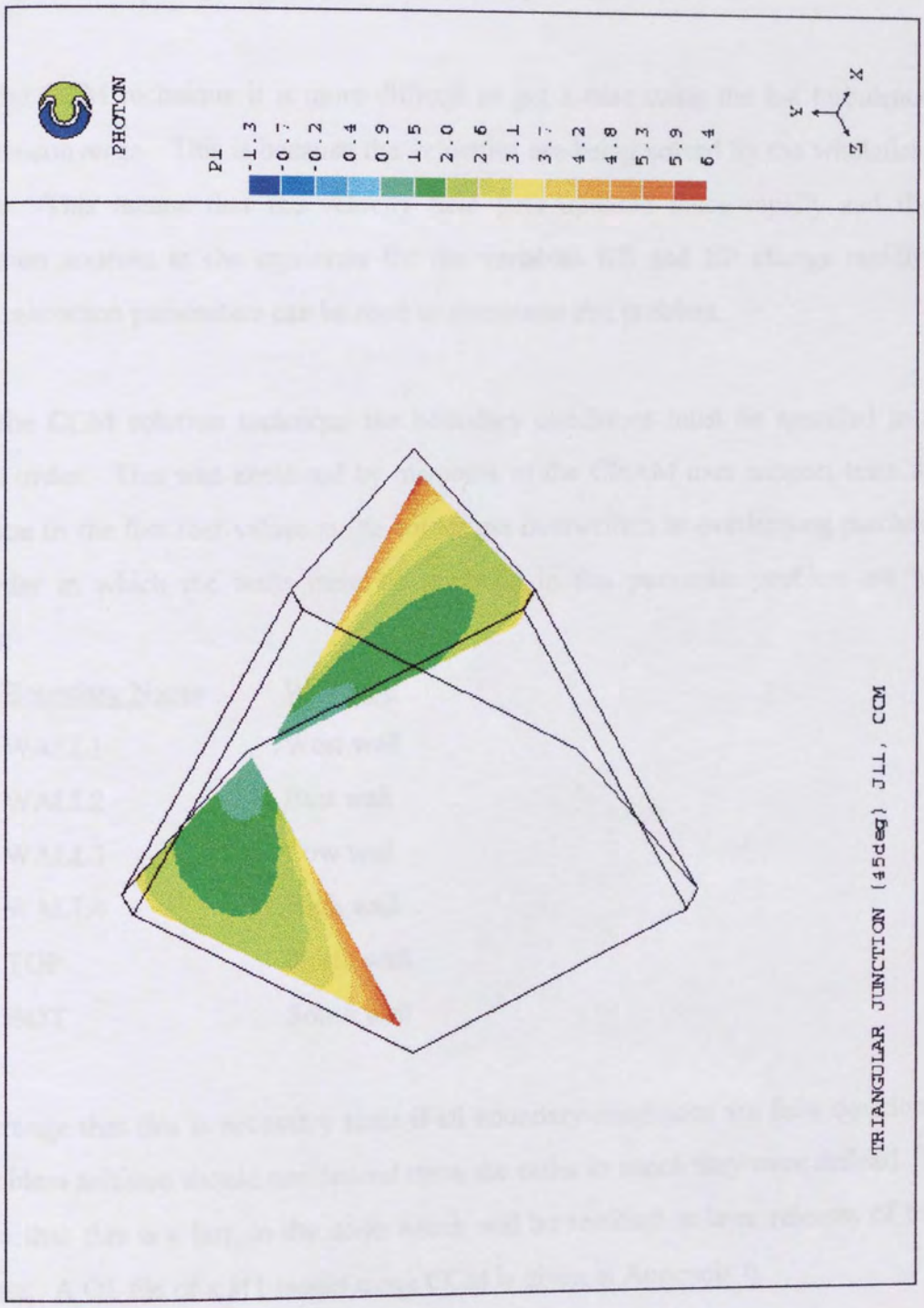

Figure 4-6(b) Pressure contours at inlets using the CCM solution method.

Figures 4-7 and 4-8 show temperature contours at the outlets of the third junction using the staggered grid and CCM methods, respectively. The overall results are similar. This is important to the work that follows since a temperature model is used as the basis of comparing efficiencies of structured packing shapes.

Using the CCM technique it is more difficult to get a case using the k-ε turbulence model to converge. This is because the velocities are being solved by the wholefield method. This means that the velocity field gets updated more rapidly and the momentum sources in the equations for the variables KE and EP change rapidly. Strong relaxation parameters can be used to overcome this problem.

Using the CCM solution technique the boundary conditions must be specified in a specific order. This was explained by members of the CHAM user support team as being due to the fact that values in the corner get overwritten at overlapping patches. The order in which the walls must be specified in this particular problem are as follows:

Boundary Name	Wall type
WALL1	West wall
WALL2	East wall
WALL3	Low wall
WALL4	High wall
TOP	North wall
BOT	South wall

It is strange that this is necessary since if all boundary conditions are fully described the problem solution should not depend upon the order in which they were defined. It may be that this is a bug in the code which will be rectified in later releases of the software. A Q1 file of a J11 model using CCM is given in Appendix 6.

In some of the following sections results from both methods are shown for comparison.

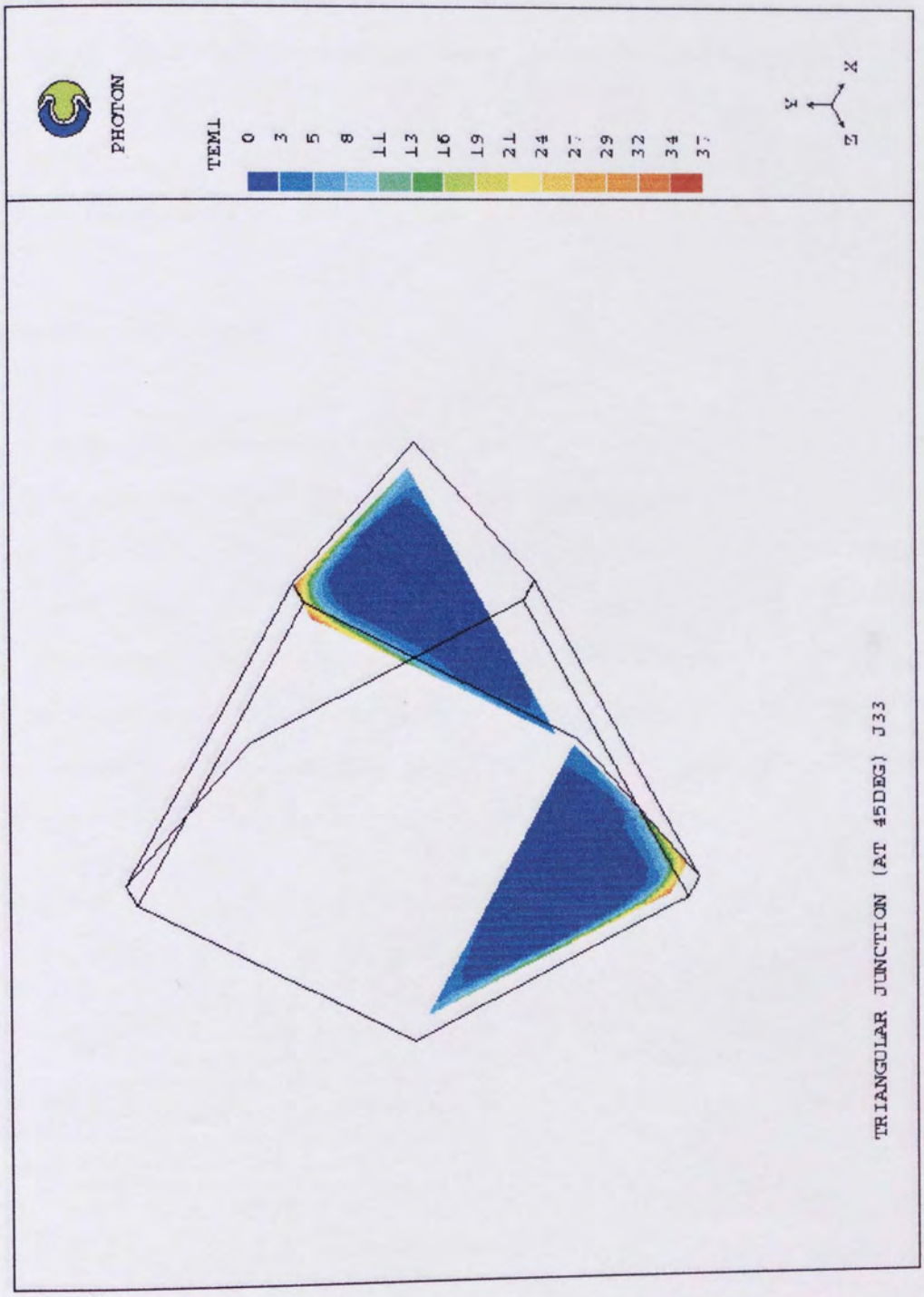

Figure 4-7 Temperature contours at outlets of third junction using the staggered grid solution method.

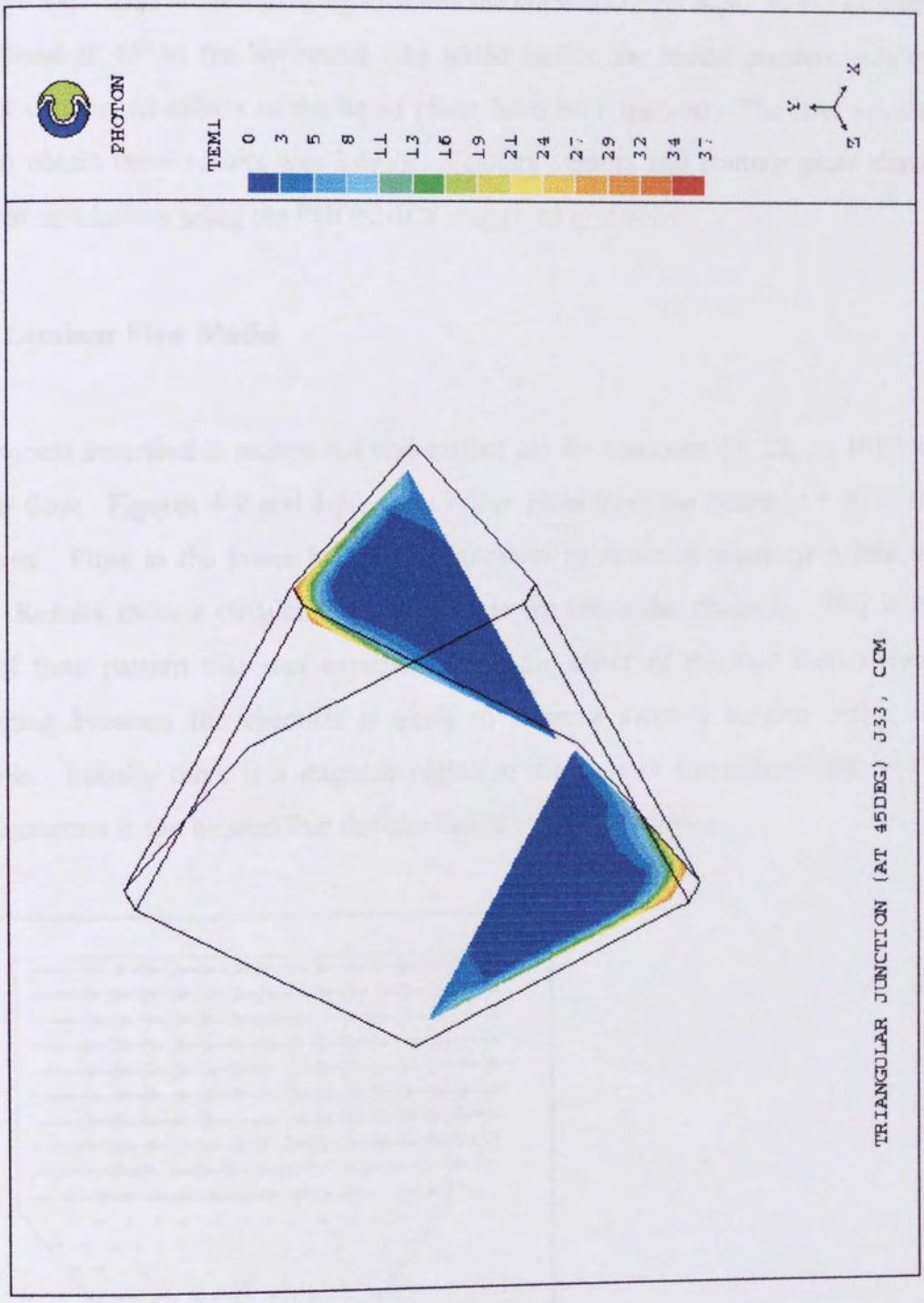

Figure 4-8 Temperature contours at outlets of third junction using the CCM solution method.

4.6 Fluid Flow Model

This section shows some of the results obtained using the mesh for the junction shown in Figure 4-2. This models packing in which the channels cross at 90^0 so the channels are inclined at 45^0 to the horizontal. As stated earlier, the model predicts only the flow of vapour; all effects of the liquid phase have been ignored. The inlet velocity used to obtain these results was 3.6m/s. Velocity vectors and contour plots shown are from simulations using the PHOENICS staggered grid solver.

4.6.1 Laminar Flow Model

The process described in section 4.4 was carried out for junctions 11, 22, ... 1010 for laminar flow. Figures 4-9 and 4-10 show vector plots from the centre (z = 8) of the junctions. Flow in the lower half of the junctions (z direction channel) is into the page. Results show a circulation developing in the triangular channels. This is the type of flow pattern that was expected, since the effect of the two fluid streams interacting between the channels is likely to cause a swirling motion within the channels. Initially there is a stagnant region in the base of the channel but by the eighth junction it can be seen that the circulation is well developed.

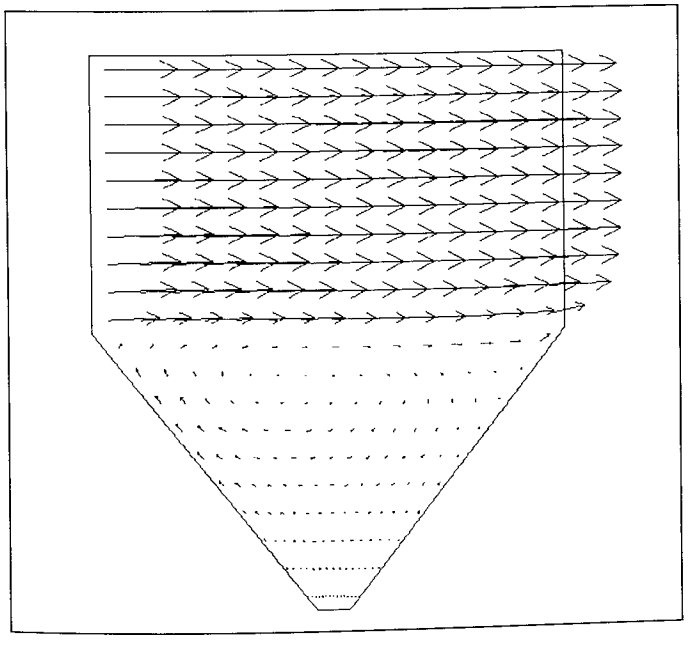

Figure 4-9 Junction 22 velocity vectors.

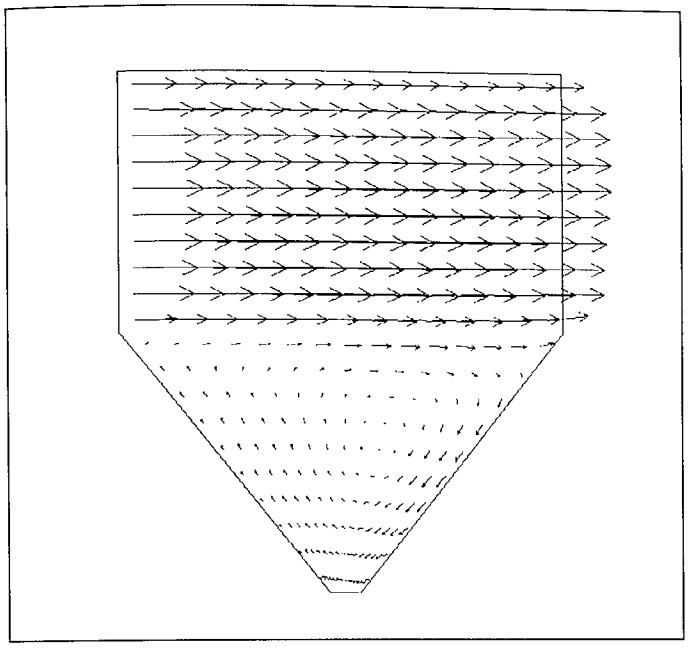

Figure 4-10 Junction 88 velocity vectors.

4.6.2 Turbulent Flow Model

The process was repeated using the widely known k-ε turbulence model which is supplied in PHOENICS. Experimental results indicate that the vapour phase is in the turbulent flow regime. As expected, a circulation can be seen developing in the channels. However, as Figure 4-11 shows, the circulation can be seen sooner and has developed by junction 33.

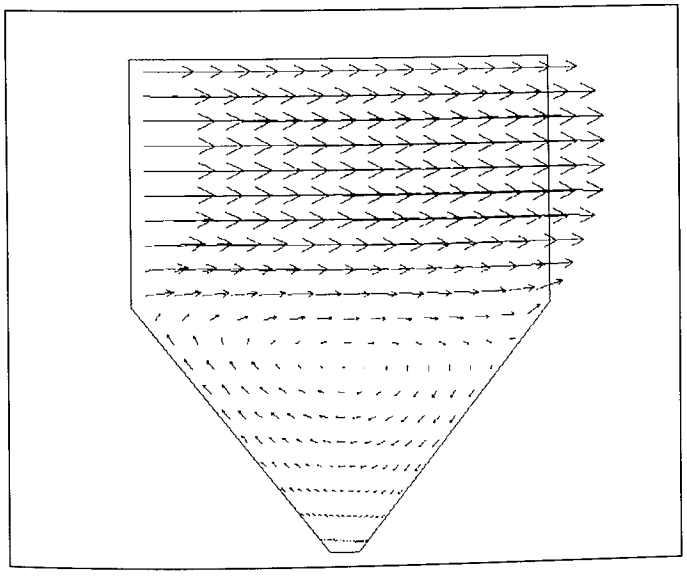

Figure 4-11 Junction 33 velocity vectors.

4.6.3 Validation of Method

A grid was created to model a section of packing having three overlapping channels i.e. up to junction 33 to validate the method outlined in the preceding sections. A converged solution could be reached for the laminar case only and the staggered grid method was used. Vector plots, for junctions 11, 22 and 33, from this simulation compared well with those obtained by performing successive simulations on the one junction, hence validating the method.

4.6.4 Mixing Between Channels

The concentration of a scalar quantity, A, was used to investigate the degree of mixing between the channels. The concentration of A was specified over the inlet of the z-direction channel (INB) of junction 11; arbitrary values of concentration of 1 and Prandtl number of 1 were used.

Figures 4-12 and 4-13 show contours of the concentration of A in the x-direction channel of the fifth junction, for laminar and turbulent cases respectively. As expected, the mixing between channels for laminar flow is significantly less than that for turbulent flow. However, Figure 4-13 shows that, despite turbulent flow, the component A is not being mixed to all areas of the neighbouring channel. Designs of future packings might aim to improve this degree of mixing.

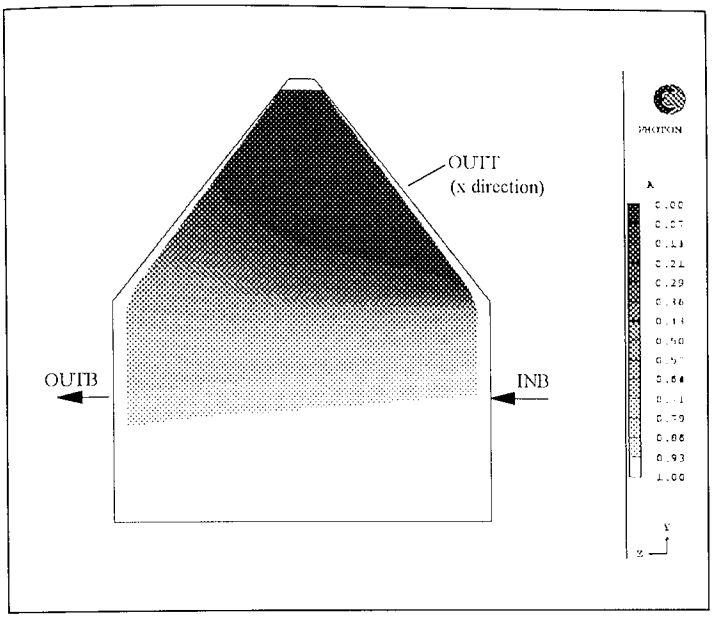

Figure 4-12 Contours of A - Laminar flow model.

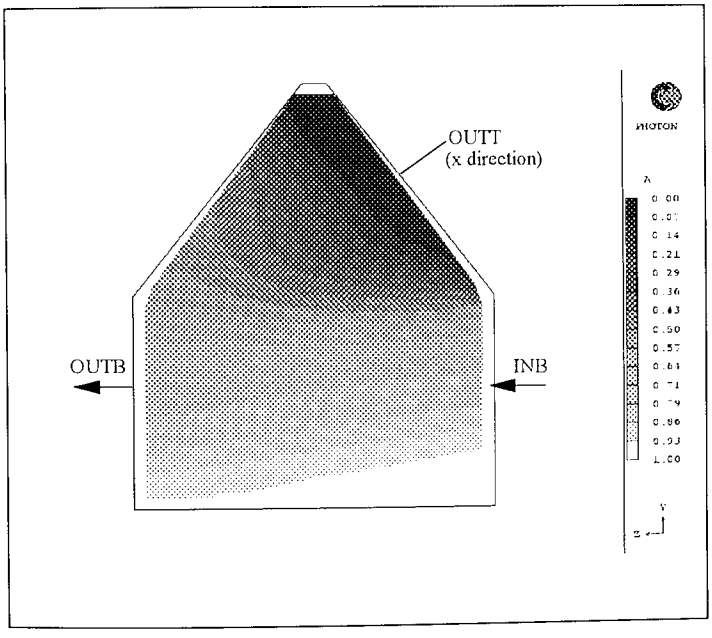

Figure 4-13 Contours of A - Turbulent flow model.

4.6.5 Pressure Drop

The average dry pressure drop across the junction was calculated from the pressures predicted at the inlet and outlet of both channels. Figure 4-14 shows how total pressure drop increases with block height. Results are given for both the PHOENICS staggered grid solver and the newer CCM solver. The difference in total pressure drop predicted after six junction is approximately 10%.

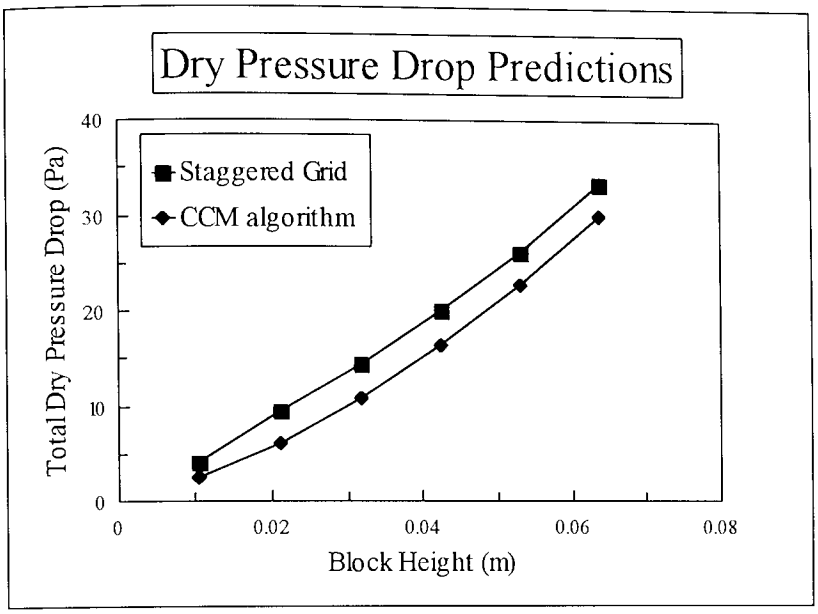

Figure 4-14 Comparison of dry pressure drop predictions.

4.6.6 Throughput and Channel Inclination Angle

Simulations were also carried out for inlet flowrates of 2.5m/s and 1m/s to model the effects of vapour throughput. The inclination of the corrugations with respect to the horizontal was investigated by performing simulations using grids representing angles of 30^0, 45^0 and 60^0.

Several workers have published experimental results of dry pressure drop through various packings. Data is usually presented plotted against the gas load F-factor, and is a straight line on a logarithmic plot. Spiegel and Meier (1987) give results for both Mellapak 250Y and 500Y. Figure 4-15 shows that the PHOENICS results for the standard 45^0 channel type packing compare well with those results published by Spiegel and Meier for similar packing.

As would be expected the results predict that the higher the channel angle with respect to the horizontal the lower the pressure drop.

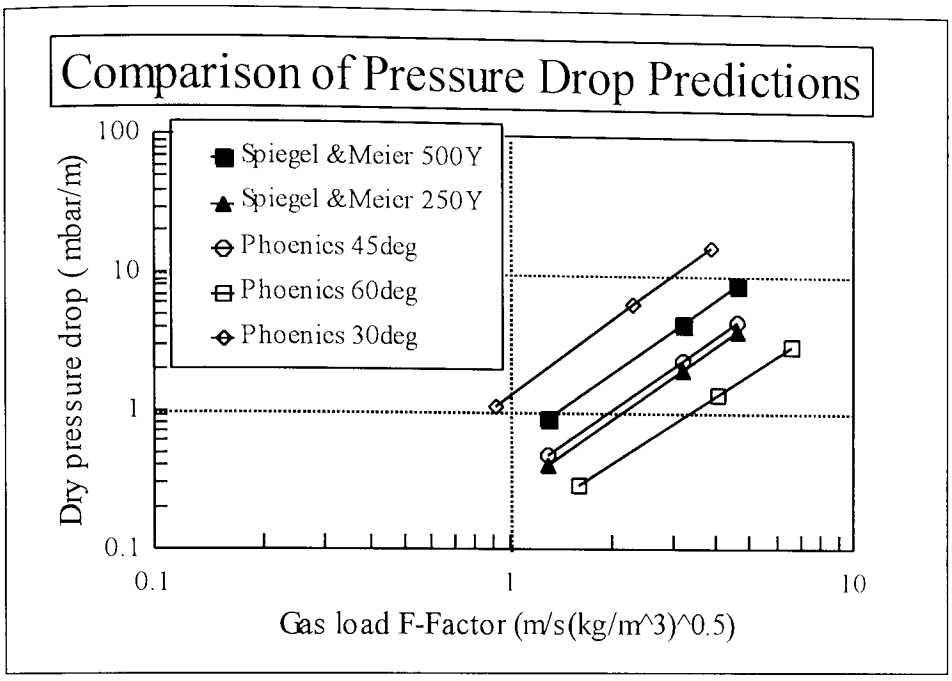

Figure 4-15 Comparison of pressure drop predictions.

4.7 Heat Transfer Model

The basic flow model was developed into a heat transfer model. This was chosen in preference to a mass transfer model as it was easier to implement within PHOENICS and, as heat and mass transfer equations are analogous, results are also valid in terms of mass transfer. This has enabled values of the rate of heat transfer and heat transfer coefficients to be calculated from the heat balance performed by PHOENICS. In addition, a value for the number of transfer units (NTU) has been calculated for each junction, based on average temperatures across the inlets and outlets. These results are valuable in assessing which areas of the packing should be modified in an attempt to increase the overall efficiency.

4.7.1 Energy Equation

By modifying the energy conservation equation, the variable TEM1 (temperature of first phase) was solved for directly, rather than being derived from enthalpy. The enthalpy term can easily be used to denote temperature by using the PIL variable HUNIT, a multiplying factor to convert the built in enthalpy source terms to

alternative units. Therefore, in this case, to convert enthalpy to temperature HUNIT is set equal to $1/C_p$ (PHOENICS Encyclopedia entry HUNIT).

4.7.2 Boundary Conditions

The boundary conditions set were for constant wall temperature, rather than constant flux. The actual choice of value was fairly arbitrary but an initial temperature difference of 50^0C seemed reasonable. The following additional boundary conditions were inserted into the Q1 file:

All walls:	$T_w = 50$
Initial fluid temperature:	$T_f = 0$

4.7.3 Wall Heat Transfer

PHOENICS reports the results of a heat balance in the RESULT file and this breaks down the total heat transfer into values of the rate of heat transfer at each boundary wall. By investigating the values of the rate of heat transferred from the wall to the fluid for a particular wall information can be obtained on which areas in the packing have the lowest efficiency in terms of heat or mass transfer .

4.7.4 Number of Transfer Units

By performing a heat balance over a section, of length dx, in which the temperature rise is dT, the number of transfer units can be expressed in terms of temperature in a similar fashion to the more commonly quoted NTU for mass transfer. The number of transfer units can be expressed as:

$$NTU = \int_{T_{in}}^{T_{out}} \frac{dT}{(T_w - T)}$$

Integrating over the length of the duct, T_{in} and T_{out} being the inlet and outlet fluid temperature, gives;

$$NTU = \ln\left(\frac{T_w - T_{in}}{T_w - T_{out}}\right) \quad \text{or} \quad NTU = \ln\left(\frac{inlet\ driving\ force}{outlet\ driving\ force}\right)$$

Driving forces were calculated from area averaged temperatures across the inlets and outlets of junctions.

4.8 Results

4.8.1 Heat Transfer Rates

The results of the heat transfer model can be viewed in a number of ways to get a complete picture of the variation both in the junctions as a whole but also in each part of the junction. Figure 4-16 shows the heat transfer in each junction for the model using an inlet velocity of 3.6m/s and using the standard PHOENICS staggered grid solver. The initial decrease is sharp as the fluid starts to heat up. Around junction 44 a slight increase is seen which may be due to the circulation in the flow pattern becoming developed. A fairly constant value is then reached.

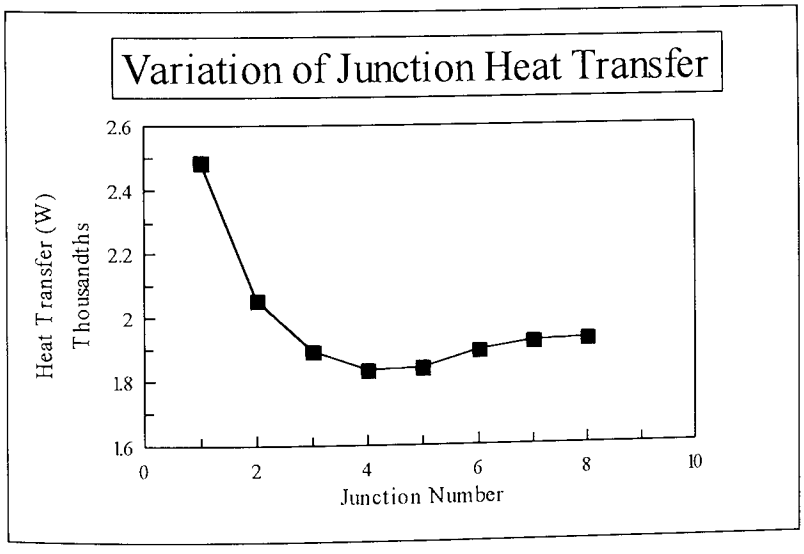

Figure 4-16 Variation of Junction Heat Transfer.

A more detailed analysis of the way in which heat transfer rates vary within the junctions can be seen in figure 4-17. Heat transferred to the fluid from each wall of the junction for the first eight junctions is plotted. It is clear that walls TOP and BOT - the walls at the apex of the triangular channels - transfer around only half the amount of heat to the fluid compared to the side walls and hence these areas perform less efficiently in terms of heat or mass transfer. A similar result is given when using values reported from simulations using the CCM solver. As fluid flows more slowly in the corners of the channels its temperature approaches that of the wall. Contour plots of temperature (Figure 4-18) show fluid in the apex reaching a fairly high temperature whilst the central portion of the flow is still relatively cold.

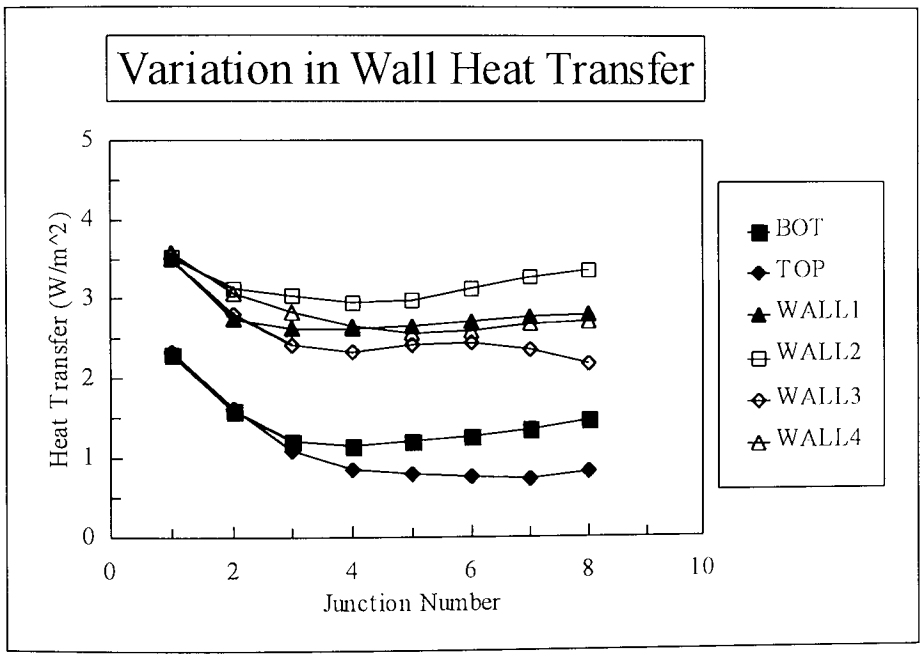

Figure 4-17 Variation of heat transfer for each wall of junction.

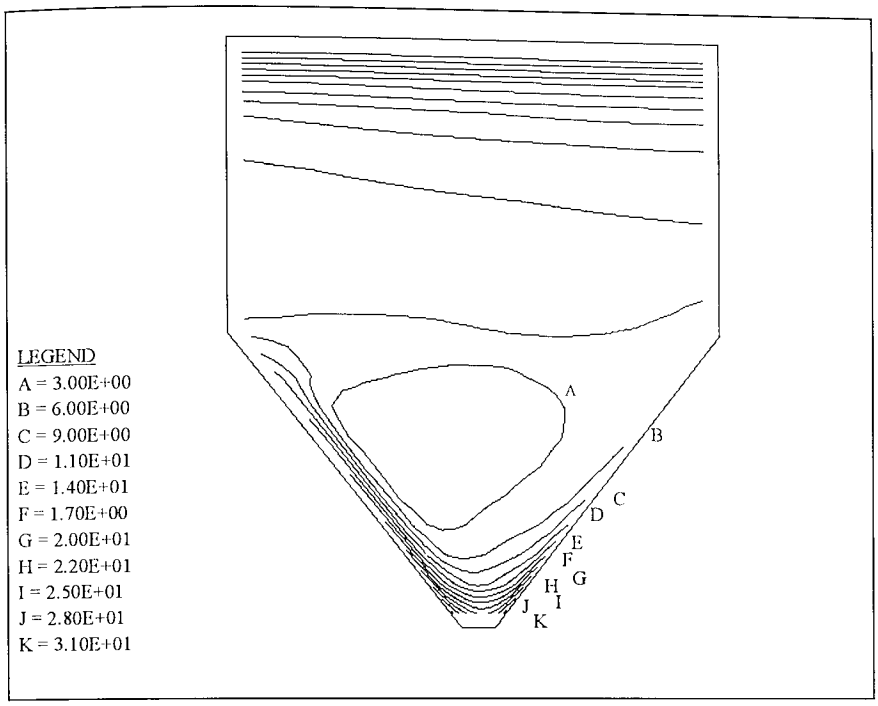

Figure 4-18 Contour plots of temperature at centre of fifth junction.

4.8.2 Number of Transfer Units

A value of NTU was calculated from average temperatures across the inlets and outlets of the junctions. It can be seen in figure 4-19 initially this value falls as the junction number increases. However, it then starts to rise again at junction 44, which may again be due to the circulation in the channels having become fully developed.

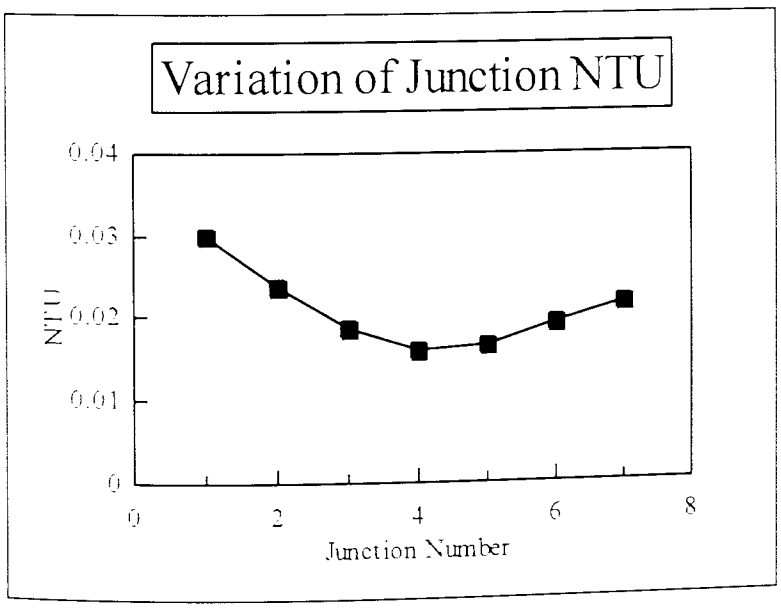

Figure 4-19 Variation of NTU with junction number.

It can be concluded that the regions of the packing blocks where the highest rates of heat or mass transfer take place are at the lower edges. An overall value of NTU was also calculated, assuming that the packing was infinitely wide, so that junctions other than 11, 22, 33 etc. could be ignored. Figure 4-20 shows the variation of overall NTU/N, where N is the number of junctions, against block height. The height is calculated assuming that the channels are at 45°.

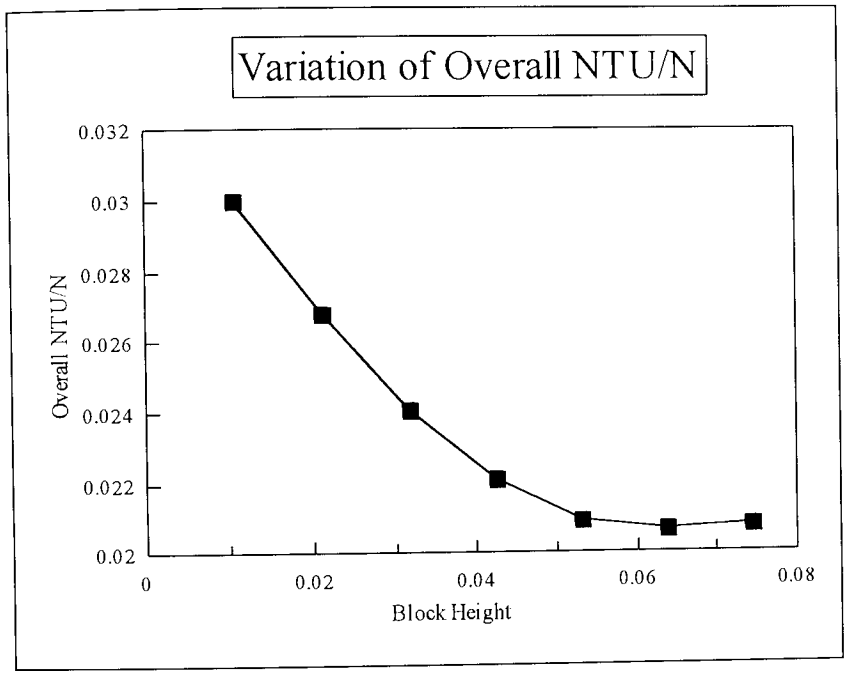

Figure 4-20 Overall NTU/N against block height.

Hence it can be said that if:

$$\frac{NTU_1}{N_1} > \frac{NTU_2}{N_2} \quad \text{or} \quad \frac{Q_1}{N_1} > \frac{Q_2}{N_2}$$

where Q is the overall heat transfer, the overall efficiency of packing 1 will be greater.

These results also indicate that there may be a small scale-up effect. Since the lower numbered junctions occur not only in the lower region of the packing block but also around the outer edges of the block, it would be expected that the packing efficiency would be higher when in a column of smaller diameter. Clearly, once the column diameter becomes very large any increase in efficiency due to the edge effects will become negligible.

4.9 Effect of Sheet Width

The heat transfer model has been used further to investigate the effects of column diameter on the overall heat/mass transfer efficiency. In all work described so far the column diameter has been assumed to be infinite so that junctions other than those numbered 11, 22 and so on could be ignored. The case of packing in a column of finite diameter is now considered and the CFD technique used to model flows and heat transfer in the junctions around the edge of the packing block.

4.9.1 Edge Junctions

An edge junction will be defined as one that is named other than J11 etc. e.g. J35, J62, or, a junction which is named 11, 22 etc. but which is at some other height in the block than if the column were infinitely wide. Figure 4-21 shows the junction numbering in a section of packing at the bottom left hand edge. Again numbers relate to how many cross overs, or junctions, the fluid has passed through in the particular direction.

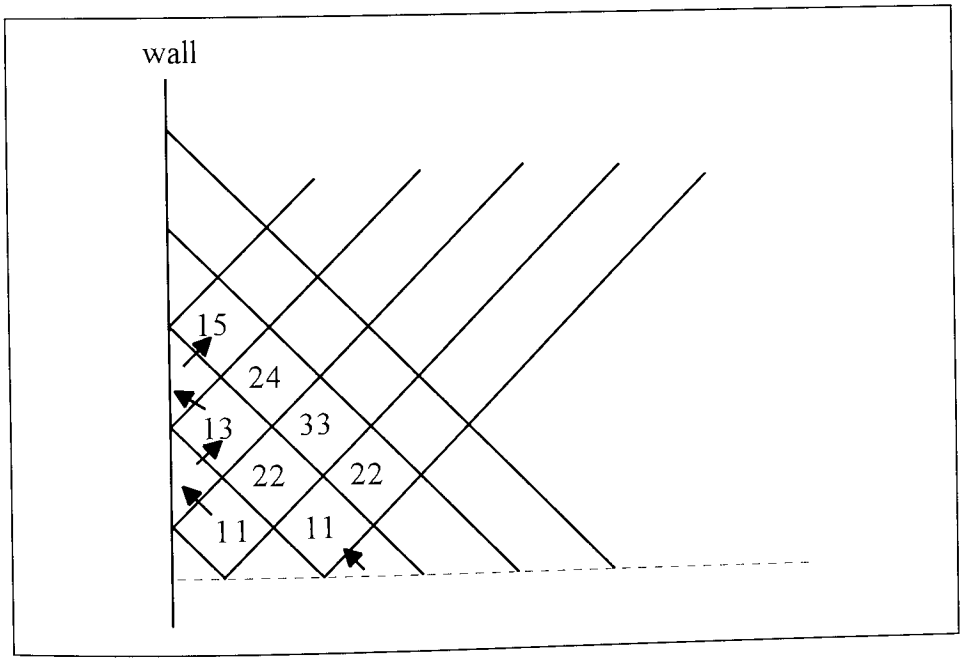

Figure 4-21 Numbering of edge junctions.

It has been shown that the overall value of NTU/N and the rate of heat transfer decreases with increasing junction number. It is expected that the presence of edge junctions will increase the value of NTU for a sheet over that predicted for the same block height in an infinitely wide column.

4.9.2 Model Assumptions

Several assumptions are made in order to develop the model further. It is assumed that the presence of the wall has a mixing effect such that fluid at the wall, after leaving a channel, is at the average temperature of fluid leaving the junction from which it emerged. For example, the fluid entering the lower half of J15 (see Fig 4-21) with a flat velocity profile is assumed to be at the average temperature of fluid leaving J33 (i.e. the upper half of J13). It is also assumed that edge junctions on the left hand side of the sheet of packing will be identical to those on the right hand side. Perhaps the most gross assumption in the modelling of sheets of a given width is that standard numbered junctions, e.g. J66, which are not at the usual height in the block had it been infinitely wide, are assumed to be identical to those that are at their usual height. This reduced the total number of simulations that had to be performed. However, by studying the trend in the NTU results it is likely to slightly decrease the average NTU that is calculated for a given sheet width; as such, any conclusions that are drawn on the effect of width will be on the conservative side.

4.9.3 Number of Transfer Units

Several PHOENICS simulations were performed and the value of NTU calculated from average temperatures at the inlets and outlets for each particular edge junction. The number of transfer units in a sheet of given width were calculated by averaging the individual junction NTUs for each row of junctions. This was then used to calculate the overall sheet NTU from:

$$NTU_{sheet} = \ln(e^{NTU\,(row1)} \times e^{NTU\,(row2)} \times \ldots\ldots e^{NTU\,(rowN)})$$

4.10 Results

4.10.1 Number of Transfer Units

Figure 4-22 shows the relative increase in NTU above the value for an infinitely wide column.

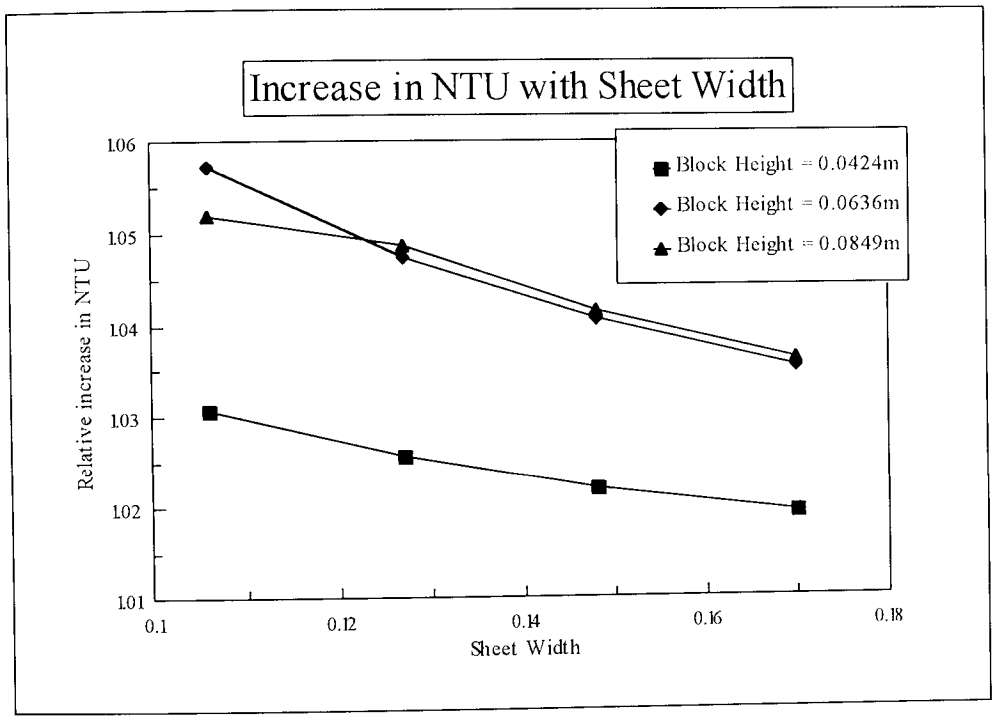

Figure 4-22 Increase in number of transfer units with column width.

This indicates that a 3-6% increase in the packing efficiency may be observed if standard sized packing is tested in columns having diameters less than approximately 15cm. We can therefore be confident of the results obtained from the Aston test rig (described later) since the structured packings are tested in a column with an internal diameter of 0.3 m.

4.11 Summary

A technique for modelling the processes occurring within the channels of structured packings has been proposed. The model, which has been implemented in the CFD

code PHOENICS, consists of a single junction. Coding, written within the subroutine GROUND, enables successive simulations to be carried out with inlet conditions being set from outlet data of the preceding simulation.

The consistency of the results has been discussed. A particular inconsistency was observed in the results predicted by PHOENICS. Two alternative solution methods, available within the code, have been used to perform the model calculations and the results discussed.

The flow patterns predicted by the model show a circulation developing due to the interactions between the two streams. A heat transfer model, which is an extension of the fluid flow model, shows that the highest rates of heat transfer occur in the lower regions of the packing block. This agrees with experimental results that shorter blocks have a higher efficiency than taller ones.

5. PACKING DEVELOPMENT

5.1 The New Shape

From results of the CFD model of the Tianjin packing it has been seen that the model predicts that fluid in the apex of the triangular channels quickly reaches equilibrium with the walls. If this model reflects reality sufficiently, the same effect will happen in the real packing. The assumption is made here that the efficiency of a packing would be improved if this effect was removed or diminished. One way of testing this is to devise modifications of the shape and test them using a CFD model derived from the model of the Tianjin packing. The model predictions would then suggest modifications for a real packing. This chapter describes such modelling work.

A new packing shape was devised by Prof. K.E. Porter, having slots and tabs punched out at the apex of the channels, in an attempt to mix the colder fluid, from the central area of the junction, with the hotter fluid in the apex of the channels. Tabs protruding into the flow of vapour in the triangular corrugation of the neighbouring sheet should 'scoop' fluid from the cold central core of the flow through the slot into the apex of the next corrugation. The profile of this shape, illustrated in Figure 5-1 has the attraction that it should be relatively easy to manufacture and should mix the fluid both vertically and laterally through the packed section.

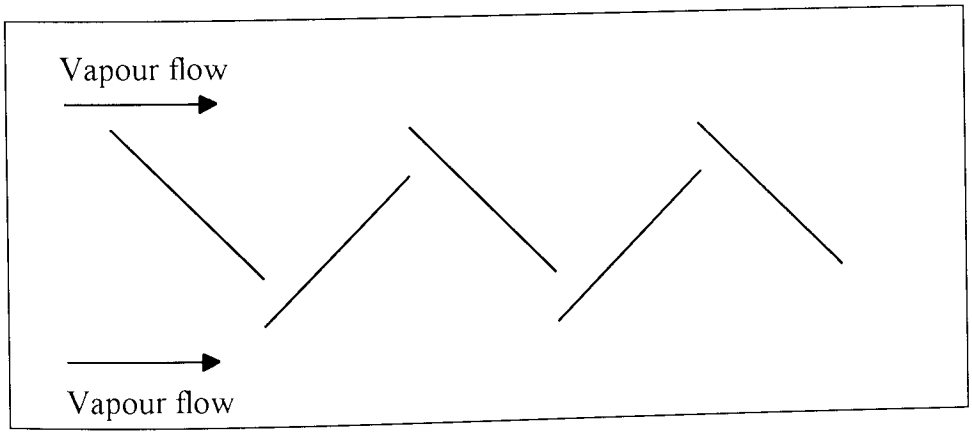

Figure 5-1 Profile of new shape of packing.

The CFD model described in the previous chapter has been developed to model the proposed modified packing. This can be done using the same strategy as before by working on a single junction, and proceeding in a stepwise fashion, the outlet data (i.e. velocity vectors, temperatures etc.) of both the main and slot flows forming the inlets for the next simulation. This has enabled comparisons to be made between the different designs, on the assumption that if the model of the new packing shows a difference of performance then a real packing would also show a different performance.

5.2 CFD Model

5.2.1 Model Geometry

Due to the additional slots for mixing the fluid in a lateral direction, the CFD model is more complicated than the model of the traditional packing structures presented previously. It is now necessary to consider three neighbouring sheets of packing in order to determine the flow path of the fluid and hence set the appropriate boundary conditions for the grid. The previous model of a junction, which was shown in Figure 4-2, had the bulk fluid flow in the bottom half of the junction in the z-direction (i.e. W1) and that in the top half in the x-direction (i.e. U1). In the new model fluid is being transferred from one side of a sheet to the other, so modelling of the flow path through the slots requires the use of another junction, rotated through 90°, such that the bulk flows are the reverse of the original ones. These junctions were numbered using the same system followed by 'opp', to distinguish the orientation of the junction. The two geometries, with inlet and outlet boundaries indicated, are shown in Figures 5-2 and 5-3.

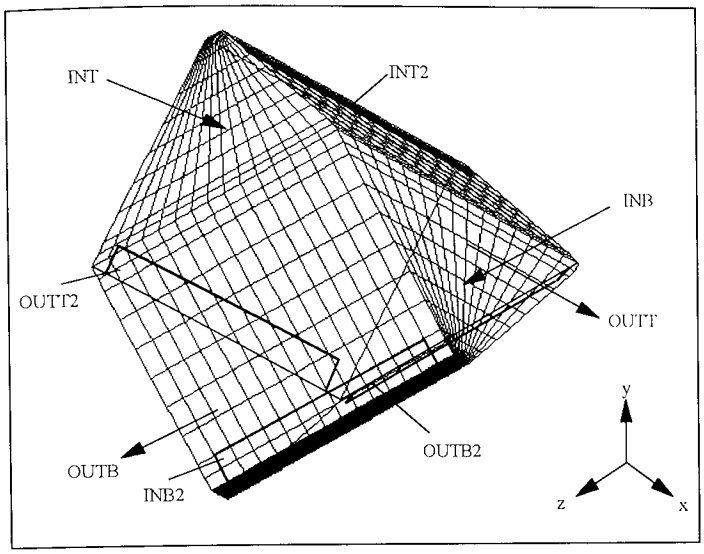

Figure 5-2 Geometry of original junction.

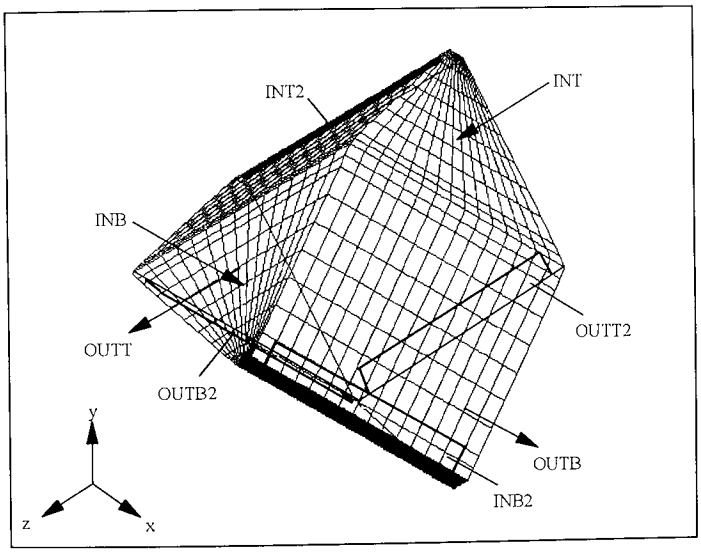

Figure 5-3 Geometry of opposite junction.

5.2.2 Fluid Flow Path

The flow of the bulk fluid follows the same pattern as previously, with outlets from each half of the junction feeding into the inlet of the corresponding half of the next junction; i.e.:

$$J11 \rightarrow J22 \rightarrow J33 \rightarrow J44 \text{ etc.}$$

and similarly for the opposite junctions:

$J11opp \rightarrow J22opp \rightarrow J33opp \rightarrow J44opp$ etc.

The flow of fluid through the slots is not so easy to describe but does follow a regular pattern. Figure 5-4 shows a 2-D slice through three neighbouring sheets of packing. The junction numbers and the slot names are given. A similar diagram would represent the flows at 90^0 to the ones shown.

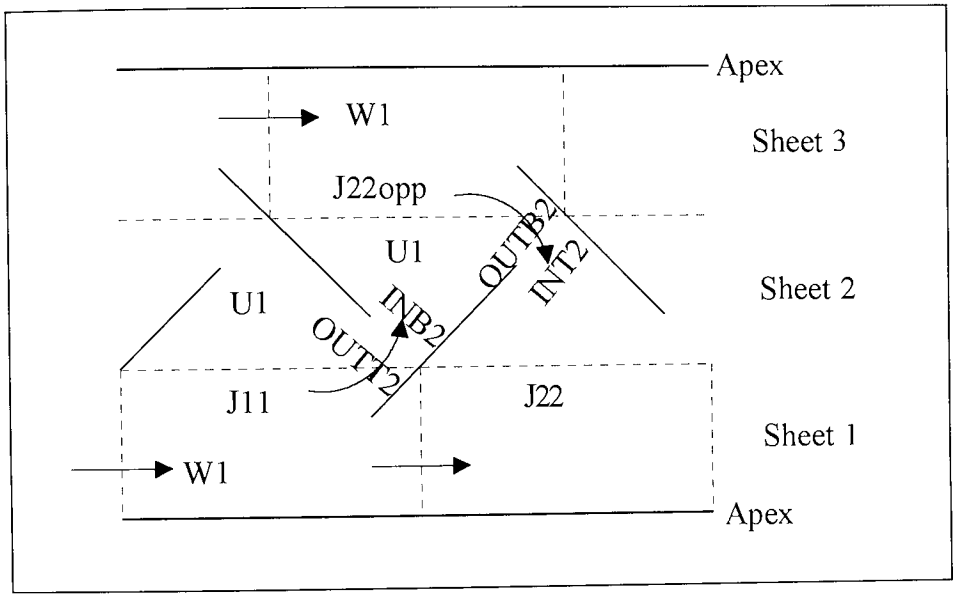

Figure 5-4 Slot and bulk fluid flows at a 2-D plane through packing.

The naming of J22opp is fairly arbitrary as it could equally well have been numbered J11opp. As with the plain junction case only whole junctions are considered so the bottom of the block of packing is assumed to be corrugated.

The flow path of fluid through the slots can be written more succinctly as shown in Figure 5-5.

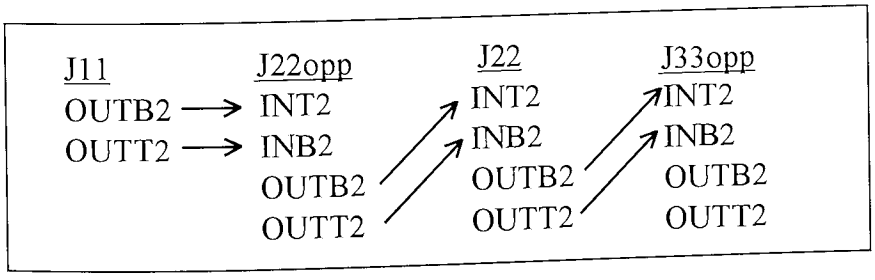

Figure 5-5 Flow path through slots.

5.2.3 Boundary Conditions

The additional inlets and outlets which are shown in Figures 5-2 and 5-3 were made as wide as possible such that the model represents a theoretical maximum. This eliminated any recirculation which developed behind the slot inlets, causing the problem of inflow through the main outlets.

It has been assumed that the process of making slots will lead to small tabs of metal which can either be completely removed (a loss of metal area) or pushed out in some direction. The proposed shape would ideally have the tabs in the plane of the corrugation, as shown in Figure 5-1, but due to the limited griding abilities of PHOENICS this was not possible so various other positions of the tab were considered. Three main variations of tab were modelled:

1. Tab completely removed, therefore slot only.
2. Tab in horizontal position, therefore inside junction.
3. Tab in vertical position, therefore blocking portion of main inlets/outlets.

Figure 5-6 shows a 2-D slice representing the three different variations. In the case of the horizontal and vertical tab the tab was assumed to extend across the width of the channel. The effect of changing the frequency with which the tabs and slots occur was also investigated by modelling the tab and slot on alternate junctions.

A vertical tab pushed inside the junction was also modelled. This was parallel to the main flow direction and not affecting the corrugation below. Thin vertical tabs protruding into the centre of the neighbouring channel were also gridded and coded into GROUND. However, results were not obtained since the presence of such a tab caused a circulation resulting in fluid flowing in through the outlet and convergence could not be reached.

a) Tab completely removed.

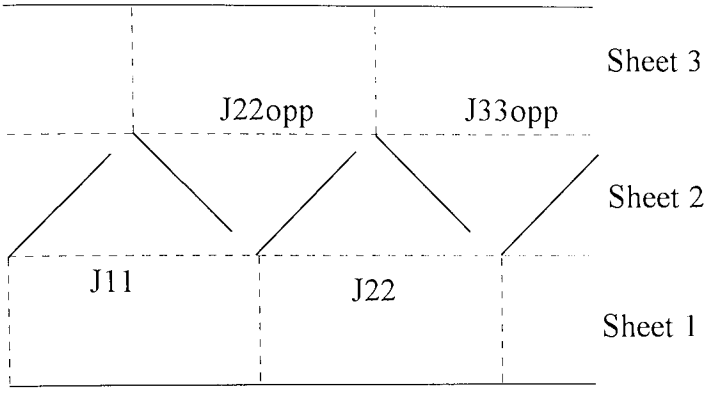

b) Tab in horizontal position.

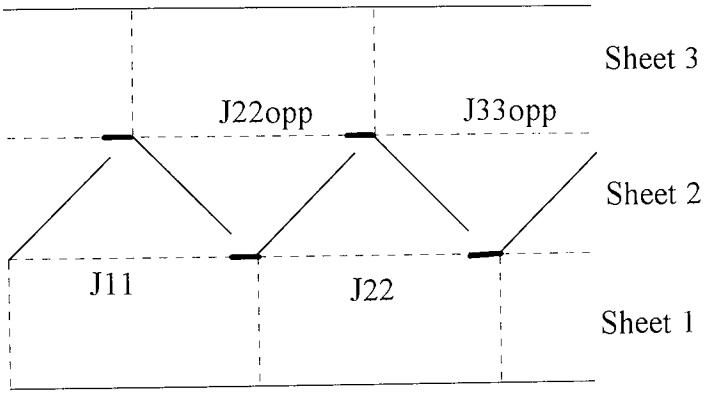

c) Tab in vertical position.

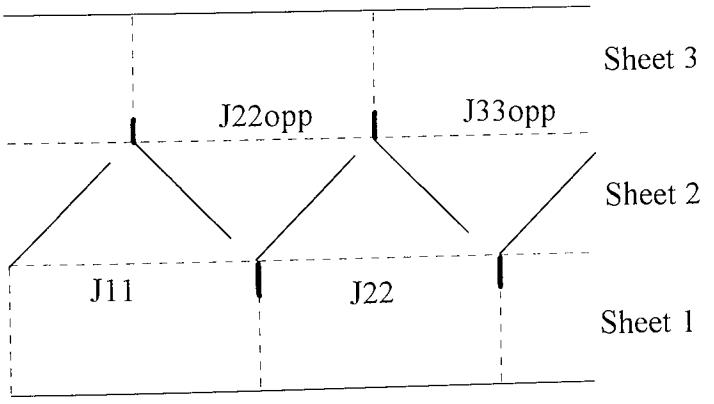

Figure 5-6 2-D representations of new packing models.

5.2.4 Ground Coding

Additional GROUND coding was required to facilitate the reading and writing of data for the new slot inlets and outlets. This was similar to that written previously for the main openings but had the added complication that the local grid directions at the outlets were not identical to those at the corresponding inlets. As the grid is non-orthogonal Cartesian components of velocity are used to supply the inlet values of U1, V1 and W1, which are the velocity components in the local grid direction. Mass flowrates at inlets were calculated from the value of pressure at the corresponding outlet and the coefficient of the variable P1. Since the additional outlets resulted in a division of the flow, slot outlets being parallel rather than normal to the direction of bulk flow, it was not possible to calculate mass flowrates from velocities, as discussed in section 4.4. Appendix 7 gives the additional Ground coding for the slots. The GROUND shown does not allow for a series of runs with data being stored and transferred automatically. However, this extension could easily be made.

5.2.5 Limitations of Present Model

Due to the requirement of the PHOENICS solver to have a topologically cartesian structured grid dealing with triangular shapes is inherently difficult. The exact desired position and shape of the slot and tab could not be represented using the PHOENICS grid generator. Various other positions, being at either end of the range of possible positions it could have taken, had to be used. The shapes of the slot and tab were dictated by what could be fitted easily to the mesh. The pre-processing package, Powermesh, from ICEM, which was available for use did not have at the time a suitable interface with PHOENICS. It was stated by the suppliers that this should be available by mid 1996 which would mean that such limitations of the model could be overcome and a more detailed optimisation of shape and size of the tab and slot carried out. This could be the subject of further studies.

The model is only able to consider downstream effects i.e. it can only march forwards through the sequence of junctions and therefore, as an example, J22, being downstream of J22opp, can have no effect on J22opp. This means that the boundary conditions at the slot inlets are not an exact representation since at this point parallel flows occur which the model predicts to have different velocities. Two options for the user defined slot inlet boundary condition were considered. Either all the velocity components were read in or the bulk velocity component was ignored and only the two components perpendicular to the bulk flow were read as the inlet condition. However, since the slow flowing fluid in the apex of a junction will have some deceleration effect on the faster flowing fluid in the central portion of the preceding junction, it would probably be more appropriate to read back the bulk velocity reduced by some suitable resistance factor. However, the two options described above should envelop the range of possible results.

5.3 Results

Various combinations of tab and slot, as described previously, were investigated. The models fall into two categories depending on the slot inlet boundary conditions i.e. those where bulk velocity was ignored and those where bulk velocity was transferred at the slot inlet boundary condition. The table describes the models and the legend used to denote each one.

Model	Name	Symbol	Description
1	Plain	■	The original model i.e. no slots or tabs
2	Horz (15%)	◆	Tabs: Horizontal Slots: 15% of side wall area Inlet: Bulk velocity ignored Notes: Tab does not protrude into adjacent channel
3	Slots only	▲	Tabs: None Slots: 10% of side wall area Inlet: Bulk velocity ignored Notes:

4	Vert	□	Tabs: Vertical Slots: 10% of side wall area Inlet: Bulk velocity ignored Notes: Tab protruding into adjacent channel
5	Horz (10%)	✧	Tabs: Horizontal Slots: 10% of side wall area Inlet: Bulk velocity ignored Notes: As Horz (15%)
6	Alt Horz (10%)	✷	Tabs: Horizontal Slots: 10% of side wall area Inlet: Bulk velocity ignored Notes: Tab/slot placed at alternate junctions
7	Thin (2a)	●	Tabs: None Slots: 10% of side wall area Inlet: Bulk velocity included in BC Notes: Thin slot in centre of side wall
8	Alt Horz (2a)	★	Tabs: Horizontal Slots: 10% of side wall area Inlet: Bulk velocity included in BC Notes: As Alt Horz (10%)
9	Vert (2a)	▼	Tabs: Vertical Slots: 10% of side wall area Inlet: Bulk velocity included in BC Notes: As Vert
10	Int Vert	○	Tabs: Vertical Slots: 10% of side wall area Inlet: Bulk velocity ignored Notes: Tab inside junction parallel with bulk flow

Table 5-1 Summary of model simulations.

As discussed previously the actual shape designed, which would have tabs at 45^0 could not be modelled. Hence the vertical and horizontal tabs modelled bound the range of positions the tab could take. The aim of the new shape is to maximise the mixing of fluid from the apex with that in the centre of the junction for the minimum pressure drop. Having a tab protruding into the vapour flow channels is likely to increase pressure drop and reduce capacity through the packing so any increase in separation efficiency needs to be large enough to compensate for the penalties incurred in pressure drop and capacity.

The results obtained are now discussed.

5.3.1 Fluid Flow Patterns

Velocity vectors from the centre of the third and fifth junctions of two models - horizontal and vertical tabs - are shown below. By comparing these with the flow patterns produced in the plain junctions by the interaction of just two streams (figure 4-11) it can be seen that the effect of the additional flow through the slots is to disrupt the circulations. The benefit of this is that the boundary layer will not become fully developed and heat and mass transfer will be higher.

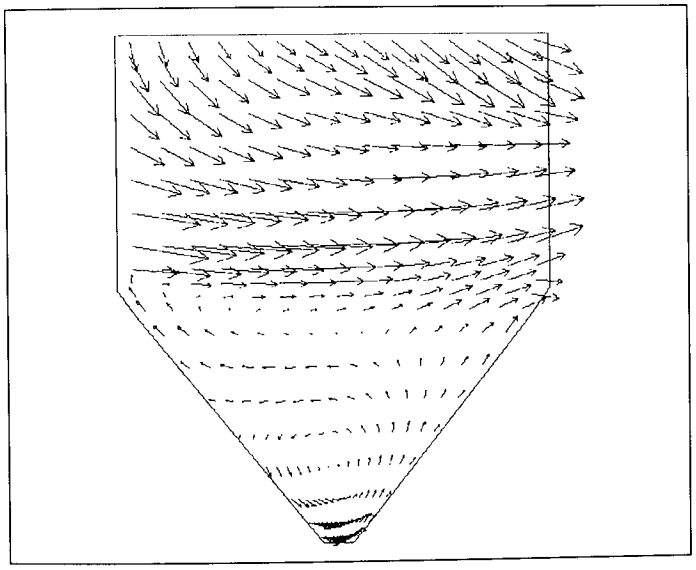

Figure 5-7 Horizontal tabs - Junction 33.

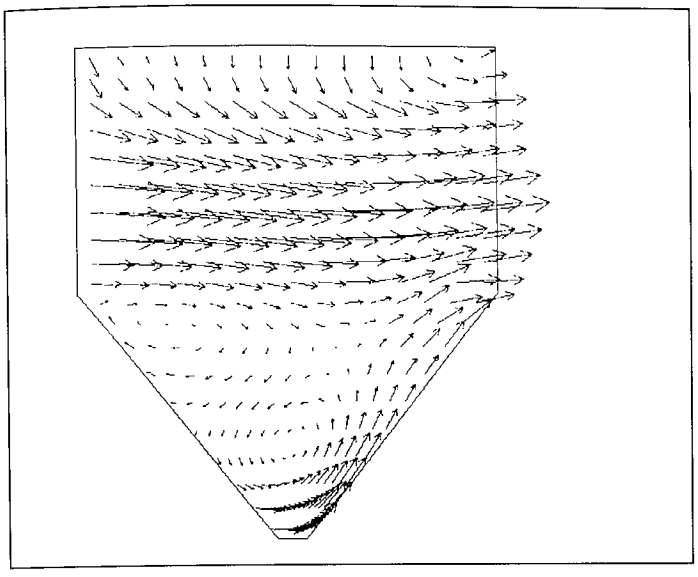

Figure 5-8 Horizontal tabs - Junction 55.

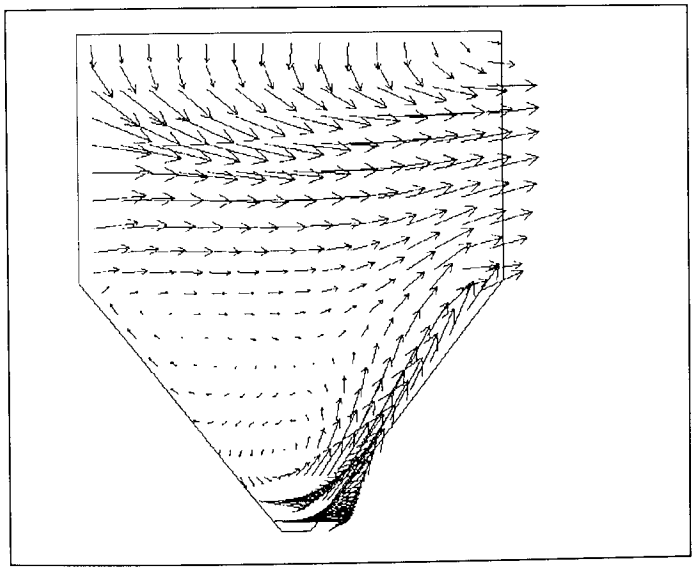

Figure 5-9 Vertical tabs - Junction 33.

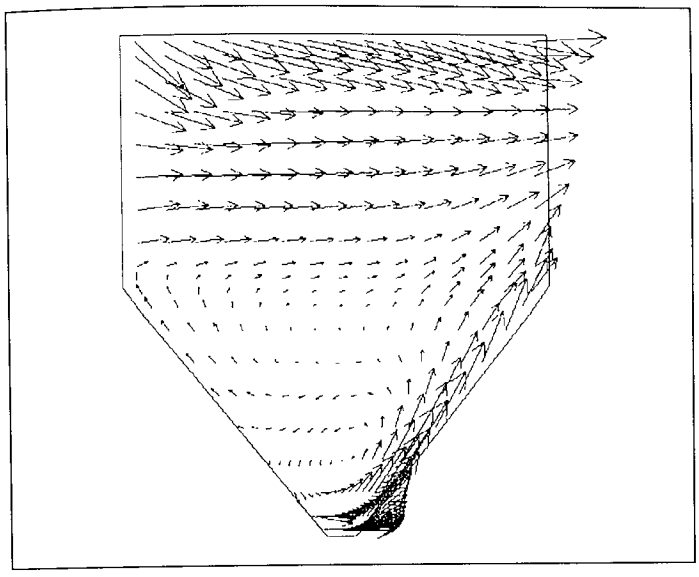

Figure 5-10 Vertical tabs - Junction 55.

5.4 Heat Transfer Modelling

5.4.1 Junction Heat Transfer

Figure 5-11 shows the way in which the heat transferred from the walls to the fluid as it passes through each junction varies for the different models. Initial 'blips' in the heat transfer in junction 22 show up in most models of the new packing. This could simply be due to the rather arbitrary choice of junction numbers at the start of the process. However, by the third junction most models show an increase in the rate of heat transfer when compared to the plain junctions. It is interesting to note that even the slot only model, which has less surface area for heat transfer, can show a higher junction heat transfer than plain junctions. This indicates that the concept behind the new shape is predicted to improve the efficiency of the packing.

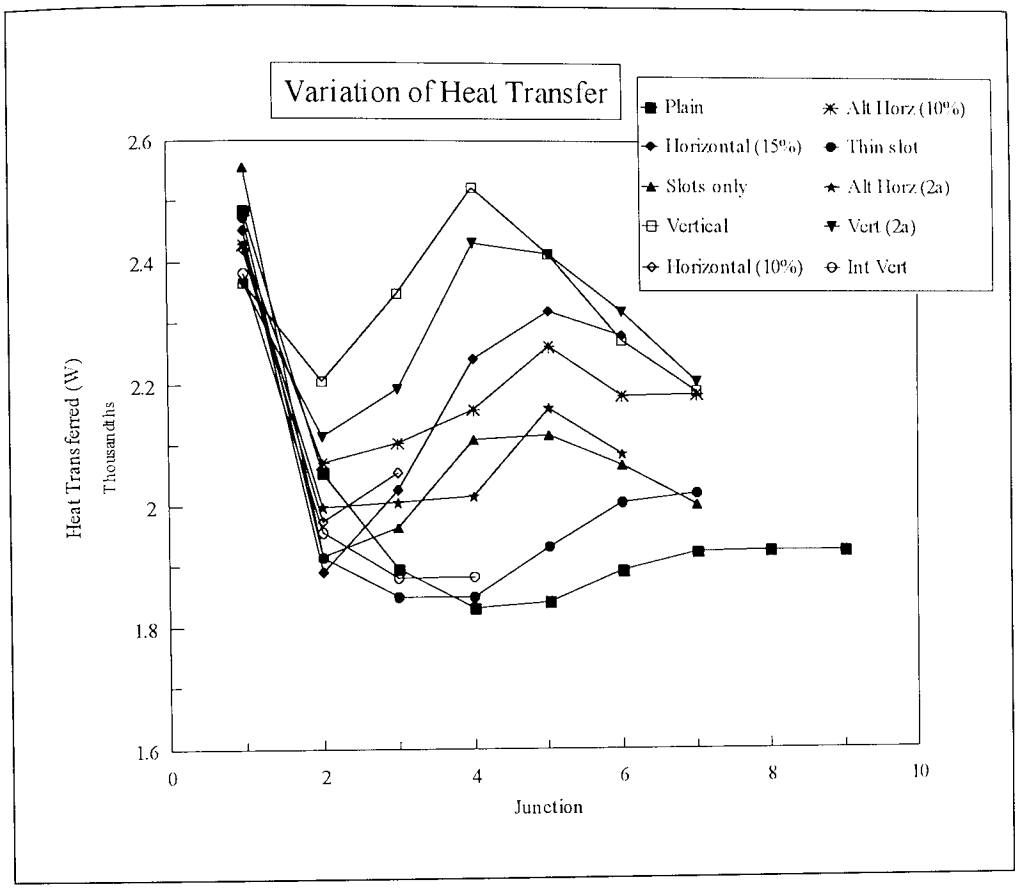

Figure 5-11 Variation of junction heat transfer.

5.4.2 Overall Average Heat Transfer

The same data may be represented slightly differently. By plotting the overall heat transferred/N, the number of junctions, the cumulative effect of this improved heat transfer in individual junctions over the total height can be seen. Figure 5-12 shows this and it can be seen that the new packing shape is predicted to increase the overall efficiency by 5-17%.

The first seven junctions only were considered although this required fourteen simulations in order to get both the main and slot flows, (J11 and J11opp etc.). Also, because of the non-symmetrical predictions of flows, transferring fluid through the slots at the same time as bulk flow through the main inlets/outlets, lead to increases in the total mass flowrate above the mass flowrate at the inlet of the first junction. Once the mass flowrate was approximately 10% above the initial value the simulations were

stopped since results would no longer be valid. Such an increase in mass flowrate occurred around the seventh junction.

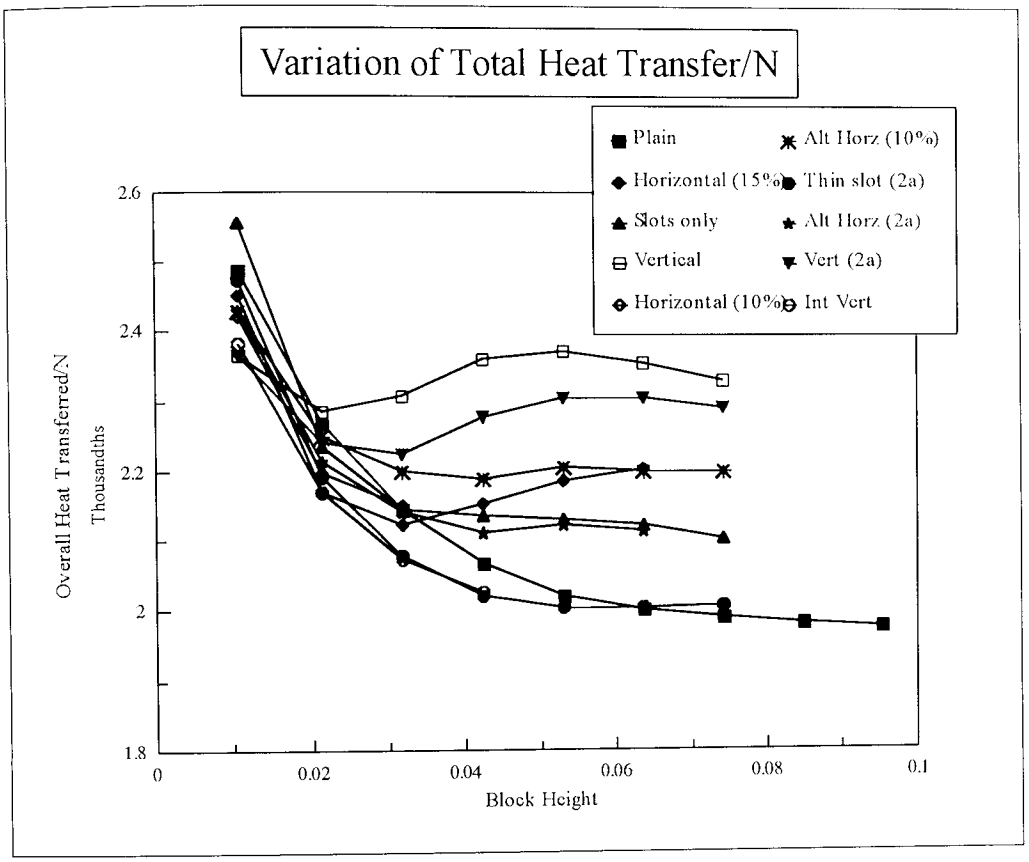

Figure 5-12 Variation of total heat transfer/N.

It has been discussed previously (section 4.8.2) that standard sheet metal structured packings have a higher efficiency if the block height is shorter. However, it is predicted that using the new shape will allow higher block heights to be used with reduced loss of efficiency since many of the new models reach a constant value of overall average heat transfer or even show a slight increase as the block height increases whereas the original model continues to decrease. It is likely that the tabs and slots have a similar mixing effect to that which is achieved when the fluid leaves one block and is redirected upon entering the next block which is turned at 90^{0} to the previous one. A similar mixing effect is accomplished by the Norton packing by turning peaks into troughs and vice versa.

It can also be seen that the different slot inlet boundary conditions have a slight effect on the results. Comparing the two sets of like simulations, vertical tabs and alternate

horizontal tabs, shows approximately 3% greater rate of overall heat transfer when the bulk velocity is ignored. This is explained by the fact that ignoring the bulk velocity at the slots slows the fluid in the apex further, hence allowing time for heating, whereas including the bulk flowrate in the boundary condition increases the speed of fluid in the apex regions. It will be seen later that the effect of the two different boundary conditions has a greater effect on the results of predicted pressure gradient.

5.4.3 Wall Heat Transfer

The heat transfer in the junctions can be investigated in more detail by considering the heat transfer at each wall. Figures 5-13 and 5-14 show the heat transfer rate from individual walls for the models having horizontal tabs and vertical tabs. Comparing these with Figure 4-17 which shows the same results for the original model, it is seen that not only has the rate of heat transfer from all walls been increased, (as expected since the junction heat transfer has increased) but the walls TOP and BOT, at the apexes, are now performing significantly better. This is due to the fact that the driving force in this area has been kept higher. Figure 5-15 shows contour plots of temperature at the centre of the fifth junction for the slots-only model: this should be compared with figure 4-18 for the plain model.

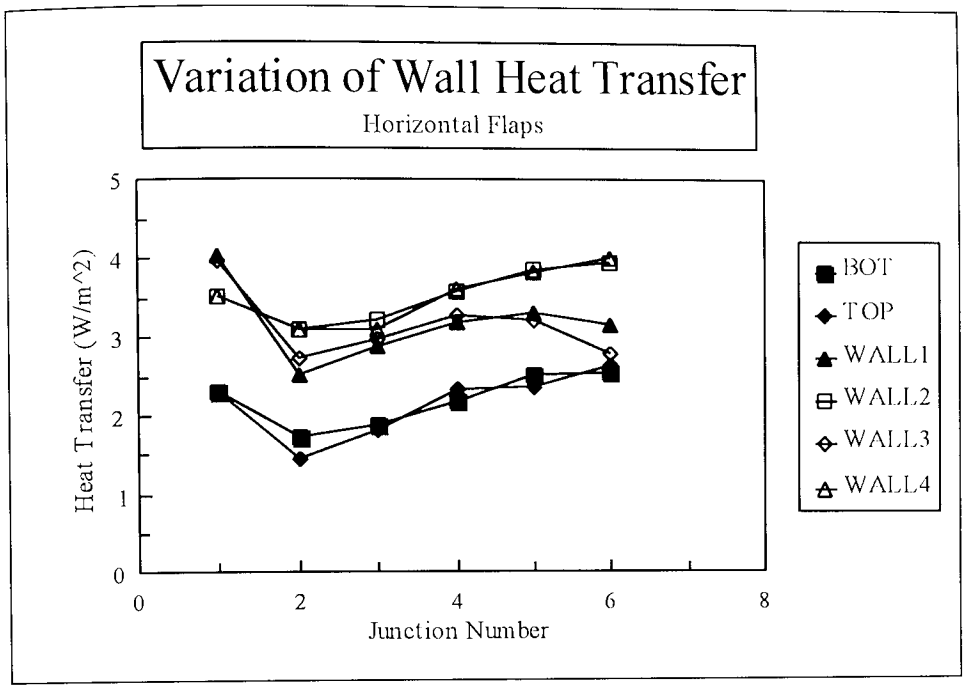

Figure 5-13 Variation of heat transfer at each wall - horizontal tabs.

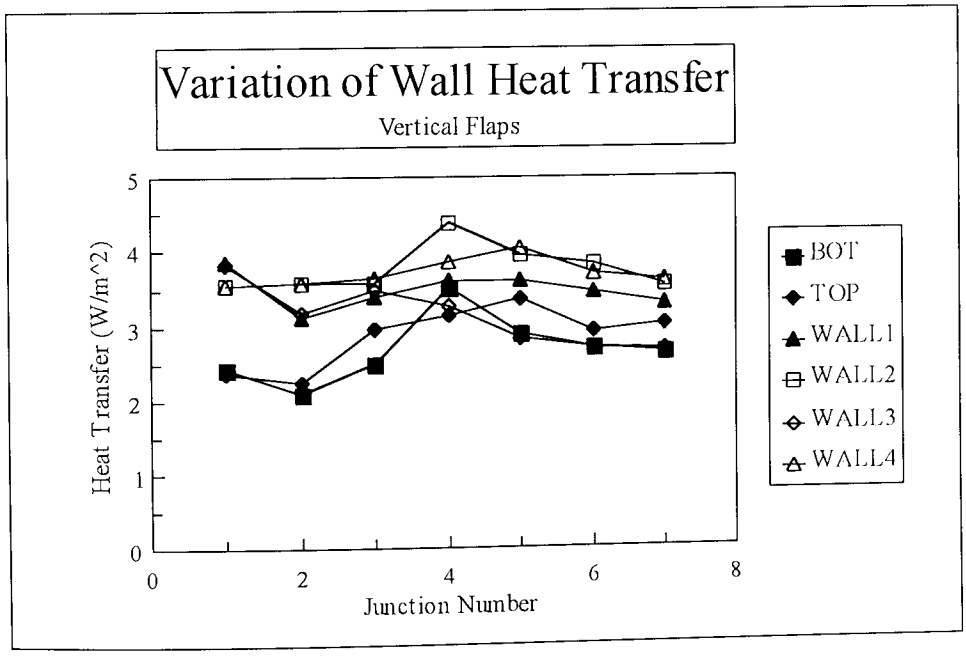

Figure 5-14 Variation of heat transfer at each wall - vertical tabs.

The table gives the value of the heat transfer rate averaged over junctions J11-J66 for each wall, for three models. Heat transfer in the region of the apex has been increased by 50-130%.

	Average Heat Transfer (W/m^2)		
	Plain	Horizontal	Vertical
BOT	1.452	2.198	2.682
TOP	1.236	2.147	2.833
WALL1	2.803	3.180	3.507
WALL2	3.119	3.530	3.811
WALL3	2.648	3.157	3.218
WALL4	2.874	3.533	3.735

Table 5-2 Average wall heat transfer rates.

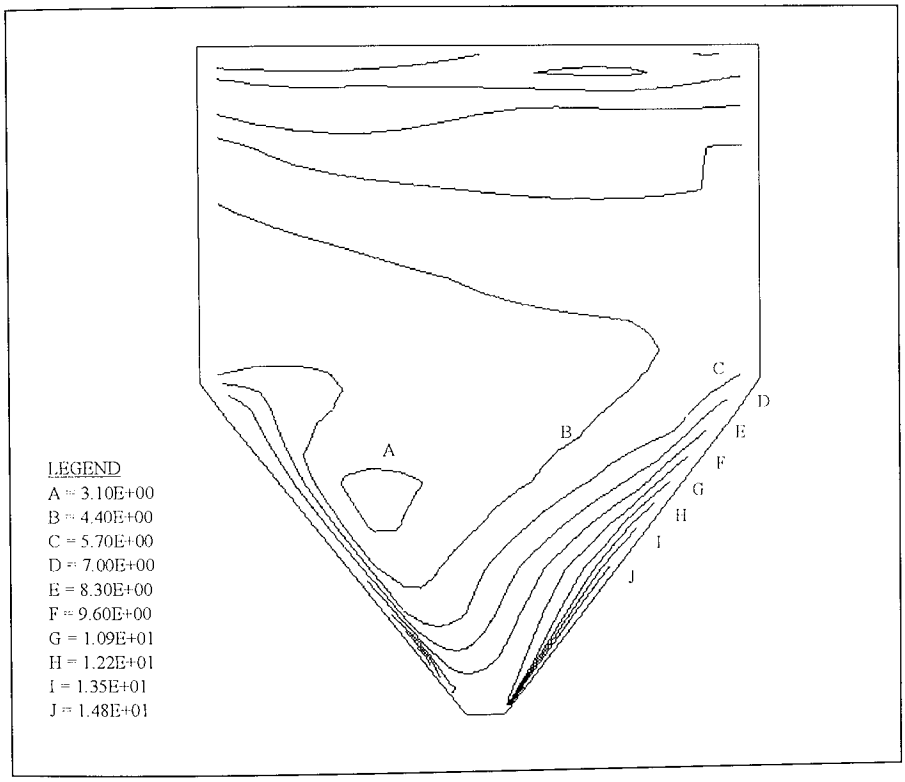

Figure 5-15 Temperature contours centre of 5th junction - slot only model.

5.4.4 Number of Transfer Units

The concept of NTU was not found to be useful in the evaluation of the performance of the new shape. A value could be calculated, taking into account both the main and slot inlets and outlets, but this produced odd results. It was noted that average temperatures of fluid leaving a junction through slot outlets often appeared less than that for fluid entering the junctions through the slot inlets i.e. fluid seemed to cool down. This may be due to the way in which boundary conditions are set in

PHOENICS. Since the boundary condition is added as a source term to the equation, it is not actually on the boundary but at the centre of the first cell. The line of cells in the slot inlet closest to either BOT or TOP will also have the source term for the wall boundary condition. This meant that the average temperature calculated for fluid at a slot inlet was higher than the temperature calculated for the same stream as it left the previous junction, there being no adjacent TOP or BOT wall boundary condition at a slot outlet. Since such spurious results were observed, the value of NTU was not used when assessing the possible advantages of the new shape.

5.4.5 Pressure Drop

As mentioned in section 4.5.3 in reference to the pressure drop predicted for the original plain junction model, the results were not symmetrical about the top and bottom half of the junction when the PHOENICS staggered grid solver was used. Further problems were incurred when predictions of pressure drop for the new model geometries were studied. The cause of the problem became apparent when looking at the velocity vectors at the slot inlets and outlets. One large vector sometimes appeared in one cell at one end of the top inlet slot. It is not known why this should have happened since the vector was not apparent in the corresponding slot outlet, from where the data was taken. Also, the vector was seen appearing at either end of the slot for different sets of simulations. Once the vector started to appear it became self-propagating and simply got larger. A converged solution for the new model shape was not achieved using the alternative CCM solver.

It can be seen from Figure 5-16 that there is a wide variation in the total pressure drops predicted for the different models. Despite the fact that the results may not be reliable it can give us some indication of the worst possible scenario - the pressure may almost triple. It is also seen that the boundary condition on the slot inlets makes a considerable difference in the pressure drop. The model ignoring the bulk flow velocity component at the slot predicts over 50% greater pressure drop than the same model where the bulk flow was included in the boundary condition. This is due to the whole flow through the slot being at 90^0 to the channel flow that it is joining.

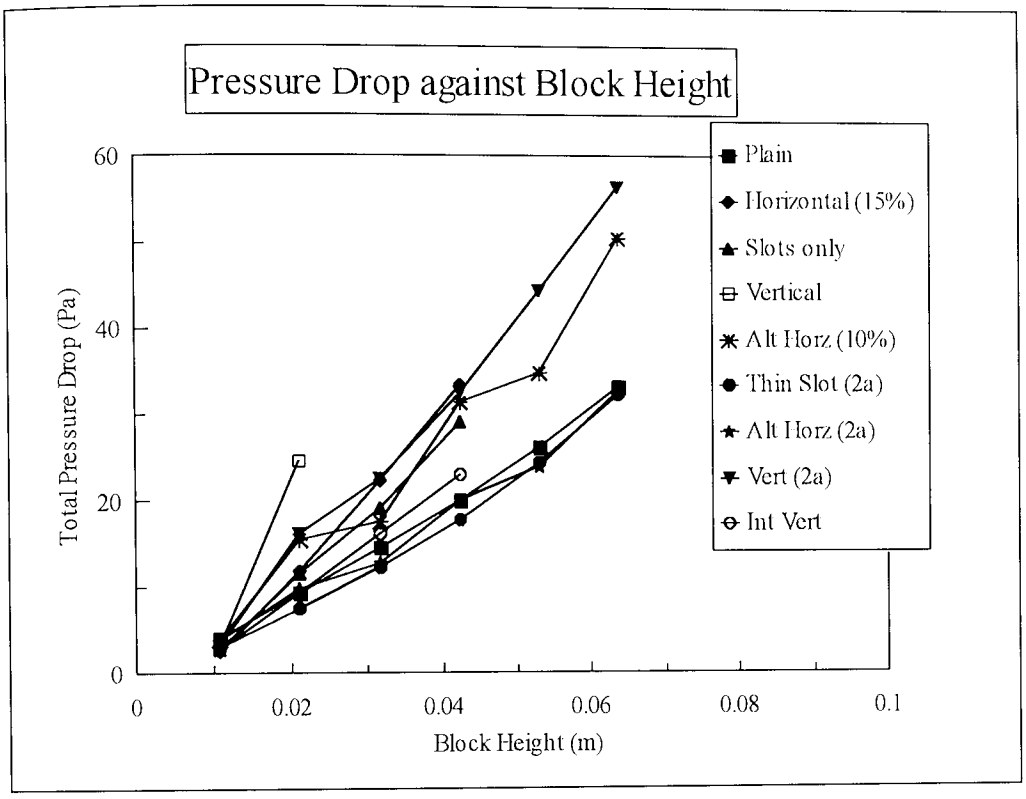

Figure 5-16 Pressure drop predictions for new shaped packing.

5.5 Summary

A new shaped packing, having tabs and slots at the channel apexes, has been devised and a model for it implemented in PHOENICS following the ideas described in Chapter 4. The exact shape of the packing was limited by the gridding capabilities of PHOENICS but various positions of the tab were investigated. It was also found that the results obtained were dependent on the boundary conditions used at the slots and two different conditions were used. The flow patterns produced show that the circulation that develops in standard packing shapes is disrupted by the additional flows and a more even distribution of temperature is obtained. Results indicate that the new packing can increase the overall efficiency by 5-17%. This should result in an economically advantageous packing.

6. EXPERIMENTAL WORK

6.1 Aim of Experimental Work

The experimental work had two main aims. Firstly the effect of block height was investigated. This followed on from the work carried out by Higginbotham (1993). He tested a Tianjin Mellapak 350 m^2/m^3 packing with a block height of 100mm, which is half the standard block height, and found an unexpectedly high separation efficiency. This suggested that reducing the block height of structured packings could be used to increase their efficiency. Tests were needed to confirm such a suggestion. Two Tianjin Mellapak 350m^2/m^3 packings, with block heights of 100mm and 200mm, were tested in the 1 ft diameter test rig designed and built by Higginbotham. This work is discussed in the first section of the chapter.

Secondly it was hoped that the test rig could be used to test any new packing developed in the light of the CFD work, described in chapters 4 and 5. Results could then be compared with those from tests of existing packings, and would give an indication of the success, or otherwise, of designing new packing shapes using the CFD method. In practice, insufficient of the new packing could be made to fill the 1ft diameter rig so this was tested in a smaller scale rig. This work is discussed in the second section of the chapter.

As initial runs of the rig showed it not to be functioning correctly it was first necessary to recommission the rig before tests could begin.

6.2 The Large Scale Test Rig and Experiments Carried Out

6.2.1 Description of Large Scale Rig

A detailed description of the design and operation of the distillation test rig is given by Higginbotham (1993). A brief description is given here. The stainless steel flanged

column, which has a diameter of 1 ft, can accommodate packed heights of up to 2 m. It is designed to operate at atmospheric pressure and can flood packings with a specific surface area as small as 250 m^2/m^3. The size of the rig was the largest possible given the maximum capabilities of the departmental steam boiler and water cooling system. A vertical, shell and tube, thermosyphon steam reboiler is mounted below the bottom of the column. The shell and tube water condenser is mounted below the level of the top of the column to avoid difficulties in placing it near the roof of the laboratory, which means that the reflux has to be pumped back to the top of the column.

A support and access structure allows access to the rig at ground level and two raised levels. A hoist system is included to allow the column to be dismantled and the packing to be changed.

The column was operated at total reflux using the test mixture chlorobenzene/ethylbenzene. The aim of the experiments is to determine the efficiency and pressure gradient in the packing at various flows through it.

6.2.2 Operation of Test Rig

Safe operation of the test facility and data logging are executed by a suite of programmes written in TURBO PASCAL. The computer is situated outside the hazardous area in a laboratory adjoining the flameproof laboratory which houses the test rig. The rig is equipped with four flow meters, twelve resistance thermometers and several pressure measuring devices. Nozzles are provided at various points to allow withdrawal of samples.

6.2.3 Recording and Processing of Experimental Data

Throughout the operation of the rig a wide range of experimental data is logged by the computer. Manual recordings of column pressure drop, steam rate and reflux rate are made. At each different flowrate through the column three liquid samples are

taken; these are of the reflux back into the column, liquid below the packing and liquid below the column bottom. Each sample is analysed using an Anton Paar densitometer and the time period of the U-tube oscillation is recorded from the digital display.

The automatically and manually logged data is finally transferred to a computer containing the programs to process the raw data. These programs were written by Higginbotham (1993) who gives a detailed account of them. The data is processed and various parameters, such as flowrate, expressed as the F-factor, efficiency, expressed as HETP or number of theoretical plates per metre (NTP/m), and pressure gradient are computed.

6.2.4 Recommissioning the Rig

Preliminary runs of the column were carried out. However, results could not be obtained over a wide range of operating conditions and results did not compare well with those obtained previously. The initial hypothesis was that the test mixture had become contaminated in some way; possibly by dirt particles, from the sample bottles, or the packing, or by the grease covering the packings when they are delivered from China. However, these possibilities were ruled out by testing samples from the rig, and pure components and known mixture compositions of chlorobenzene and ethylbenzene in both the gas chromatograph and density meter.

It was discovered that to run the rig successfully the control valves needed to be operated manually. The problem was tracked down to the steam control valve which was not moving between fully open and fully closed but between about 40-80% open. This was due to two burnt out capacitors in the digital to pneumatic converter. C these had been replaced the column was operated successfully.

6.2.5 Packings Tested

The packings tested were the Tianjin Mellapak 350Y with block heights of 200mm and 100mm. The packings are made in the packing factory at Tianjin University in PR of China. The Tianjin Mellapak is basically a copy of the Mellapak packings made by Sulzer.

Prior to the tests suitable wall wiper bands had to be fitted to the 200mm blocks. The ones fitted by the Chinese were of a metal which was too stiff to bend easily and they were also too loose to hold the sheets of packing tightly together. Wall wipers, designed by Higginbotham (1993) were made from brass strip and fitted to the packing blocks with the aid of a large jubilee clip. The wall wiper is needed to prevent wall flow of liquid which significantly reduces the packing's efficiency.

6.2.6 Results

To compare the performance of the various packings the column pressure drop and NTP/m is used. Figures 6-1 and 6-2 show the results of tests on the two different block heights of Tianjin Mellapak 350 m^2/m^3. The results of these tests are shown to compare well with those obtained by Higginbotham. This means that other results of Higginbotham can be used for comparing efficiencies of any new packings tested in the future.

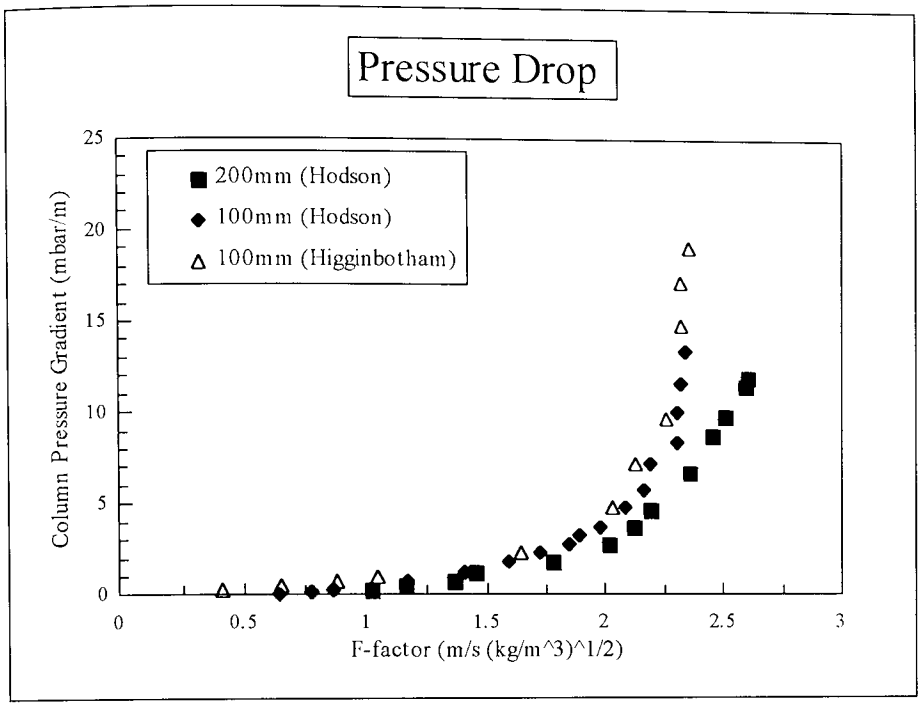

Figure 6-1 Comparison of column pressure gradient against F-factor for two block heights of Tianjin Mellapak 350 m^2/m^3.

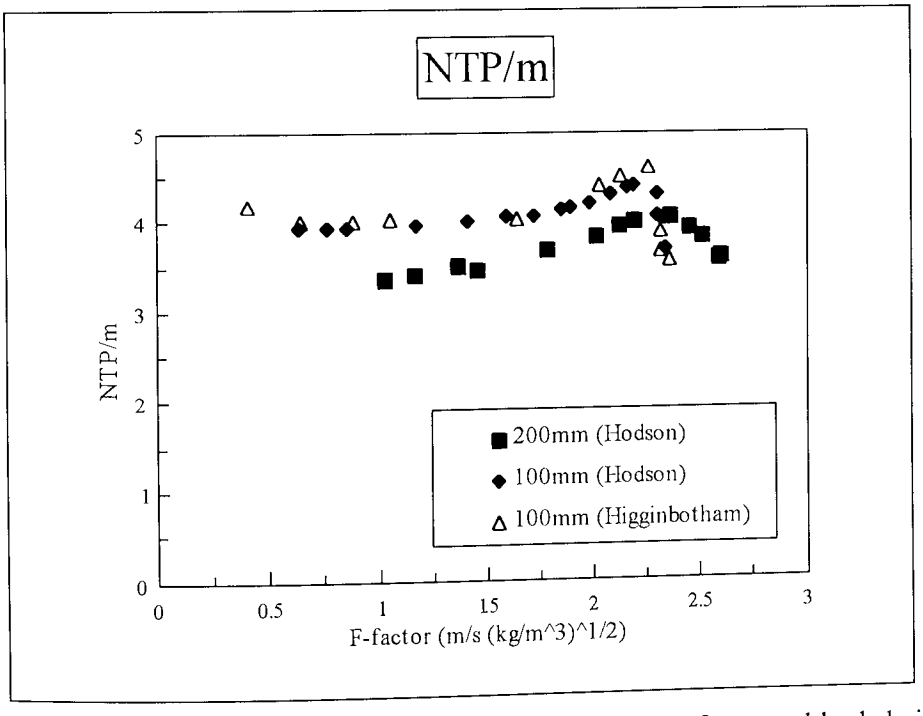

Figure 6-2 Comparison of NTP/m against F-factor for two block heights of Tianjin Mellapak 350 m^2/m^3.

Overall the shape of both the pressure gradient and NTP/m against F-factor plots are the same for both packings. However the magnitude of these values is clearly

dependent on the block height. A shorter block height means that the vapour has to change direction more frequently. This increases the pressure gradient for a given vapour flow. An additional pressure drop is associated with the entrance region of a block where the boundary layer is not fully developed and there is greater momentum transfer to the walls. These results suggest that the total pressure gradient can be split into three component parts: the skin friction, the pressure drop due to changes in direction and the pressure drop caused by entrance effects.

It is also noted that the capacity, or maximum vapour flowrate, is reduced (approximately 11%) by a reduction in block height. It has been suggested (Higginbotham, 1993) that flooding in packed columns starts between the blocks of packing. However, this would imply that flooding would occur at a given vapour rate, regardless of the number of block intersections.

The shapes of the NTP/m plots are typical of a structured packing. At low flowrates the mass transfer efficiency remains almost constant. At higher F-factors, when the vapour and liquid interact (i.e. above loading), the NTP/m reaches a maximum before decreasing sharply as the column starts to flood. It can be seen that the shorter block height has a higher mass transfer efficiency (approximately 14%) suggesting that mass transfer is also higher in the entrance region of the block.

Reducing the block height of structured packing may lead to economic advantages in that the column height and hence capital cost is reduced. However this must outweigh the extra operational cost resulting from the higher pressure gradient.

6.3 Manufacturing the New Packing

6.3.1 The Design Specifications

A design specification for a new packing was made. This was as a result of the predictions of the CFD model that the general principle of mixing fluid between the

apex and central region of the channel corrugation would lead to an improvement in the mass transfer performance of the structured packing. Details of the design are given in figure 6-3.

Given that the tabs are in the plane of the corrugation this design will lead to approximately 13% of the channel cross section being blocked by the tab. This is in keeping with the areas modelled using CFD.

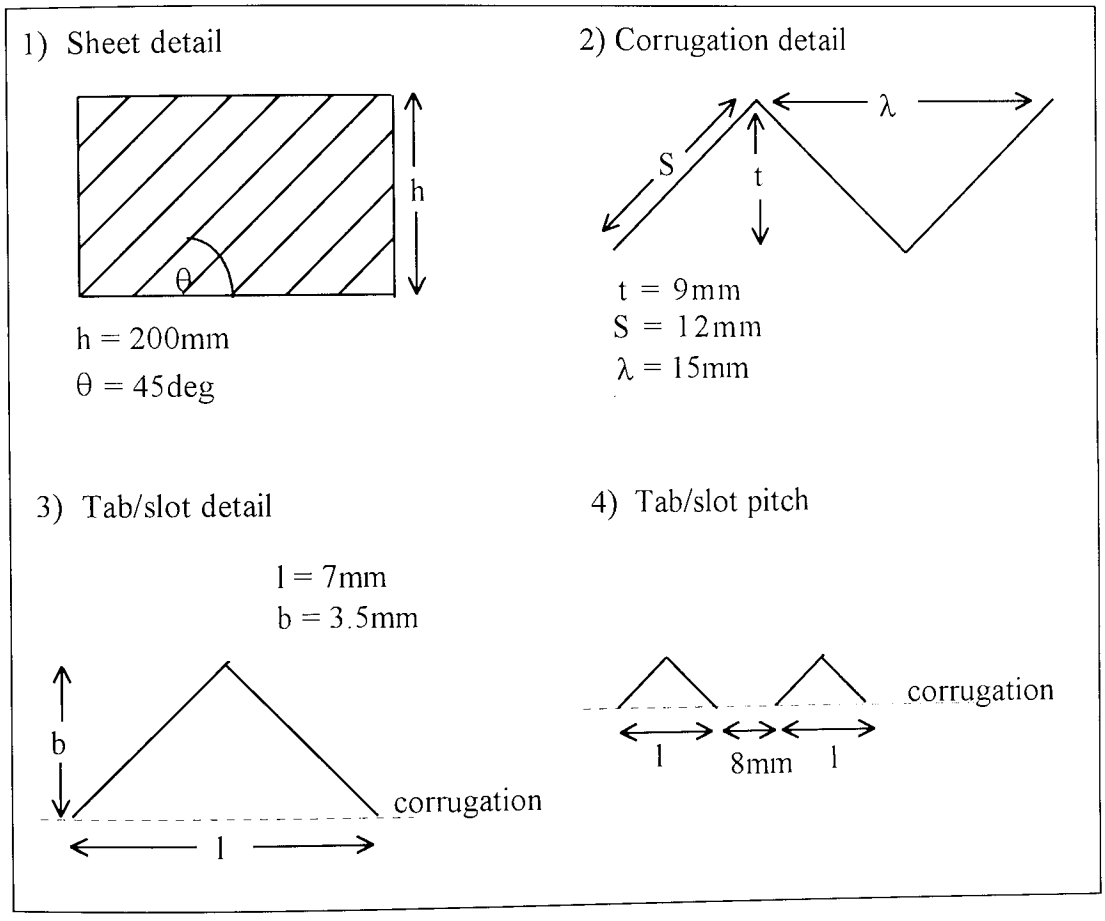

Figure 6-3 Details of new packing design.

In order that the tests would be comparable with others already conducted in the Aston test rig as many features of the packing as possible were kept the same as the standard Tianjin Mellapak 350 m^2/m^3. Stainless steel metal, of 0.17mm thickness, having the fluted surface texture but no perforations was supplied by the Tianjin Packing Factory. The width of strip was 0.24m such that once corrugated a packing block height of approximately 0.2m was achieved.

6.3.2 Manufacturing Method

Two companies were initially approached and discussions held on the feasibility of manufacturing the new shaped packing.

1) Mason and King - a fairly large company in Leicester who supply trays to BOC.
A successful method of manufacturing sheets of corrugated metal having tabs and slots was devised and tested using 0.2mm aluminium sheets as stainless steel from Tianjin had not been received. Briefly, the method involved programming the shape of tab and slot required and then laser cutting the metal sheet. The cut sheet was then corrugated using a tool that was specifically designed to bend only the webs between the slots. Once the first corrugation had been placed the following corrugations were done automatically as the sheet was fed through the tool.

This method of manufacture, although very precise, was also costly due to the time taken to laser cut the slots. Given the approximate cost of the two prototype sheets it was estimated that the cost of manufacturing enough corrugated, slotted sheets to construct packing blocks to fill the test rig would be around £5000. It was anticipated that using the fluted stainless steel metal would be more difficult since it raised the question of exactly where the laser beam should be focused. Hence it was decided that a more 'rough and ready' manufacturing process should be sought.

2) Pugh Engineering - A small engineering firm in Birmingham specialising in metal work.
The manufacturing process devised here was very labour intensive and in the first instance highly unsatisfactory. Briefly, the method involved corrugating the sheets using a tool formed to press out the required corrugations. The edges of each sheet were then cut square before the tabs were punched out. This was done manually, one at a time, by clamping each corrugation in a specially designed jig and hitting a punch through with a hammer. This gave a method of producing sheets of the packing and such a sheet is shown in figure 6-4.

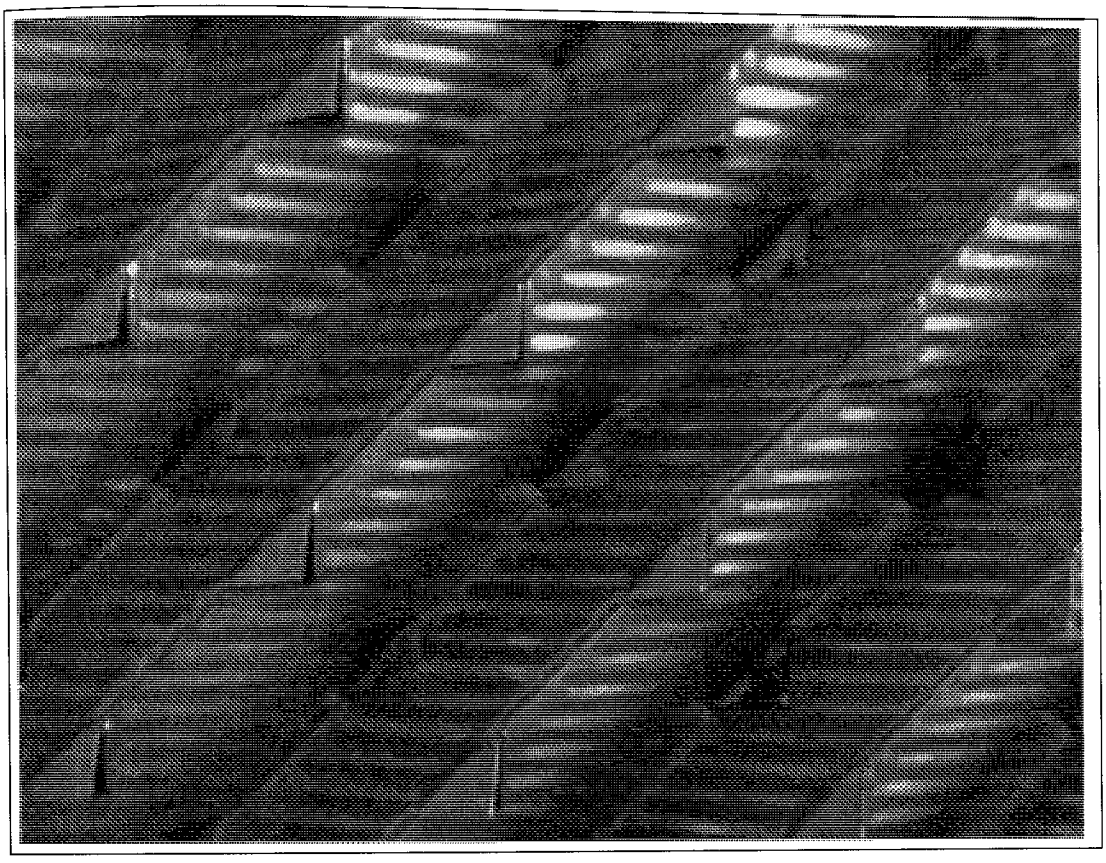

Figure 6-4 A sheet of the new packing.

Further problems were encountered in placing the sheets such that the tabs were correctly aligned in the channel centres. Initially this was due to the poor tolerance in producing uniform corrugations. However, once the uniform corrugations were obtained a method of positioning the sheets accurately was devised. The corrugated sheets were held together by two bolts inserted through the block and a file was used to mark the channel centres on the corrugation apexes of the neighbouring sheets. The blocks could then be dismantled, the tabs punched out and the block reassembled with the sheets in the correct places.

Unfortunately this process was very labour intensive and it became clear that time and money were not available to manufacture enough packing to fill the distillation column previously used to test packings. Another, smaller test rig was designed.

Large scale manufacture of the packing sheet should be possible using a tool and press in a similar manner to which the sheets are corrugated at the Tianjin Packing Factory (see Higginbotham (1993) for description of process). Obviously the tool

would have to be more complex and must allow for tabs protruding from both sides of the sheet. It may also be necessary to have some sort of stripping plate to remove the packing sheet from the tool.

6.4 The Small Scale Test Rig and Experiments Carried Out

6.4.1 Description of Small Scale Rig

The small scale rig was designed and built using QVF glassware around a rectangular steel test section. The column was designed to operate at atmospheric pressure and at total reflux. Figure 6-5 shows a diagram of the apparatus.

It was important to use a similar height of packing to that used in the large rig so that the results were not affected by the inlet zones of the packing, where liquid and vapour may not be fully distributed. The column section was constructed from four pieces of stainless steel plate bolted together to form a square section with sides of 105mm. A chemical resistant sealant was used to seal the joins. The height of the steel column was 2m. This was attached to 6" flanges drilled to match the QVF flanges. The reboiler section consisted of three flameproof electrical reboilers, each of 6kW. Two were vertical thermosyphon reboilers and the third was a horizontal pool boiler. The heating capacity of the reboilers was calculated to vapourize sufficient liquid to flood a Tianjin Mellapak 350m^2/m^3 packing. The column section and reboilers were lagged to minimise the heat losses. The condenser was mounted vertically above the column and reflux divider. It was supplied with cooling water from the mains supply. A distributor having four drip points was made so that the liquid was distributed evenly over the top of the packing.

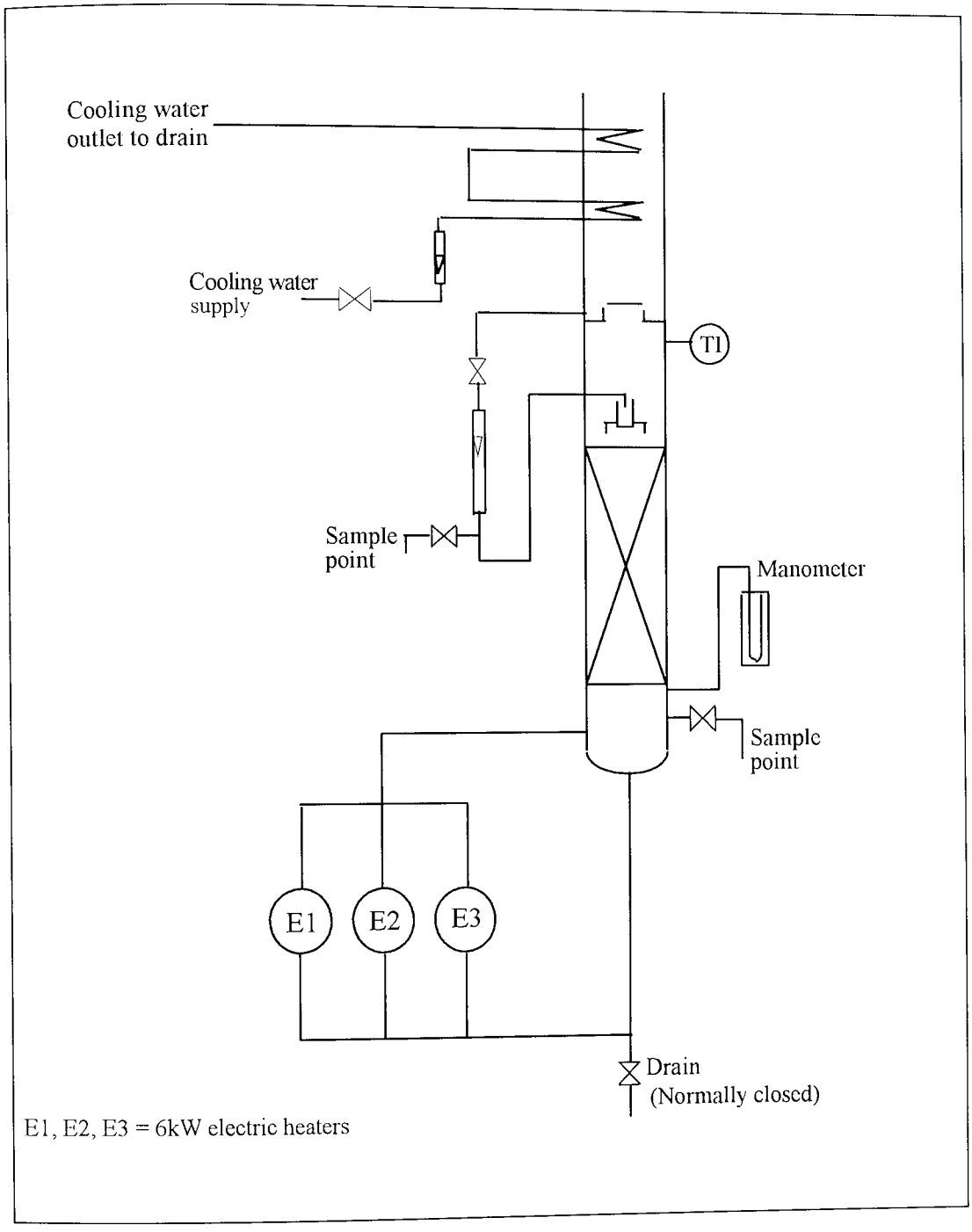

Figure 6-5 Flowsheet of the small scale test rig.

6.4.2 Operation of the Test Rig

The test rig could be run safely by one person. The control panels and isolating switches for the electrical reboilers were mounted outside the flameproof area. The power to both the thermosyphon reboilers could be varied, whereas the third reboiler was either on or off.

The flowrate of the liquid reflux was measured by a rotameter before being returned to the top of the packing. A P550 platinum resistance thermometer was used to measure the temperature at the top of the column.

Two nozzles were provided to allow samples to be taken above and below the packing. The pressure drop was measured using a manometer. A nitrogen purge was supplied from a cylinder, set to 0.5 barg, to purge the lines to the manometer.

6.4.3 Recording and Processing of Experimental Data

Throughout the operation of the rig data was logged manually every ten minutes. The flowrate of reflux through the rotameter, the column pressure drop and the top temperature were recorded. The column was allowed to reach equilibrium for a given power setting of the reboilers and once the readings taken were constant the samples were taken. The top sample was taken from the reflux return line to measure the composition just above the packing. The bottom sample was a vapour sample taken just below the bottom of the packing.

The samples were analysed using an Index Instruments automatic refractometer GPR 11-37-X. The densitometer which had been used previously was found to be non-operational. The refractometer was calibrated using standard mixtures of chloro-/ethylbenzene made up by weight using 4 place scales. A logarithmic curve fit was used to fit the calibration points.

The data recorded during the operation of the test rig was entered into a spreadsheet. Parameters such as the F-factor and HETP could then be calculated from the data.

6.4.4 Packings Tested

Two packings were tested. These were the new packing and the Tianjin Mellapak. The Tianjin packing was tested to give a comparison of the performance of the new packing, and a comparison between the results obtained from the two test rigs. The

block heights of both packings was approximately 200mm. Brass wall wiper bands were used to ensure that the blocks fitted tightly against the column walls.

6.4.5 Results

Results obtained for the packings tested in the small rig are shown in figures 6-5 and 6-6. A full set of results for the first test, carried out on the new packing, was not obtained. This was because one of the electrical reboilers was not properly connected and this fact was not discovered until the second test run. In the limited time available it was felt it would be better to obtain data for another test run rather than repeating the first data set. The new packing was put back into the column upside down as compared to the design, i.e. the tabs were pointing up the column, rather than down as illustrated in Figure 6-4. This configuration was not modelled using the CFD model although in the model in which the tabs are vertical the tabs would appear the same to the vapour flow regardless of its direction in relation to them. The flow pattern would not be as predicted by the model though since the slots would be on the reverse side of the tab rather than below it as modelled.

The only packing which was actually observed to be flooding was the new packing when it was upsidedown. This was reasonable as it was expected that the capacity of the new packing would be less than that of Tianjin Mellapak. The actual power of the reboiler section, after heat losses, may not have been sufficient to flood the Mellapak packing. The true capacity of the new packing can only be estimated because the reflux line at the top of the column was too small. A maximum reading was recorded on the rotameter and the remainder of the flow was through the centre of the reflux divider. The capacity of the Mellapak was estimated from heat losses because the tests at higher flowrates were carried out after the reboilers had been correctly connected and it was known that this provided an additional 4kW.

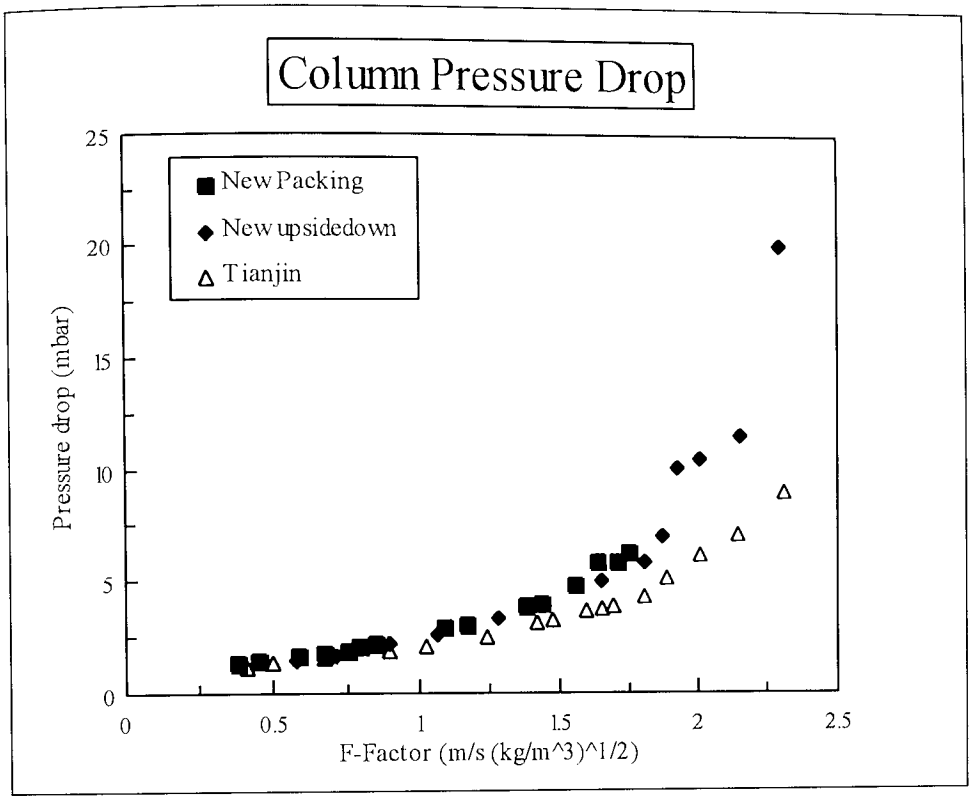

Figure 6-5 Column pressure drop for packings tested in small rig.

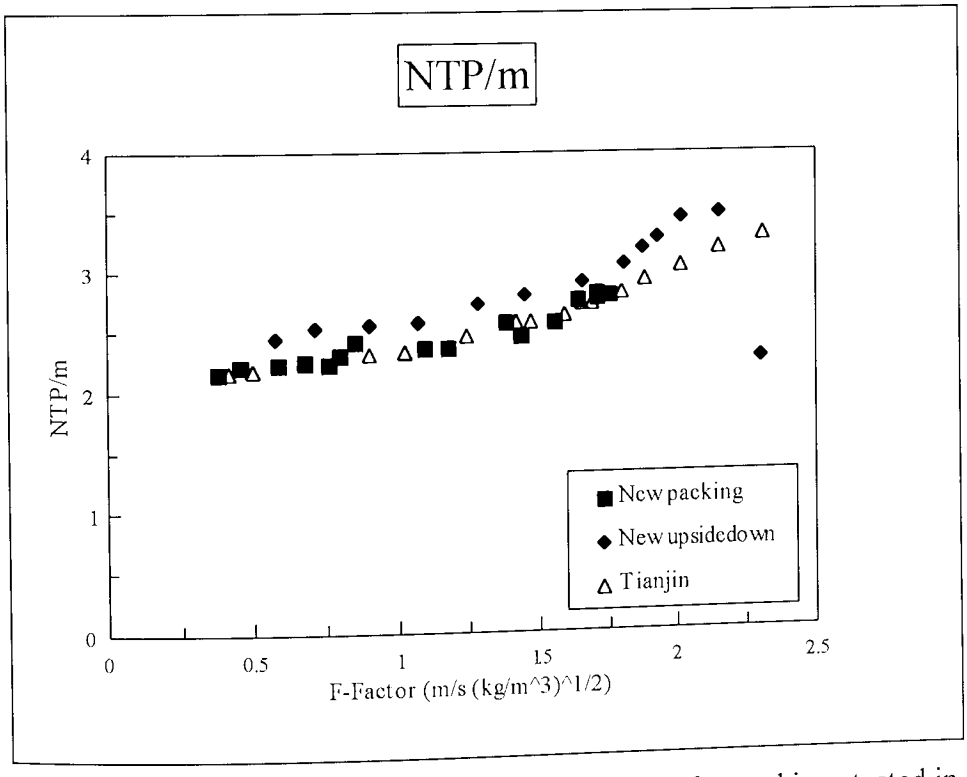

Figure 6-6 Number of Theoretical Stages per metre for packings tested in small rig.

The number of theoretical stages per metre of packing for all packings increases as the vapour flowrate increases. In general structured packings have a relatively constant

value of NTP/m with flowrate except in the region close to flooding. Results for the new packing compared with the Tianjin packing do not show any difference in efficiency and the pressure drop is higher for the new packing. However, placing the new packing upside down gave an increase in efficiency by approximately 10% over the whole range of operation. The pressure drop is higher than the Tianjin Mellapak. The pressure drop was expected to be higher since the tabs are partially blocking the vapour flow channels. The flow patterns of vapour and liquid which result in an improved efficiency can only be postulated since to model the situation using CFD would require a two phase model. It may be that it is the liquid rather than vapour that passes through the slot. As vapour flows up over the tab liquid may be sucked through the slot and sprayed from the tab point by the upward flow of vapour. Such a flow would increase the surface area of liquid and lead to improved mass transfer between the two phases.

Figure 6-7 shows the comparison between the results of NTP/m for the Tianjin Mellapak packing tested in both rigs. It is possible that the results presented for NTP/m are affected by wall flow, or corner flow, despite the fact that suitable wall wiper bands were used and the packing was a tight fit inside the column. It was found be Higginbotham (1993) that wall flow could reduce the NTP/m by up to 25%. This is supported by the fact that the NTP/m obtained from the small rig is approaching that obtained in the large rig as flooding is approached. Fair (1988) suggests that the smallest column that can be used to obtain reliable results on the performance of structured packings is 100mm. The experimental results from this study indicate that a larger column should be used. Although the results from the small rig do not compare well with those obtained in the large rig the conditions for all three test runs using the small rig were the same so comparisons between these results can be made.

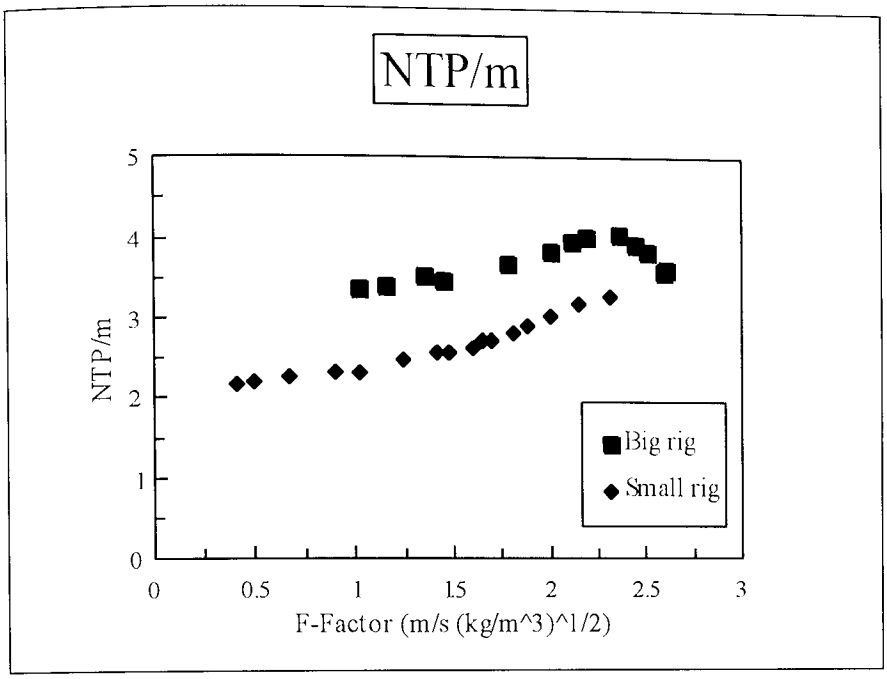

Figure 6-7 Comparison of NTP/m for Tianjin Mellapak tested in two rigs.

6.5 Summary

Experimental tests on structured packings have been carried out using two different distillation rigs. The effect of block height was investigated using a 300mm diameter column. A shorter block height gave an increased separation efficiency of approximately 14%, but for a higher pressure drop. The capacity is reduced by approximately 11%.

A new structured packing with tabs and slots was designed and manufactured. A 100mm column was designed and built in order to test the new packing. An improved separation efficiency of approximately 10% was shown when the tabs were pointing up the column in the same direction as vapour flow. The pressure gradient for the new packing is higher than that for the standard Tianjin Mellapak packing.

7. DISCUSSIONS AND CONCLUSIONS

Currently the design of structured packing is more of an art than a science with new shapes developed from intuitive guesses. This is costly and time consuming especially if no improvement is found once experiments have been carried out. The main aim of this work has been the development of a model for structured packing using the technique of computational fluid dynamics. The aim is that by using CFD the design of packings can be more scientific and shapes can be 'tested' by a computer model, rather than in a laboratory experiment.

It appears that the idea of using CFD to model structured packings is fairly new and no detailed model has been published in the open literature. However, the very competitive nature of the structured packing business means that the major research into their performance may be undertaken by the vendors themselves who would obviously not wish to divulge any competitive lead they may have come up with.

It seems that CFD is booming at the present time and many companies sell codes. However, although it is used for modelling many situations it can not provide answers to all problems. In fact, some mathematicians decry the whole concept of being able to represent highly non-linear differential equations by linear equations, which is the basis of the finite volume technique and used by the code chosen for this work. Although commercial CFD packages have been being developed for around fifteen years, and have been used extensively it would be naive simply to believe the results one obtains. The equations involved are highly complex and interlinked but this can easily be forgotten by the user since the CFD packages endeavour to hide this fact behind simple graphical interfaces.

The use of CFD in the chemical process industries is increasing but complaints of difficulties with gridding complex shapes and modelling of complex phenomena are common. The first problem may be eased by the use of specialised grid generation packages but the second can only improve with increased understanding of the process involved.

7.1 Simplifications

The process of distillation taking place inside structured packings is very complex and involves not only two phase fluid flow, but also heat and mass transfer. The development of the model requires many assumptions to be made in order to make a model possible.

The idea behind the development of the CFD model presented in chapter 4 is to use the regular structure of the packing to simplify the region that needs to be modelled. Rather than modelling a large area of packing the region is reduced to one intersection of the channels since the packing block is composed of many such junctions, all of which have the same geometry. The model implemented within the CFD code is further simplified in that it considers the flow of one phase only - the vapour. Also the model does not include mass transfer. Heat transfer is used to give an indication of the profiles developed inside the channel of the packing. Further development of the model could include a mass transfer element modelled in conjunction with heat transfer.

Structured packings are not usually made from plain sheet metal; the surface is textured in some proprietary way in an attempt to increase the efficiency. Such surface texture, or the interface between the two phases, is ignored in this model, but a suitable wall boundary condition could allow for such an effect. Also, since the model only considers flow of fluid on one side of the sheet the effect of holes are ignored. The actual effect of the holes, either quantitatively or qualitatively is not known or understood. If a larger section of packing was modelled this could be investigated.

Such simplifications mean that the model cannot give quantitative results that can be compared directly with experimental ones. However, as with many new developments it is possible to qualitatively assess the results in the light of experimental data and conclude how the model may be improved and developed at a later stage.

7.2 Problems and Limitations

Any new method must inevitably encounter a number of problems and this case was no exception. A major reservation that must be placed on the results is due to anomalies thrown up by the CFD package itself. Although the problem posed was a symmetrical one the predicted pressures and velocities were not symmetrical. Also predictions of pressure and velocities differed depending on the orientation of the grid with respect to the axis. This was observed when using the standard PHOENICS staggered grid technique. Although the more recently developed CCM method, which uses a cell centred method, did predict symmetrical results it was only possible to use this method with the basic model. The method proved to be very unstable with the addition of extra boundary conditions which were introduced as part of the model described in chapter 5. These simulations could not be made to converge. Ideally such problems with the CFD code would have been investigated by using a number of different codes to model the same problem. However, it was not the aim, nor within the scope of this project, to investigate the various CFD packages or the mathematical techniques employed.

Another problem relates to the calculation of mass flowrates and those reported in the RESULT mass balance section. Pressure must influence the flowrate through a boundary but this should also relate to the velocity vectors through that boundary. With the addition of inlet and outlet boundary conditions at 90^0 to the bulk flow the mass rate through these boundaries had to be calculated from cell pressure data rather than velocity vectors in order that the mass balance corresponded to that given in RESULT.

It would be desirable to be able to model a larger portion of the packing such that the slots were not modelled as inlet and outlet boundary conditions but as a gap in a wall. This would allow an investigation into how the two neighbouring stream flows interact. The model predicts these flows to be of different velocities since one is at the apex and the other the centre. This is not accurately accounted for in the model

using a single junction, instead two extremes are considered for the boundary condition.

Modelling of the new shaped packing was limited by the capabilities of the grid generator. The shapes actually modelled did not include several of those thought up since it was not possible to grid such shapes. It may be possible to use a more general grid generation packing to accomplish this but only once a suitable interface between the grid generator and PHOENICS exists.

7.3 Current State of Structured Packing Models

The published literature relating to structured packings is increasing and experimental test data becoming more widely available. From such results several groups of workers have developed comprehensive models that correlate important parameters involved in packed column design. These models can now give predictions of packing performance in all operational regions from below loading up to flooding. However, since these models are validated against data from tests on a limited number of packings (possibly only one) and using a limited number of test mixtures they have a narrow range of application i.e. they can only safely be applied to that packing. The models generally include a factor that accounts for differences in predicted and experimental results; this may be for a family of packings or just one size. This limits these models to use on existing packings. Since they do not include effects of geometrical features etc. they cannot predict the performance of a new packing. Some include the corrugation side length, which is a characteristic length of the packing e.g. Rocha et al. (1992). The models do not allow for effects such as block height. Hughmark's (1986) method of splitting the pressure drop could be developed further to account for the various contributions to the overall pressure drop (section 6.2.6). The other model which has a different basis is the block model of Stoter et al. (1993) but this again uses experimentally obtained friction factors, and does not attempt any solution of the Navier Stokes equations. Otherwise this has the basis of a more fundamental, equation solving method rather than a correlation.

7.4 Current State of Structured Packings

The majority of structured packings are based on the same shape and this dates back to 1965 as Sulzer's first gauze Mellapak. Many patents have been published regarding structured packings but overall the difference in performance is minimal. The Norton packing IMTP gives good performance and is one which uses a novel design whereby peaks become troughs, and vice versa, within the height of a block. Other than that the new inventions have only been slight modifications of the standard sheet. Jaegar Max-Pak has already used the idea of tabs and slots but these are in the side wall of the channel i.e. parallel with the flow direction, rather than at the apex as in the new shape described in chapter 5. The benefit is said to be that such tabs are positioned at specific places and allow a weaving flow path and create drip points for liquid. The nested packing described by Yeoman (1994) will have the effect of disrupting the vapour/liquid flow at the channel apexes. It is not clear if this was the main intention of the design or whether it was merely intended to increase efficiency by increasing the specific surface area. Sulzer's new packing Optiflow, which the vendor literature states has been optimised using CFD, is the most radically different new packing although even this starts life as the standard shape before a large amount of metal is removed. However, this does then allow for more than one direction for vapour flow.

Major improvements in structured packings along the lines of the standard channel shapes have probably been exhausted, and such improvements will have to come from a radical new concept of packing.

7.5 Results and Predictions

Since the results of the computational model are as yet only preliminary and cannot be said to represent the full distillation process in any way it is not possible to make any quantitative comparison with experimental results. However, one statement that can be made in the light of the results and observations of temperature contours is that the highest rates of heat transfer, and by analogy mass transfer, take place in junctions

with the lowest number. This is where the driving force between the wall and fluid is highest and the boundary layer is not fully developed. This implies that the effect of shorter blocks is to increase the separation efficiency, as shown in section 4.8.2. This is confirmed by the experimental work (figure 6-2) which showed that for Tianjin Mellapak 350 halving the block height increased efficiency by 14%. This is also supported by results published by Bauermann and Benhamou (1983) and Billet and Mackowiak (1988) who both tested Montzpak B1-300. Nutter (1987) state that the block height is 203mm whereas Bauermann and Benhamou give it as 125mm. Comparison of their results show that the shorter blocks had a 5-10% higher efficiency.

However, the computational predictions of pressure drop are not reconcilable with those from experimental work. The CFD predictions are that the junction pressure drop increases as the junction number increases. This is the opposite effect to what would be predicted in pipe flow where there is an additional pressure drop associated with the entrance region (Sparrow (1964)). This means that the CFD predicts that a shorter block height would have a lower pressure drop. This is even so if the extra pressure drop associated with the block intersections is included by the addition of 0.075mbar per intersection that is estimated by Higginbotham. This value is too small to affect the overall trend that the CFD predicts smaller blocks (i.e. more block intersections) to have a lower pressure drop. Experimental results show that in fact the taller block heights have a lower pressure drop.

Experimental results also show that the capacity, or maximum vapour throughput, is reduced by a reduction in block height. Tests on Tianjin Mellapak showed a reduction in capacity of 10-12% and comparison of the two sets of results, previously mentioned for Montzpak, show a 15% lower capacity for the shorter block. This is in contrast to the statement made by Higginbotham that the capacity appeared to be unchanged. He also suggested that flooding occurs between the blocks and that increasing the number of block boundaries would not change the flooding velocity. These results show this not to be true.

7.6 Packing Development

The new shaped packing was developed with the aim of enhancing heat and mass transfer by keeping the driving forces high. To do this additional flow paths are created for the fluid at 90^0 to the direction of flow to increase mixing. The results of the CFD model shows that this would increase the efficiency by 5-17%. It is not known from the CFD results what effect on capacity the new shape will have. However, it might be expected, due to the more tortuous flow path and higher pressure drop that the capacity will be reduced. This was confirmed experimentally. Experimental results for the new packing also show that the separation efficiency can be increased by approximately 10% if tabs are pointing in the same direction as the vapour flow.

7.7 Final Conclusions

1. A comprehensive survey of the CFD vendors and the capabilities of a wide range of commercial packages is presented.

2. The use of CFD can increase understanding of the processes occurring within structured packings. However, the results must be carefully investigated and treated with caution.

3. Structured packings have regular shapes and this has been exploited as the basis of a CFD model. Rather than computing results for a large area of structured packing a single intersection, or junction, between channels has been modelled and successive simulations performed.

4. The CFD model of standard Mellapak type packing predicts:

    i) A circulating flow pattern develops due to the interaction of the two streams.

ii) Fluid temperature reaches equilibrium with the walls in the apex region of the channel.

iii) Heat transfer rates fall as the junction number increases. Therefore a shorter block height will have higher efficiency.

iv) Pressure drop increases as junction number increases.

5. Experimental tests of Tianjin Mellapak 350 m^2/m^3 with block heights of 100mm and 200mm show that with a shorter block:

i) NTP/m is increased (HETP reduced), i.e. higher separation efficiency.

ii) Pressure drop is increased.

iii) Capacity is reduced, i.e. flooding velocity is lower. Therefore the number of block intersections does affect the flooding velocity.

6. The CFD model of the newly devised structured packing predicts that:

i) Circulations are disrupted by the additional flow directions.

ii) Driving forces are maintained higher by mixing regions of cold and hot fluid.

iii) Heat transfer is increased.

7. Experimental tests of Tianjin Mellapak and a new packing both with block heights of 200mm show that:

i) The new packing has a higher pressure drop.

ii) Capacity is reduced by the new packing.

iii) The new packing with the tabs pointing down shows no improvement in separation efficiency.

iv) The new packing with the tabs pointing up provides a 10% improvement in separation efficiency.

8. A new shaped packing devised with the aid of the CFD technique may have economic advantages since the efficiency is increased.

9. Manufacture of the new shaped packing is difficult without the investment of time and money.

7.8 Suggestions For Further Work

It is important that before the model is developed further the CFD package and the mathematical technique being used give consistent and believable results. This can be done by using a variety of the commercially available packages to perform the same problem.

Various properties of current packings, such as surface texture and particularly perforations, could be investigated by modelling a larger portion of packing. This could be done if a suitable grid generation package was used. These effects could then be incorporated into the model using the single junction.

The model should ideally include both phases since in reality two phases are present within the structured packing. However, modelling of two phase flow is at present difficult (or impossible). It may be possible though to include a wall boundary condition that mimics the effect of the second phase and accounts for mass transfer related to heat transfer. It would need to include some equilibrium data in order to do this. Results could then be used to predict HETP. However, it is unlikely that the present state of knowledge regarding the phenomena of two phase flow and turbulence could provide a complete model of the distillation process.

Due to the unexpected differences in performance of the standard packing when tested in the large and small column the new packing should be tested in the large column. These results should also be compared with the CFD model.

Both the theoretical and practical experimentation should be carried out using a different geometry packing. This will allow further verification of the method.

NOMENCLATURE

Greek Letters

ρ_g	Density, gas phase	(kg/m^3)
γ	contact angle between solid and liq film	(deg)
π	3.14159.....	
ρ_l	Density, liquid phase	(kg/m^3)
ϕ	general variable, crimp half angle	
σ	Surface tension	(N/m)
ξ	Flow factor function	(-)
μ	Dynamic viscosity	(kg/ms)
δ	Film thickness	(m)
Γ_ϕ	general diffusion coefficient	(m^2/s)
δ^+	Dimensionless film thickness	(m)
S_ϕ	general source term	
λ	wavelength of corrugation	(m)
α	Fraction of pressure drop producing shear	(-)
τ	Shear stress	(Pa)
ε	Rate of dissipation of turbulent kinetic energy	

a	specific area of packing	(m^2/m^3)
a	Finite volume equation coefficient	
a_e	Effective interfacial area	(m^2/m^3)
a_h	Wetted/hydraulic area	(m^2/m^3)
B	specific liquid load	(m^3/m^{2}h)
C	general constant	(-)
C_E	Correction factor	(-)
c_G	Gas capacity factor $u_{gs}\sqrt{\rho_g/(\rho_l-\rho_g)}$	
c_L	Liquid capacity factor $u_{ls}\sqrt{\rho_l/(\rho_l-\rho_g)}$	
c_p	Specific heat capacity	(J/kgK)
D	Diffusion coefficient	(m^2/s)
d_e	Equivalent/hydraulic diameter	(m)
$(dp/dz)_{irr}$	Irrigated pressure drop	(N/m^2)
$(dp/dz)_{dry}$	Dry bed pressure drop	(N/m^2)
$(dp/dz)_{flood}$	Flood point pressure drop	(N/m^2)
E	East face of PHOENICS cell	(-)
EL1	Length scale	
ENUT	Turbulent, or eddy viscosity	
EP	Rate of dissipation of turbulent kinetic energy	
f_1, f_2, f_3	multiplying factors in Sp+M model	(-)
F_p	Packing factor	(m)
F_v	F-Factor $u_{gs}\sqrt{\rho_g}$	(m/s (kg/m^3)$^{1/2}$)
G	Gas mass flowrate	(kg/s)
g	Gravitational constant	(m/s^2)
H	High face of PHOENICS cell	(-)

h	block height	(m)
h_l	Liquid Hold-up	(m^3/m^3)
$h_{l, fl}$	Liquid hold-up at flooding	(m^3/m^3)
h_o	Liquid hold-up below loading	(m^3/m^3)
K	Constant	(-)
k	Turbulent kinetic energy	
k	Thermal conductivity	(W/mK)
KE	Turbulent kinetic energy	
k_g	Mass transfer coefficient, vapour phase	(m/s)
k_l	Mass transfer coefficient, liquid phase	(m/s)
L	contact length	(m)
L	Liquid mass flowrate	(kg/s)
L	Low face of PHOENICS cell	(-)
l	specific liquid load	(m^3/m^2s)
m	Slope of Wallis diagram line	(-)
N	North face of PHOENICS cell	(-)
P	PHOENICS cell centre	(-)
P	Pressure	(N/m^2)
PHASEM	Mass of phase in cell	(kg)
PRT	Turbulent Prandtl number	
S	Side length of corrugation	(m)
S	South face of PHOENICS cell	(-)
T	PHOENICS time step	(s)
T	Temperature	(^0C)
t	time	(s)
t	corrugation depth	(m)
u	velocity component	(m/s)
u	x-direction velocity component	(m/s)
u^*	Shear velocity = $\sqrt{g\,\rho}$	(m/s)
u_g	vapour velocity	(m/s)
$u_{g, flood}$	Vapour velocity at flooding	(m/s)
u_{ge}	Effective velocity, gas phase	(m/s)
u_{gs}	superficial vapour velocity	(m/s)
$u_{l, eff}$	Effective velocity, liquid phase	(m/s)
u_{ls}	superficial liquid velocity	(m/s)
u_s	Superficial velocity	(m/s)
v	y-direction velocity component	(m/s)
W	West face of PHOENICS cell	(-)
w	z-direction velocity component	(m/s)
x	distance	(m)

Dimensionless Groups

Fr	Froude number	$u^2/d_{eq}\,g$
Re	Reynolds number, liquid phase	$(\rho_l\,u_{ls}\,d_e)\,/\,\mu_l$
Sc	Schmidt number	$\mu/(\rho\,D)$
Sh	Sherwood number	$(k\,d_e)/D$
We	Weber Number, liquid phase	$(u_s^2\,\rho\,d_e/\sigma)$

Sub And Super Scripts

l	liquid phase
g	gas phase
s	superficial
e	effective
fl, flood	flood point

Abbreviations

BC	Boundary condition

REFERENCES

Adderley, C.I.; Foumeny, E.A. and Griffin, H.E. (1995) The Numerical Simulation of Heat Transfer and Laminar Flow in Corrugated Ducts. IChemE Research Event. 405-407

AEA Technology, CFDS Update. No. 10 Autumn 1995

Alekseev, V.P.; Prberezkin, A.E. and Gerasimov, P.V. (1972) Determination of Flooding Rates in Regular Packings. Heat Transfer-Soviet Research **4** (6) 159-163

Bakker, R.A. and Van Den Akker, K.E.A. (1994) A Computational Study of Chemical Reactors of the Basis of Micromixing Models. Transactions of the Institution of Chemical Engineers. **72** part A. Nov. 733-738

Bauermann, H.D. and Benhamou, W. (1983) Amagements internes pour las distillation sous vide. Informations Chimie. **209** 93-96

Billet, R. and Shultes, M. (1992) Advantage in Correlating Packed Column Performance. I.Chem.E.Symposium Series 128 B129-B136

Billet, R. and Mackowiak, J. (1988) Application of Modern Packings in Thermal Separation Processes. Chem. Eng. Technol. **11** 213-227

Billet, R. and Schultes, M. (1987) Determination of Liquid Hold-up in Gas-Liquid Two-Phase Countercurrent Mass Transfer Columns. I.Chem.E.Symposium Series 104 A159-A170

Billet, R. (1987) Modelling of Fluid Dynamics in Packed Columns. I.Chem.E.Symposium Series 104 A171-A182

Bode, J. (1994) Computational Fluid Dynamics Applications in the Chemical Industry. Computers and Chemical Engineering. 18 suppl. S247-S251

Boysen, H.F. (1994) Breaking the Barriers of CAD-Connectivity: The New FLUENT Grid Generator. CFD News, **4**, (1) May

Bragg, (1957) Goodloe Column Packing. Ind. Eng. Chem. **49** 1063-1066

Bravo, J.L.; Rocha, J.A. and Fair, J.R. (1986) Pressure Drop in Structured Packings. Hydrocarbon Processing. March 45-49

Bravo, J.L; Rocha, J.A. and Fair, J.R. (1985) Mass Transfer in Gauze Packings. Hydrocarbon Processing. January. 91-95

Bravo, J.L.; Rocha, J.A. and Fair, J.R. (1991) How Surface Treatment and Geometry Affect the Performance of Structured Packing. AIChE Annual Meeting Nov 17-22 Los Angeles, USA

Bschorer, S. and Schierhoz, W. (1993) Simulation Programs for Non-Newtonian Fluids. Rheology. Sept. 198-201

Chen, G.K. and Chuang, K.T. (1989) Recent Developments in Distillation. Hydrocarbon Processing. Feb. 37-44

Chen, G.K. and Acerra, M. (1987) Structured Tower Packing. Euro patent 0270 050 A2

Choudhury, D.; Foumeny, E.A., and Benyahia, F. (1993) CFD. Chemical Engineering Progress. April. 8-10

Dombrowski, N.; Foumeny, E.A., Riza, A. (1993) Know the CFD codes. Chemical Engineering Progress. Sept. 46-48

Douglass, R.W. and Ramshaw, J.D. (1994) Perspective: Future Research Directions in CFD. Transactions of the ASME, Journal of Fluids Engineering. **116**, June, 212-215

Fair, J.R. (1988) Distillation: Whither, not Whether. Chem. Eng. Res. Des. **66** July 363-370

Fair, J.R. and Bravo J.L. (1990) Distillation Columns Containing Structured Packing. Chem. Eng. Prog. January 19-29

Fair, J.R. and Bravo, J.L (1987) Prediction of Mass Transfer Efficiencies and Pressure Drop for Structured Tower Packings in Vapour/Liquid Service. I.Chem.E.Symposium Series 104 A183-A201

Fokema, M.D., Kresta, S.M. and Wood, P.E. (1994) Importance of Using the correct Impeller Boumdary Conditions for CFD Simulations of Stirred Tanks. Canadian Journal of Chemical Engineering. **72** April. 177-183

Forsyth, Jr. W.L.; Stack, T.G.; Wolf, J.E. and Conn, A.L. (1947) Performance of McMahon Packing. Ind. Eng. Chem. **39** (6) 714-718

Foumeny, E. A. (1996) Computational Fluid Dynamics: Theory and Trends Proceedings of the 1996 IChemE Research Event. Vol 1 6-11

Freitas, C.J. (1995) Perspective: Selected Benchmarks from Commercial CFD Codes. Transactions of the ASME, Journal of Fluids Engineering. **117**, June, 208-218

Gaiser, G. and Kottke, V. (1989) Flow Phenomena and Local Heat and Mass Transfer in Corrugated Passages. Chem. Eng. Technol. **12** 400-405

Hanley, B.; Dunbobbin,B. and Bennett, D. (1994) A Unified Model for Countercurrent Vapour/Liquid Packed Columns. 1. Pressure Drop. Ind. Eng. Chem. Res. **33** 1208-1221

Hanley, B.; Dunbobbin,B. and Bennett, D. (1994) A Unified Model for Countercurrent Vapour/Liquid Packed Columns. 2. Equations for the Mass-Transfer Coefficients, Mass-Transfer Area, the HETP, and the Dynamic Liquid Holdup. Ind. Eng. Chem. Res. **33** 1222-1230

Hartle, S.L. Neural Network Grid Generation. Presented to CFDCC Seminar, University of Bristol. Sept 1995

Hayter, A.J. (1952) A High-Efficiency Corrugated Gauze Packing for Controlled Flow Distillation. Ind. Chem. **28** 59-64

Henriques de Brito, M; von Stockar, U. and Bomio, P. (1992) Predicting the Liquid Phase Mass Transfer Coefficient - k_l - for the Sulzer Structured Packing Mellapak. I.Chem.E.Symposium Series 128 B137-B144

Henriques de Brito, M.; von Stockar, U.; Menendez Bangerter, A.; Bomio, P, and Laso, M. (1994) Effective Mass-Transfer Area in a Pilot Plant Column Equipped with Structured Packings and with Ceramic Rings. Ind. Eng. Chem. Res. **33** 647-656

Higginbotham, P. (1993) Structured Packing in Air Distillation. PhD Thesis, University of Aston, Birmingham, UK

Hsia, M.A. (1987) Tower Packing Element. US patent 4 670 196

Huber, M. (1980) Packing Element of Foil like Material for an Exchange Column. US patent 4 186 159

Huber, M. (1967) Sulzer Rectification Columns. Sulzer Tech. Rev. **1** 30-

Hughmark, G.A. (1986) Packed Column Efficiency Fundamentals. Ind. Eng. Chem. Fundam. **25** 405-409

Jaeger, (1988) Metal Max-Pak Product Bulletin 500. Jaeger Products Inc., Spring, USA

Kister, H.Z. and Gill, D.R. (1992) Flooding and Pressure Drop Prediction for Structured Packings. I.Chem.E.Symposium Series 128 A109-A123

Kolev, N; Billet, R.; Semkow, R.; Mackowiak, J. and Nakov, Sv. (1994) On the Optimal Form of Stacks in Packed Columns. Fat Sci. Technol. 7 267-

Kolev, N and Nakov, Sv. (1993) Performance Characteristics of a Packing with Boundary layer Turbulisers. Part 1. Pressure Drop and Loading Point. Chem. Eng. Proc. **32** 389-385

Laso, M.; Henriques de Brito, M.; Bomio, P. and von Stockar, U. (1995) Liquid-side Mass Transfer Characteristics of a Structured Packing. The Chemical Engineering Journal **58** 251-258

McGlamery, G.G. (1988) Liquid Film Transport Characteristics of Textured Metal Surfaces. PhD Thesis. University of Texas at Austin.

McMahon, H.D. (1947) Efficient Packing for Rectifying Columns. Ind. Eng. Chem. **39** (6) 712-714

Meier, W (1981) Packing for an Exchange Column. US patent 4 296 050

Meier, W. (1984) Packing for an Exchange Column. US patent 4 455 339

Meier, W.; Stoecker W.D. and Weinstein B. (1977) Performance of a New, High Efficiency Packing. Chem. Eng. Prog. **73** (11) 71-

Monclova, L.A, and Fornay, L.J. (1995) Numerical Simulation of a Pipeline Tee Mixer. Ind.Eng.Chem.Res. **34**. 1488-1493

Nakov, Sv. and Kolev, N. (1994) Performance Characteristics of a Packing with Boundary layer Turbulisers. Part 2. The Packing Dynamic Hold-up. Chem. Eng. Proc. **33** 101-105

Nutter, (1987) Montz High-efficiency Structured Packings. Bulletin B-1, Nutter Engineering Ltd., Tulsa, USA

Oakley, D.E. (1994) Scale up of Spray Dryers with the Aid of CFD. Drying Technology. **12** (1&2) 217-233

Parsons, I.M. (1991) Gas Distribution in Shallow Packed Beds. Ph.D. Thesis. Aston University, Birmingham, UK.

Patankar, S.V. (1980) Numerical Heat Transfer and Fluid Flow. Publ. Hemisphere, New York.

Patel, B.R.; Dombrowski, N.; Foumeny, E.A., and Riza, A. (1994) CFD Codes; Chemical Engineering Progress. Jan. 8

Porter, K.E. (1995) Why Research is Needed in Distillation. Trans. IChemE. **73** part A, May, 357-362

Porter, K.E. and Jenkins, J.D. (1979) The Interrelationship between Industrial Practice and Academic Research in Distillation and Absorption. IChemE Symposium Series 56, 75-121

Regehr, U. (1975) Contact Body for Transfer of Heat and/or Substances. US patent 3 887 664

Riza, A.; Introduction to CFD Codes. Internal Report. Department of Chemical Engineering, University of Leeds.

Robbins, L.A. (1991) Improve Pressure-Drop Prediction with a New Correlation. Chem. Eng. Prog. May. 87-91

Rocha, J.A; Bravo, J.L. and Fair, J.R. (1992) A Comprehensive Model for the Performance of Columns Structured Packings. I.Chem.E.Symposium Series 128 A439-A458

Rocha, J.A; Bravo, J.L. and Fair, J.R. (1993) Distillation Columns Containing Structured Packings: A Comprehensive Model for their Performance 1. Hydraulic Models. Ind. Eng. Chem. Res. **32** 641-651

Rocha, J.A; Bravo, J.L. and Fair, J.R. (1996) Distillation Columns Containing Structured Packings: A Comprehensive Model for their Performance 2. Mass Transfer Model. Ind. Eng. Chem. Res. **35** 1660-1667

Scofield, R.C. (1950) Industrial Fractionating Tower Packing. Chem. Eng. Prog. **46** (8) 405-

Seah, A.M. (1986) Structured "WV" Packing Elements. Euro patent 0218 417 A1

Shaw, C.T. (1992) Using CFD. Publ. Prentice Hall.

Shi, M.G. and Mersmann, A. (1985) Effective Interfacial Area in Packed Columns. Ger. Chem. Eng. **8** 87-96

Sparrow, E.M.; Lin, S.H. and Lundgren T.S. (1964) Flow Development in the Hydrodynamic Entrance Region of Tubes and Ducts. The Physics of Fluids. 7 (3) 338-347

Sperandio, A. (1962) Sulzer Technical Reveiw **4**

Spiegel, L. and Meier, W. (1987) Correlations of the Performance Characteristics of the Various Mellapak Types. I.Chem.E.Symposium Series 104 A203-A215

Spiegel, L. and Meier, W. (1992) A Generalized Pressure Drop Model for Structured Packings. I.Chem.E.Symposium Series 128 B85-B94

Stedman, D.F. (1937) Fractionating Columns of High Efficiency. Trans. Am.I.Chem.E. **33**, 153-161

Stichlmair, J.; Bravo, J.L. and Fair, J.R. (1989) General Model for Prediction of Pressure Drop and Capacity of Countercurrent Gas/Liquid Packed Columns. Gas Separation and Purification **3** 19-28

Stoter, F; Olujic, Z. and de Graauw, J. (1992) Modelling of Hydraulic and Separation Performance of Large Diameter Columns Containing Structured Packings. I.Chem.E.Symposium Series 128 A201-A210

Stoter, F; Olujic, Z. and de Graauw, J. (1993) Modelling and Measurement of Gas Flow Distribution in Corrugated Sheet Structured Packings. Chemical Engineering Journal **53** 55-66

Sulzer Brothers, (1966) Improvements Relating to Liquid/Vapour Material Exchange Column. UK patent 1 020 190

Sulzer Chemtech, - Optiflow Brochure

Sulzer Bothers, (1965) Swiss patent 398503 Sulzer A.G.

Sulzer Chemtech Ltd., (1994) Optiflow. Sulzer Chemtech Ltd., Separation Columns, Winterthur, Switzerland.

Watson, H.E. (1949) The Separation of Closely Boiling Liquids. Ind. Chem. **25** 503-506

Weedman, J.A. and Dodge, B.F. (1947) Rectification of Liquid Air in a Packed Column. Ind. Eng. Chem. **39** (6) 732-744

Wilhelm, G. (1992) Multilayer Angular Packing. US patent 5 158 712

Wilhelm, G. (1989) Vortex-inducing Packing of Pyramid-type Elements and Process for its Assembly. US patent 4 830 792

Yeoman, N.; Buchholz, M. and Maltke, F.E. (1994) Nested Packing for an Exchange Column. WO 94/12258

APPENDIX 1 - SUMMARY OF CFD COMPANIES AND PRODUCTS

NOTE: All prices quoted (excluding VAT) are for non-commercial, university use, for supporting the program on a Unix workstation (i.e. a Sun Sparc). The information supplied was correct at Jan 1994.

ADINA R&D Inc; 71 Elton Avenue, Watertown, MA, 02172, USA Tel:(617) 926-5199 Fax:(617) 926-0238	Product: Price:	**ADINA-F** $2,400 Perpetual Licence
Fluent Europe Ltd; Hutton's Building, 146 West Street, Sheffield, S1 4ES Tel:(0742) 780861 Fax:(0742) 795086	Product: Price:	**FLUENT** **NEKTON** **RAMPANT** Fluent: £2,200 Nekton: £2,200 Both Above: £3,300 Annual Licence Rampant: N/A
Applied Computing & Engineering Ltd; The Genesis Centre, Garrett Field, Science Park South, Birchwood, Warrington, WA3 7BH Tel:(0925) 830085 Fax:(0925) 826460	Product: Price:	**FIDAP** £900 Annual Licence
Polyflow; Place de l'Universite 16, B-1348 Louvain-la-Neuve, Belgium Tel: 32 (0)10 452861 Fax: 32 (0)10 453009	Product: Price:	**POLYFLOW** 100,000 BEF Perpetual

CHAM Ltd;
Bakery House,
40 High Street,
Wimbeldon,
London, SW19 5AU

Tel: 081 947 7651
Fax: 081 879 3497

Product: **PHOENICS**

Price: No information

Flowsolve Ltd;
130 Arthur Road,
Wimbeldon Park,
London SW19 8AA

Tel: 081 944 0940
Fax: 081 944 1977

Product: **PHOENICS**

Distributors for CHAM

Computational Dynamics Ltd;
Olympic House,
317 Latimer Road,
London, W10 6RA

Tel: 081 969 9639
Fax: 081 968 8606

Product: **STAR-CD**

Price: £2,000 Annual Licence

AEA Technology;
Computational Fluid
Dynamics Services,
8 Harwell, Didcot,
Oxfordshire, OX11 0RA

Tel: 0235 432822
Fax: 0235 432989

Product: **FLOW 3D**

Price: £3,900 Fee +
£1,200 Annual Licence

Nuclear Electric Plc.;
Berkeley Technology Centre,
Berkeley,
Gloucester, GL13 9PB

Tel: 0453 812009
FAx: 0453 812791

Product: **FEAT**

Price: No information

Control Data Systems Inc.; ICEM Marketing, ARH290, 4201 Lexington Avenue North, Arden Hills, MN 55126-6198, USA Tel: 1-612-482-6736 Fax: 1-612-482-2000	Product: Price:	**ICEM CFD/CAE** No information
PDA Engineering, Rowan House, Woodlands Business Village, Basingstoke, Hants, RG21 2JX Tel: 0256 331313 Fax: 0256 840296	Product: Price:	**P3/CFD** No Information
Strucom Strucom House, 188-196 Canterbury Road, Croyden, Surrey, CR0 3HF Tel: 081 683 3999 Fax: 081 683 3933	Product: Price:	**FLOWTRAN** No information
Innovative Research Inc; 2800 University Avenue SE, Minneapolis, MN 55414, USA Tel:(612) 378-0302 Fax:(612) 378-0535	Product: Price:	**COMPACT-2D -3D** $2,000/$4,000 Annual $5,000/$10,000 Perpetual
McMaster University; Prof J Vlachopoulos, Chemical Engineering, Hamilton, Ontario, Canada, L8S4L7 Tel:(905) 521-8815 Fax:(905) 522-5004	Product: Price:	**POLYCAD + 7 Others** $20,000 Perpetual Others $5,000-$18,000

IKV Software;
Institut fur
Kunststoffverarbeitung,
Pontstrasse 49,
D-5100 Aachen, Germany

Tel: 0241 803806
Fax: 0241 404551

Product: **MICROPUS**

Price: Not commercially available any more

Prof S Tsangaris;
National Technical,
University of Athen,
Box 6470,
15710 Zografou, Greece

Tel:(01) 77 13 060
Fax:(01) 77 06 545

Product: **U.I.N.S.**

Price: Not commercially available

Institut fur Kunstoff-
technologie der
Universitat Stuttgart;
Boblinger Strabe 70,
D-70199 Stuttgart, Germany

Tel: -
Fax: -

Product: **SIMFLOW**

Price: No information

Appendix 2 - Summary of Capabilities of Commercially Available CFD Packages

Company:	CHAM(1)	FLUENT EUROPE LTD			CD LTD(2)
Program Name:	PHOENICS	RAMPANT	FLUENT	NEKTON	STAR-CD
Method:					
Finite Volume	√	√	√	√	√
Finite Element	-	-	-	-	-
Dimension:					
2D	√	√	√	√	√
3D	√	√	√	√	√
Time Dependency:					
Steady State	√	√	√	√	√
Transient	√	√	√	√	√
Solution Algorithm:					
Direct		-	√	√	-
Iterative	√	√	√	√	√
Multinodal		-	√	-	-
No. of Additional Equations	No limit	None	No limit	No limit	50 scalars
Position/Time Dependancy:					
$\rho(x)$	√	√	√	-	√
$\rho(t)$	√	√	√	-	√
$\mu(x)$	√	√	√	√	√
$\mu(t)$	√	√	√	√	√
$C_p(x)$	√	√	√	√	√
$C_p(t)$	√	√	√	√	√
$\lambda(x)$		√	√	√	√
$\lambda(t)$		√	√	√	√
Non-Newtonian Model:					
General	Power-Law	Power-Law	Power-Law Carreau	Power-Law Carreau	Power-Law
Newtonian				Bingham	
Plastic	Bingham				

	PHOENICS	RAMPANT	FLUENT	NEKTON	STAR-CD
Subroutines & Included Derivatives:					
User Developed	√	-	√	√	√
1.		-	√	√	-
2.		-	√	√	-
Mixed		-	-	√	-
Free Surfaces:					
Internal		-	√	√	-
External	√	-	√	√	-
Transient BC	√	√	√	√	-
Processors:					
Pre	√	√	√	√	√
Post	√	√	√	√	√
Grids/Mesh:					
BFC	√	√	√	-	√
Structured	√	√	√	√	-
Unstructured	-	√	√	√	√
Rotating Co-ordinate system	√	√	√	-	√
Fine Grid Embedding	√	√	√	√	√
Solution Adaptive		√	√	√	-
Sliding Mesh	√	√	√	√	√
Capability with CAD Packages:	√	√	√	√	√
Turbulence Models:					
Constant Eddy Viscosity	√	-	-	-	√
k-l	√	-	-	√	√
k-ε	√	√	√	√	√
Low Re k-ε	√	-	-	-	√
RSM(3)	√	-	√	-	-
DSM(4)		-	√	-	-
RNG(5)	√	√	√	-	√
Differential Re flux		-	-	-	-
Two layer model	√	-	-	-	√

	PHOENICS	RAMPANT	FLUENT	NEKTON	STAR-CD
Other Features:					
Porous media	√				√
Conjugate heat transfer	√		√	√	√
Radiation	√				√
Combustion modelling	√			√	√
Particle tracking	√				√
Compressible	√	√	√		√
Multiphase	√	-	√	-	√
Phase change					
Operating System:	DOS UNIX	UNIX	DOS UNIX	UNIX	All

Company:	CFDS(6)	PDA	NE(7)	STRUCOM	FD INT(8)	ADINA
Program Name:	FLOW3D	P3/CFD	FEAT	FLOTRAN	FIDAP	ADINA-F
Method:						
Finite Volume	√	-	-	-	-	√
Finite Element	√	√	√	√	√	√
Dimension:						
2D	√	√	√	√	√	√
3D	√	√	√	√	√	√
Time Dependency:						
Steady State	√	√	√	√	√	√
Transient	√	√	√	√	√	√
Solution Algorithm:						
Direct	-		√	-	√	√
Iterative	√		-	√	√	√
Multinodal	-		-	-	-	-
No. of Additional Equations	No limit				15	-
Position/Time Dependancy:						
$\rho(x)$	√		-		√	√
$\rho(t)$	√		-		√	-
$\mu(x)$	√		√		√	√
$\mu(t)$	√		√		√	√
$C_p(x)$	√		-		√	√
$C_p(t)$	√		-		√	√
$\lambda(x)$	√		√		√	√
$\lambda(t)$	√		√		√	√
Non-Newtonian Model:						
General	Power-Law		-		Power-Law	Power-Law
Newtonian	Carreau				Carreau	Carreau
Plastic	Bingham				Bingham	

	FLOW3D	P3/CFD	FEAT	FLOTRAN	FIDAP	ADINA-F
Subroutines & Included Derivatives:						
User Developed	√		√		√	√
1.	-		-		√	-
2.	-		-		√	-
Mixed	-		-		√	-
Free Surfaces:						
Internal	√		-	-	√	√
External	√		-	-	√	√
Transient BC	√		-	-	√	√
Processors:						
Pre	√	√	√	√	√	√
Post	√	√	√	√	√	√
Grids/Mesh:						
BFC	√		-	-	-	-
Structured	√		-	-	√	-
Unstructured	√		√	√	√	√
Rotating	√		-	√	√	√
Co-ordinate system						
Fine Grid	√		√	-	√	-
Embedding						
Solution Adaptive	√	√	√		-	-
Sliding Mesh						
Capability with CAD Packages:	√	√	√	√	√	-
Turbulence Models:						
Constant Eddy Viscosity	√	-	√	-	-	√
k-l	√	-	√	-	√	√
k-ε	√	√	√	√	√	√
Low Re k-ε	√	-	-	-	-	
RSM	√	-	-	-	-	
DSM	√	-	-	-	-	
RNG	√	-	-	-	-	
Differential Re flux	√	-	-	-	-	
Two layer model	-	-	-	-	-	

	FLOW3D	P3/CFD	FEAT	FLOTRAN	FIDAP	ADINA-F
Other Features:						
Porous media			✓			✓
Conjugate heat transfer	✓		✓		✓	
Radiation	✓		✓		✓	
Combustion modelling					✓	
Particle tracking	✓					
Compressible	✓			✓	✓	✓
Multiphase	✓				✓	
Phase change					✓	✓
Operating System:			UNIX	All	All	UNIX DOS

NOTES

(1) - CHAM = Concentration, Heat and Momentum Ltd
(2) - CD LTD = Computational Dynamics Ltd
(3) - RSM = Reynolds Stress Model
(4) - DSM = Differential Stress Model
(5) - RNG = Renormalisation Group Theory
(6) - CFDS = Computational Fluid Dynamics Services
(7) - NE = Nuclear Electric
(8) - FD INT = Fluid Dynamics International

APPENDIX 3 - Q1 FILE FOR FLOW IN A TRIANGULAR DUCT

```
TALK=T;RUN( 1, 1);VDU=X11-TERM
IRUNN  =      1 ;LIBREF =      0
**************************************************************
 Group 1. Run Title TEXT(TRIANGULAR CHANNEL, THETA = 11.4 )
**************************************************************
 Group 2. Transience
STEADY  =   T
**************************************************************
 Groups 3, 4, 5  Grid Information
  * Overall number of cells, RSET(M,NX,NY,NZ,tolerance)
RSET(M,10,10,135)
  * Set overall domain extent:   *       xulast  yvlast  zwlast   name
XSI= 2.000E-02;YSI= 1.000E-01;ZSI= 1.350E+00;RSET(D,CHAM    )
**************************************************************
 Group 6. Body-Fitted coordinates
BFC=T
  * Set points
XPO= 9.0000E-03;YPO= 0.0000E+00;ZPO= 0.0000E+00;GSET(P,P1  )
XPO= 1.1000E-02;YPO= 0.0000E+00;ZPO= 0.0000E+00;GSET(P,P2  )
XPO= 0.0000E+00;YPO= 1.0000E-01;ZPO= 0.0000E+00;GSET(P,P3  )
XPO= 2.0000E-02;YPO= 1.0000E-01;ZPO= 0.0000E+00;GSET(P,P4  )
  * Set lines/arcs
GSET(L,L1,P1,P2,10,1.0)
GSET(L,L2,P2,P4,10,1.0)
GSET(L,L3,P4,P3,10,1.0)
GSET(L,L4,P3,P1,10,1.0)
  * Set frames
GSET(F,F1,P1,-,P2,-,P4,-,P3,-)
  * Match a grid mesh
GSET(M,F1,+I+J,1,1,1,TRANS)
  * Copy/Transfer/Block grid planes
GSET(C,K136,F,K1,1,10,1,10,+,0,0,1.3500E+00,INC,1)
  **********
NONORT  =   T
  * X-cyclic boundaries switched
**************************************************************
 Group 7. Variables: STOREd,SOLVEd,NAMEd
 ONEPHS  =   T
    * Non-default variable names
 NAME(46) =ENUT ; NAME(47) =WCRT
 NAME(48) =VCRT ; NAME(49) =DEN1
 NAME(50) =UCRT
   * Solved variables list
 SOLVE(P1  ,U1  ,V1  ,W1  ,KE  ,EP  )
   * Stored variables list
 STORE(UCRT,DEN1,VCRT,WCRT,ENUT)
   * Additional solver options
```

```
SOLUTN(P1  ,Y,Y,Y,N,N,Y)
SOLUTN(KE  ,Y,Y,N,N,N,N)
SOLUTN(EP  ,Y,Y,N,N,N,N)
*************************************************************
Group 8. Terms & Devices
TERMS (KE  ,N,Y,Y,Y,Y,N)
TERMS (EP  ,N,Y,Y,Y,Y,N)
NEWENT =   T
*************************************************************
Group 9. Properties
RHO1   = 1.000E+03
EL1    = GRND4
ENUL   = 1.788E-06 ;ENUT   = GRND3
PRT  (EP  ) =  1.314E+00
*************************************************************
Group 10.Inter-Phase Transfer Processes
*************************************************************
Group 11.Initialise Var/Porosity Fields
RESTRT(ALL)
FIINIT(KE  ) =  2.861E-04 ;FIINIT(EP  ) =  4.120E-04
FIINIT(UCRT) =  0.000E+00
No PATCHes used for this Group
RSTGRD =   F
INIADD =   T
*************************************************************
 Group 12. Convection and diffusion adjustments
*************************************************************
Group 13. Boundary & Special Sources  PATCH
(KESOURCE,PHASEM,1,10,1,10,1,135,1,1)
COVAL (KESOURCE,KE  , GRND4   , GRND4   )
COVAL (KESOURCE,EP  , GRND4   , GRND4   )

INLET (BFCIN   ,LOW   ,#1,#1,#1,#1,#1,#1,1,1)
VALUE (BFCIN   ,P1  , GRND1   )
VALUE (BFCIN   ,U1  , GRND1   )
VALUE (BFCIN   ,V1  , GRND1   )
VALUE (BFCIN   ,W1  , GRND1   )
VALUE (BFCIN   ,KE  , 7.841E-04)
VALUE (BFCIN   ,EP  , 3.095E-03)
VALUE (BFCIN   ,WCRT, 1.980E+00)

OUTLET(OUT     ,HIGH  ,#1,#1,#1,#1,#1,#1,1,1)
VALUE (OUT     ,P1  , 0.000E+00)

PATCH (BOT     ,SWALL ,#1,#1,#1,#1,#1,#1,1,1)
COVAL (BOT     ,U1  , GRND2   , 0.000E+00)
COVAL (BOT     ,W1  , GRND2   , 0.000E+00)
COVAL (BOT     ,KE  , GRND2   , GRND2   )
 COVAL (BOT    ,EP  , GRND2   , GRND2   )
```

```
PATCH (TOP    ,NWALL ,#1,#1,#1,#1,#1,#1,1,1)
COVAL (TOP    ,U1  , GRND2    , 0.000E+00)
COVAL (TOP    ,W1  , GRND2    , 0.000E+00)
COVAL (TOP    ,KE  , GRND2    , GRND2   )
COVAL (TOP    ,EP  , GRND2    , GRND2   )

PATCH (WALL1  ,WWALL ,#1,#1,#1,#1,#1,#1,1,1)
COVAL (WALL1  ,V1  , GRND2    , 0.000E+00)
COVAL (WALL1  ,W1  , GRND2    , 0.000E+00)
COVAL (WALL1  ,KE  , GRND2    , GRND2   )
COVAL (WALL1  ,EP  , GRND2    , GRND2   )

PATCH (WALL2  ,EWALL ,#1,#1,#1,#1,#1,#1,1,1)
COVAL (WALL2  ,V1  , GRND2    , 0.000E+00)
COVAL (WALL2  ,W1  , GRND2    , 0.000E+00)
COVAL (WALL2  ,KE  , GRND2    , GRND2   )
COVAL (WALL2  ,EP  , GRND2    , GRND2   )

BFCA   = 1.000E+03
************************************************************
Group 14. Downstream Pressure For PARAB
************************************************************
Group 15. Terminate Sweeps
LSWEEP =   1000
SELREF =   T
RESFAC = 1.000E-03
************************************************************
Group 16. Terminate Iterations
ENDIT (P1  ) =  1.000E-03 ;ENDIT (U1  ) =  1.000E-03
ENDIT (V1  ) =  1.000E-03 ;ENDIT (W1  ) =  1.000E-03
ENDIT (KE  ) =  1.000E-03 ;ENDIT (EP  ) =  1.000E-03
************************************************************
Group 17. Relaxation
RELAX(P1  ,LINRLX, 7.000E-01)
RELAX(U1  ,FALSDT, 2.508E+04)
RELAX(V1  ,FALSDT, 2.508E+04)
RELAX(W1  ,FALSDT, 2.508E+04)
RELAX(KE  ,FALSDT, 2.508E+04)
RELAX(EP  ,FALSDT, 2.508E+04)
KELIN  =     1
************************************************************
Group 18. Limits
************************************************************
Group 19. EARTH Calls To GROUND Station GENK   =   T
************************************************************
Group 20. Preliminary Printout
ECHO   =   F
```

```
************************************************************
Group 21. Print-out of Variables
************************************************************
Group 22. Monitor Print-Out I
XMON  =      5 ;IYMON  =      5 ;IZMON  =     60
TSTSWP  =  12345
************************************************************
Group 23.Field Print-Out & Plot Control
numcls = 10
nxprin = 1; ixprf = 1; ixprl = 10
nyprin = 1; iyprf = 1; iyprl = 10
nzprin = 1; izprf = 130; iyprl = 130
walprn = t
ITABL  =      1
No PATCHes used for this Group
************************************************************
Group 24. Dumps For Restarts
************************************************************
MENSAV(S,RELX,DEF,2.0000E-03,1.1960E+00,15)
MENSAV(S,PHSPROP,DEF,200,0,1.0005E+03,1.7880E-06)
MENSAV(S,FLPRP,DEF,K-E,CONSTANT,AIR-CONSTANT) STOP
```

APPENDIX 4 - Q1 FILE FOR PLAIN JUNCTION, TURBULENT FLOW

```
TALK=T;RUN( 1, 1);VDU=X11-TERM
IRUNN =      1 ;LIBREF =      0
*****************************************************************
 Group 1. Run Title
TEXT(TRIANGULAR JUNCTION TURBULENT FLOW     )
*****************************************************************
 Group 2. Transience
STEADY =   T
*****************************************************************
 Groups 3, 4, 5  Grid Information
  * Overall number of cells, RSET(M,NX,NY,NZ,tolerance)
RSET(M,15,20,15)
  * Overall domain extent, RSET(D,name,XULAST,YVLAST,ZWLAST)
RSET(D,CHAM,1.500E-02,1.800E-02,1.500E-02)
*****************************************************************
 Group 6. Body-Fitted coordinates
BFC=T
  * Set points
GSET(P,P1,7.0000E-03,0.0000E+00,0.0000E+00)
GSET(P,P2,8.0000E-03,0.0000E+00,0.0000E+00)
GSET(P,P3,0.0000E+00,9.0000E-03,0.0000E+00)
GSET(P,P4,1.5000E-02,9.0000E-03,0.0000E+00)
GSET(P,P5,0.0000E+00,9.0000E-03,1.5000E-02)
GSET(P,P6,0.0000E+00,1.8000E-02,7.0000E-03)
GSET(P,P7,0.0000E+00,1.8000E-02,8.0000E-03)
  * Set lines/arcs
GSET(L,L1,P3,P1,10,1.0)
GSET(L,L2,P1,P2,15,1.0)
GSET(L,L3,P2,P4,10,1.0)
GSET(L,L4,P4,P3,15,1.0)
GSET(L,L5,P3,P6,10,1.0)
GSET(L,L6,P6,P7,15,1.0)
GSET(L,L7,P7,P5,10,1.0)
GSET(L,L8,P5,P3,15,1.0)
  * Set frames
GSET(F,F1,P1,-,P2,-,P4,-,P3,-)
GSET(F,F2,P3,-,P5,-,P7,-,P6,-)
  * Match a grid mesh
GSET(M,F1,+I+J,1,1,1,TRANS)
GSET(M,F2,+K+J,1,11,1,TRANS)
  * Copy/Transfer/Block grid planes
GSET(C,K16,F,K1,1,15,1,10,+,0,0,1.5000E-02,INC,1)
GSET(C,I16,F,I1,11,20,1,15,+,1.5000E-02,0,0,INC,1)
  **********
NONORT =   T
  * X-cyclic boundaries switched
*****************************************************************
```

```
 Group 7. Variables: STOREd,SOLVEd,NAMEd
ONEPHS  =   T
  * Non-default variable names
NAME(46) =ENUT ; NAME(47) =WCRT
NAME(48) =VCRT ; NAME(49) =DEN1
NAME(50) =UCRT
  * Solved variables list
SOLVE(P1  ,U1  ,V1  ,W1  ,KE  ,EP  )
  * Stored variables list
STORE(UCRT,DEN1,VCRT,WCRT,ENUT)
  * Additional solver options
SOLUTN(P1  ,Y,Y,Y,N,N,N)
************************************************************
 Group 8. Terms & Devices
TERMS (KE  ,N,Y,Y,Y,Y,N)
TERMS (EP  ,N,Y,Y,Y,Y,N)
NEWENT  =   T
************************************************************
 Group 9. Properties
RHO1    = 3.400E+00
PRESS0  = 1.000E+05
EL1     = GRND4
ENUL    = 2.760E-06 ;ENUT   = GRND3
PRT   (EP  ) =  1.314E+00
************************************************************
 Group 10.Inter-Phase Transfer Processes
************************************************************
 Group 11.Initialise Var/Porosity Fields
RESTRT(ALL)
 No PATCHes used for this Group
 RSTGRD  =   F
INIADD  =   T
************************************************************
 Group 12. Convection and diffusion adjustments
************************************************************
 Group 13. Boundary & Special Sources

PATCH (KESOURCE,PHASEM,1,15,1,20,1,15,1,1)
COVAL (KESOURCE,KE  , GRND4   , GRND4   )
COVAL (KESOURCE,EP  , GRND4   , GRND4   )

PATCH (WALL1   ,WWALL ,#1,#1,#1,#1,#1,#1,1,1)
COVAL (WALL1   ,V1  , GRND2   , 0.000E+00)
COVAL (WALL1   ,W1  , GRND2   , 0.000E+00)
COVAL (WALL1   ,KE  , GRND2   , GRND2   )
COVAL (WALL1   ,EP  , GRND2   , GRND2   )

PATCH (WALL2   ,EWALL ,#1,#1,#1,#1,#1,#1,1,1)
COVAL (WALL2   ,V1  , GRND2   , 0.000E+00)
```

```
COVAL (WALL2  ,W1  , GRND2   , 0.000E+00)
COVAL (WALL2  ,KE  , GRND2   , GRND2   )
COVAL (WALL2  ,EP  , GRND2   , GRND2   )

PATCH (BOT    ,SWALL ,#1,#1,#1,#1,#1,#1,1,1)
COVAL (BOT    ,U1  , GRND2   , 0.000E+00)
COVAL (BOT    ,W1  , GRND2   , 0.000E+00)
COVAL (BOT    ,KE  , GRND2   , GRND2   )
COVAL (BOT    ,EP  , GRND2   , GRND2   )

PATCH (WALL3  ,LWALL ,#1,#1,#2,#2,#1,#1,1,1)
COVAL (WALL3  ,U1  , GRND2   , 0.000E+00)
COVAL (WALL3  ,V1  , GRND2   , 0.000E+00)
COVAL (WALL3  ,KE  , GRND2   , GRND2   )
COVAL (WALL3  ,EP  , GRND2   , GRND2   )

PATCH (WALL4  ,HWALL ,#1,#1,#2,#2,#1,#1,1,1)
COVAL (WALL4  ,U1  , GRND2   , 0.000E+00)
COVAL (WALL4  ,V1  , GRND2   , 0.000E+00)
COVAL (WALL4  ,KE  , GRND2   , GRND2   )
COVAL (WALL4  ,EP  , GRND2   , GRND2   )

PATCH (TOP    ,NWALL ,#1,#1,#2,#2,#1,#1,1,1)
COVAL (TOP    ,U1  , GRND2   , 0.000E+00)
COVAL (TOP    ,W1  , GRND2   , 0.000E+00)
COVAL (TOP    ,KE  , GRND2   , GRND2   )
COVAL (TOP    ,EP  , GRND2   , GRND2   )

INLET (BFCINB ,LOW  ,#1,#1,#1,#1,#1,#1,#1,#1)
VALUE (BFCINB ,P1  , GRND1   )
VALUE (BFCINB ,U1  , GRND1   )
VALUE (BFCINB ,V1  , GRND1   )
VALUE (BFCINB ,W1  , GRND1   )
VALUE (BFCINB ,KE  , 2.592E-03)
VALUE (BFCINB ,EP  , 6.047E-03)
VALUE (BFCINB ,WCRT, 3.600E+00)

INLET (BFCINT ,WEST ,#1,#1,#2,#2,#1,#1,#1,#1)
VALUE (BFCINT ,P1  , GRND1   )
VALUE (BFCINT ,U1  , GRND1   )
VALUE (BFCINT ,V1  , GRND1   )
VALUE (BFCINT ,W1  , GRND1   )
VALUE (BFCINT ,KE  , 2.592E-03)
VALUE (BFCINT ,EP  , 6.047E-03)
VALUE (BFCINT ,UCRT, 3.600E+00)

PATCH (OUTB   ,HIGH ,#1,#1,#1,#1,#1,#1,#1,#1)
COVAL (OUTB   ,P1  , FIXVAL  , 0.000E+00)
COVAL (OUTB   ,KE  , 0.000E+00, SAME   )
```

```
COVAL (OUTB    ,EP  , 0.000E+00, SAME    )

PATCH (OUTT    ,EAST  ,#1,#1,#2,#2,#1,#1,#1,#1)
COVAL (OUTT    ,P1  , FIXVAL   , 0.000E+00)
COVAL (OUTT    ,KE  , 0.000E+00, SAME    )
COVAL (OUTT    ,EP  , 0.000E+00, SAME    )
 BFCA   = 3.400E+00
************************************************************
 Group 14. Downstream Pressure For PARAB
************************************************************
 Group 15. Terminate Sweeps
LSWEEP  =    1000
SELREF  =    T
RESFAC  = 1.000E-02
************************************************************
 Group 16. Terminate Iterations
************************************************************
 Group 17. Relaxation
RELAX(P1  ,LINRLX, 7.000E-01)
RELAX(U1  ,FALSDT, 2.500E-04)
RELAX(V1  ,FALSDT, 2.500E-04)
RELAX(W1  ,FALSDT, 2.500E-04)
RELAX(KE  ,FALSDT, 2.500E-04)
RELAX(EP  ,FALSDT, 2.500E-04)
KELIN  =      1
************************************************************
 Group 18. Limits
************************************************************
 Group 19. EARTH Calls To GROUND Station
GENK   =    T
************************************************************
 Group 20. Preliminary Printout
ECHO   =    T
************************************************************
 Group 21. Print-out of Variables
************************************************************
 Group 22. Monitor Print-Out
IXMON  =      6 ;IYMON  =      6 ;IZMON  =     13
TSTSWP  =   12345
************************************************************
 Group 23.Field Print-Out & Plot Control
  No PATCHes used for this Group
************************************************************
 Group 24. Dumps For Restarts
************************************************************
 MENSAV(S,RELX,DEF,9.0000E-04,3.6000E+00,1)
 MENSAV(S,PHSPROP,DEF,200,409,3.4000E+00,1.0000E-05)
 MENSAV(S,FLPRP,DEF,K-E,CONSTANT,AIR-CONSTANT)
STOP
```

APPENDIX 5 - GROUND CODING FOR BASIC MODEL

```
C FILE NAME GROUND.FTN----------------------------081294
c#### dbs/hqq 08.12.94 UCONV comments provided
c#### dbs/mrm 10.08.94 new access point on group 19, section 11
      SUBROUTINE GROUND
      INCLUDE 'lp21/d_includ/satear'
      INCLUDE 'lp21/d_includ/grdloc'
      INCLUDE 'lp21/d_includ/grdear'
      INCLUDE 'lp21/d_includ/grdbfc'
CXXXXXXXXXXXXXXXXXXXXXXXX    USER SECTION STARTS:
C
C 1   Set dimensions of data-for-GROUND arrays here. WARNING: the
C     corresponding arrays in the MAIN program of the satellite
C     and EARTH must have the same dimensions.
      PARAMETER (NLG=100, NIG=200, NRG=200, NCG=100)
      PARAMETER (NGX = 50, NGY = 50)
      PARAMETER (MX = 15, MY = 2, MZ = 15)
C

COMMON/LGRND/LG(NLG)/IGRND/IG(NIG)/RGRND/RG(NRG)/CGRND/CG(
NCG)
      LOGICAL LG
      CHARACTER*4 CG
      CHARACTER*15
UOUTB,VOUTB,WOUTB,KEOUTB,EPOUTB,TOUTB,POUTB,
     +UOUTT,VOUTT,WOUTT,KEOUTT,EPOUTT,TOUTT,POUTT
      CHARACTER*15
UINB,VINB,WINB,KEINB,EPINB,TINB,PINB,UINT,VINT,
     +WINT,EPINT,KEINT,TINT,PINT
C
C 2   User dimensions own arrays here, for example:
C     DIMENSION GUH(10,10),GUC(10,10),GUX(10,10),GUZ(10)

      DIMENSION GUINB(NGX,NGY),GVINB(NGX,NGY),GWINB(NGX,NGY),

+GUINT(NGX,NGY),GVINT(NGX,NGY),GWINT(NGX,NGY),GKEB(NGX,NG
Y),

+GEPB(NGX,NGY),GKET(NGX,NGY),GEPT(NGX,NGY),GTINB(NGX,NGY),
     +GTINT(NGX,NGY),
     +GUINB2(NGX*NGY),GVINB2(NGX*NGY),GWINB2(NGX*NGY),
     +GKEB2(NGX*NGY),GEPB2(NGX*NGY),GTINB2(NGX*NGY),
     +GUINT2(NGX*NGY),GVINT2(NGX*NGY),GWINT2(NGX*NGY),
     +GKET2(NGX*NGY),GEPT2(NGX*NGY),GTINT2(NGX*NGY),
     +GVCRTB(NGX,NGY),GVCRTT(NGX,NGY),
     +GPINB2(NGX*NGY),GPINT2(NGX*NGY),
     +GPINB(NGX,NGY),GPINT(NGX,NGY),
     +GAREA(NGX,NGY)
```

```
C
C 3  User places his data statements here, for example:
C    DATA NXDIM,NYDIM/10,10/
C
C 4  Insert own coding below as desired, guided by GREX examples.
C    Note that the satellite-to-GREX special data in the labelled
C    COMMONs /RSG/, /ISG/, /LSG/ and /CSG/ can be included and
C    used below but the user must check GREX for any conflicting
C    uses. The same comment applies to the EARTH-spare working
C    arrays EASP1, EASP2,....EASP20. In addition to the EASPs,
C    there are 10 GRound-earth SPare arrays, GRSP1,...,GRSP10,
C    supplied solely for the user, which are not used by GREX. If
C    the call to GREX has been deactivated then all of the arrays
C    may be used without reservation.
C
c*****************************************************************
c
    IXL=IABS(IXL)
    IF(IGR.EQ.13) GO TO 13
    IF(IGR.EQ.19) GO TO 19
    GO TO (1,2,3,4,5,6,25,8,9,10,11,12,13,14,25,25,25,25,19,20,25,
   125,23,24),IGR
  25 CONTINUE
    RETURN
C*****************************************************************
C
C--- GROUP 1. Run title and other preliminaries
C
   1 GO TO (1001,1002),ISC
 1001 CONTINUE
C
C    User may here change message transmitted to the VDU screen
    IF(IGR.EQ.1.AND.ISC.EQ.1.AND..NOT.NULLPR)
   1  CALL WRYT40('GROUND file is GROUND.F   of:   081294 ')
      CALL WRYT40('THIS IS A PRIVATE VERSION OF GROUND    ')
      CALL WRYT40('WRITES/READS U1,V1,W1,KE,EP,TEM1       ')
      CALL WRYT40('AUTOMATIC RUN SERIES - 14/11/95        ')
C
    RETURN
 1002 CONTINUE
    RETURN
C*****************************************************************

Ground coding deleted

C*****************************************************************
C
C--- GROUP 13. Boundary conditions and special sources
```

```
C                          Index for Coefficient - CO
C                          Index for Value      - VAL
  13 CONTINUE
    GO TO (130,131,132,133,134,135,136,137,138,139,1310,
   11311,1312,1313,1314,1315,1316,1317,1318,1319,1320,1321),ISC
  130 CONTINUE
C------------------- SECTION  1 ------------ coefficient = GRND
    RETURN
  131 CONTINUE

************************************************************

Ground coding deleted

************************************************************

C------------------- SECTION 12 ------------------- value = GRND
C.. For the patch named 'INB' ie the bottom inlet
C.. ==========================================
     IF(NPATCH.EQ.'INB') THEN

       CALL GTIZYX(ASURFL,2,GAREA,NGY,NGX)

C.. Find the zero location index of the VAL
        L0VAL=L0F(VAL)

C.. For pressure set VAL=PRESSURE*COEFFICIENT
       IF(INDVAR.EQ.P1) THEN
         DO 1114 IX=IXF,IXL
           DO 1115 IY=IYF,NY/2
               I=IY+(IX-1)*NY
               F(L0VAL+I)=GPINB(IY,IX)*RG(1)
 1115        CONTINUE
 1114      CONTINUE

C.. For W1 component set VAL=W VELOCITY
       ELSEIF (INDVAR.EQ.W1) THEN
         DO 1116 IX=IXF,IXL
           DO 1117 IY=IYF,NY/2
               I=IY+(IX-1)*NY
               F(L0VAL+I)=GWINB(IY,IX)
 1117        CONTINUE
 1116      CONTINUE

C.. For V1 component set VAL=V VELOCITY
       ELSEIF (INDVAR.EQ.V1) THEN
         DO 1118 IX=IXF,IXL
           DO 1119 IY=IYF,NY/2
               I=IY+(IX-1)*NY
```

```
            F(L0VAL+I)=GVINB(IY,IX)
1119      CONTINUE
1118    CONTINUE


C.. For U1 component set VAL= U VELOCITY
      ELSEIF (INDVAR.EQ.U1) THEN
        DO 1120 IX=IXF,IXL
          DO 1121 IY=IYF,NY/2
              I=IY+(IX-1)*NY
              F(L0VAL+I)=GUINB(IY,IX)
1121        CONTINUE
1120      CONTINUE

C.. For kinetic energy of turbulence set VAL= KE
      ELSEIF (INDVAR.EQ.KE) THEN
        DO 1136 IX=IXF,IXL
          DO 1137 IY=IYF,NY/2
              I=IY+(IX-1)*NY
              F(L0VAL+I)=GKEB(IY,IX)
1137        CONTINUE
1136      CONTINUE

C.. For turbulence energy dissipation rate set VAL= EP
      ELSEIF (INDVAR.EQ.EP) THEN
        DO 1138 IX=IXF,IXL
          DO 1139 IY=IYF,NY/2
              I=IY+(IX-1)*NY
              F(L0VAL+I)=GEPB(IY,IX)
1139        CONTINUE
1138      CONTINUE

C.. For temperature set VAL = TEM1
      ELSEIF (INDVAR.EQ.14) THEN
        DO 1144 IX=IXF,IXL
          DO 1145 IY=IYF,NY/2
              I=IY+(IX-1)*NY
              F(L0VAL+I)=GTINB(IY,IX)
1145        CONTINUE
1144      CONTINUE

      ENDIF
    ENDIF


C.. For the patch named 'INT' ie the top inlet
C.. ==========================================

    IF(NPATCH.EQ.'INT') THEN
```

```
C.. Find the zero location index of the VAL
      L0VAL=L0F(VAL)

C.. For pressure set VAL=PRESSURE*COEFFICIENT
      IF(INDVAR.EQ.P1) THEN
        DO 1128 IX=IXF,IXL
          DO 1129 IY=NY/2+1,NY
              I=IY+(IX-1)*NY
              F(L0VAL+I)=GPINT(IY,IZSTEP)*RG(1)
1129        CONTINUE
1128      CONTINUE

C.. For W1 component set VAL=W VELOCITY
      ELSEIF (INDVAR.EQ.W1) THEN
        DO 1130 IX=IXF,IXL
          DO 1131 IY=NY/2+1,NY
              I=IY+(IX-1)*NY
              F(L0VAL+I)=GWINT(IY,IZSTEP)
1131        CONTINUE
1130      CONTINUE

C.. For V1 component set VAL=V VELOCITY
      ELSEIF (INDVAR.EQ.V1) THEN
        DO 1132 IX=IXF,IXL
          DO 1133 IY=NY/2+1,NY
              I=IY+(IX-1)*NY
              F(L0VAL+I)=GVINT(IY,IZSTEP)
1133        CONTINUE
1132      CONTINUE

C.. For U1 component set VAL= U VELOCITY
      ELSEIF (INDVAR.EQ.U1) THEN
        DO 1134 IX=IXF,IXL
          DO 1135 IY=NY/2+1,NY
              I=IY+(IX-1)*NY
              F(L0VAL+I)=GUINT(IY,IZSTEP)
1135        CONTINUE
1134      CONTINUE

C.. For kinetic energy of turbulence set VAL= KE
      ELSEIF (INDVAR.EQ.KE) THEN
        DO 1140 IX=IXF,IXL
          DO 1141 IY=NY/2+1,NY
              I=IY+(IX-1)*NY
              F(L0VAL+I)=GKET(IY,IZSTEP)
1141        CONTINUE
1140      CONTINUE
```

```
C.. For turbulence energy dissipation rate set VAL= EP
      ELSEIF (INDVAR.EQ.EP) THEN
        DO 1142 IX=IXF,IXL
          DO 1143 IY=NY/2+1,NY
              I=IY+(IX-1)*NY
              F(L0VAL+I)=GEPT(IY,IZSTEP)
1143        CONTINUE
1142      CONTINUE

C.. For temperature set VAL = TEM1
      ELSEIF (INDVAR.EQ.14) THEN
        DO 1146 IX=IXF,IXL
          DO 1147 IY=NY/2+1,NY
              I=IY+(IX-1)*NY
              F(L0VAL+I)=GTINT(IY,IZSTEP)
1147        CONTINUE
1146      CONTINUE
      ENDIF
    ENDIF

    RETURN
1312 CONTINUE
C------------------- SECTION 13 ------------------- value = GRND1
    RETURN
1313 CONTINUE
*************************************************************
```

Ground coding deleted

```
*************************************************************

C*************************************************************
C* Make changes to data for GROUPS 15, 16, 17, 18  GROUP 19.
C*************************************************************
C
C--- GROUP 19. Special calls to GROUND from EARTH
C
  19 GO TO (191,192,193,194,195,196,197,198,199,1910,1911),ISC
 191 CONTINUE
C   * ------------------- SECTION 1 ---- Start of time step.
C.. If IRUNN = 1 i.e. the first junction, don't want to read data
C.. from files because flat velocity profile
    IF (IRUNN.EQ.1) THEN
        GO TO 192
    ENDIF

C.. Define the character names for the files that will be
C.. read.  Will read files called .. .out, since the previous run
C.. outfiles are the new run infiles.
```

```
C.. CG(9)=J(IRUNN-1), CG(1)=U1,CG(2)=V1,CG(3)=W1,CG(4)=KE,CG(5)=EP
C.. CG(6)=T1,CG(7)=P1
C.. OUTB
     UINB=CG(9)(1:2)//CG(1)(1:2)//'OUTB'//'.OUT'
     VINB=CG(9)(1:2)//CG(2)(1:2)//'OUTB'//'.OUT'
     WINB=CG(9)(1:2)//CG(3)(1:2)//'OUTB'//'.OUT'
     KEINB=CG(9)(1:2)//CG(4)(1:2)//'OUTB'//'.OUT'
     EPINB=CG(9)(1:2)//CG(5)(1:2)//'OUTB'//'.OUT'
     TINB=CG(9)(1:2)//CG(6)(1:2)//'OUTB'//'.OUT'
     PINB=CG(9)(1:2)//CG(7)(1:2)//'OUTB'//'.OUT'
C.. OUTT
     UINT=CG(9)(1:2)//CG(1)(1:2)//'OUTT'//'.OUT'
     VINT=CG(9)(1:2)//CG(2)(1:2)//'OUTT'//'.OUT'
     WINT=CG(9)(1:2)//CG(3)(1:2)//'OUTT'//'.OUT'
     KEINT=CG(9)(1:2)//CG(4)(1:2)//'OUTT'//'.OUT'
     EPINT=CG(9)(1:2)//CG(5)(1:2)//'OUTT'//'.OUT'
     TINT=CG(9)(1:2)//CG(6)(1:2)//'OUTT'//'.OUT'
     PINT=CG(9)(1:2)//CG(7)(1:2)//'OUTT'//'.OUT'

C.. At start of time step read the velocity components into user-
C.. defined arrays from files
     OPEN(UNIT=78,FILE=UINB,FORM='UNFORMATTED')
     OPEN(UNIT=79,FILE=VINB,FORM='UNFORMATTED')
     OPEN(UNIT=80,FILE=WINB,FORM='UNFORMATTED')
     OPEN(UNIT=81,FILE=KEINB,FORM='UNFORMATTED')
     OPEN(UNIT=82,FILE=EPINB,FORM='UNFORMATTED')
     OPEN(UNIT=83,FILE=TINB,FORM='UNFORMATTED')
     OPEN(UNIT=84,FILE=UINT,FORM='UNFORMATTED')
     OPEN(UNIT=85,FILE=VINT,FORM='UNFORMATTED')
     OPEN(UNIT=86,FILE=WINT,FORM='UNFORMATTED')
     OPEN(UNIT=87,FILE=KEINT,FORM='UNFORMATTED')
     OPEN(UNIT=88,FILE=EPINT,FORM='UNFORMATTED')
     OPEN(UNIT=89,FILE=TINT,FORM='UNFORMATTED')
     OPEN(UNIT=122,FILE=PINB,FORM='UNFORMATTED')
     OPEN(UNIT=123,FILE=PINT,FORM='UNFORMATTED')

     DO 1148 I=1,NX
       DO 1149 J=1,10
         READ(78) GUINB(J,I)
         READ(79) GVINB(J,I)
         READ(80) GWINB(J,I)
         READ(81) GKEB(J,I)
         READ(82) GEPB(J,I)
         READ(83) GTINB(J,I)
           READ(122)GPINB(J,I)
1149    CONTINUE
1148 CONTINUE

     DO 1150 I=1,NZ
```

```
      DO 1151 J=11,NY
        READ(84) GUINT(J,I)
        READ(85) GVINT(J,I)
        READ(86) GWINT(J,I)
        READ(87) GKET(J,I)
        READ(88) GEPT(J,I)
        READ(89) GTINT(J,I)
          READ(123)GPINT(J,I)
1151    CONTINUE
1150 CONTINUE

C.. Check that the correct velocities are in the arrays
    WRITE(*,*)'INITIAL VELOCITIES READ FROM FILES INTO ARRAYS'
    WRITE(*,79)'GPINB:','GUINB:','GVINB:','GWINB:','GKEINB:',
   +'GEPINB:','GTINB:'
    DO 1152 I=1,NX
       DO 1153 J=1,10
         WRITE(*,80) GPINB(J,I),GUINB(J,I),GVINB(J,I),GWINB(J,I),
   +GKEB(J,I),GEPB(J,I),GTINB(J,I)
1153     CONTINUE
1152 CONTINUE
    WRITE(*,79)'GPINT:','GUINT:','GVINT:','GWINT:','GKET:',
   +'GEPT:','GTINT:'
    DO 1154 I=1,NZ
      DO 1155 J=11,NY
        WRITE(*,80) GPINT(J,I),GUINT(J,I),GVINT(J,I),GWINT(J,I),
   +GKET(J,I),GEPT(J,I),GTINT(J,I)
1155    CONTINUE
1154 CONTINUE
    CLOSE(78)
    CLOSE(79)
    CLOSE(80)
    CLOSE(81)
    CLOSE(82)
    CLOSE(83)
    CLOSE(84)
    CLOSE(85)
    CLOSE(86)
    CLOSE(87)
    CLOSE(88)
    CLOSE(89)
    CLOSE(122)
    CLOSE(123)
 79  FORMAT(1X,7(A8))
 80  FORMAT(1X,7(F8.4))

    RETURN
 192 CONTINUE
```

```
**************************************************

Ground coding deleted

**************************************************
C  * ------------------ SECTION 8 ---- Finish of time step.
C.. Define the character names for the files that will be written.
C.. OUTB
     UOUTB=CG(8)(1:2)//CG(1)(1:2)//'OUTB'//'.OUT'
     VOUTB=CG(8)(1:2)//CG(2)(1:2)//'OUTB'//'.OUT'
     WOUTB=CG(8)(1:2)//CG(3)(1:2)//'OUTB'//'.OUT'
     KEOUTB=CG(8)(1:2)//CG(4)(1:2)//'OUTB'//'.OUT'
     EPOUTB=CG(8)(1:2)//CG(5)(1:2)//'OUTB'//'.OUT'
     TOUTB=CG(8)(1:2)//CG(6)(1:2)//'OUTB'//'.OUT'
     POUTB=CG(8)(1:2)//CG(7)(1:2)//'OUTB'//'.OUT'
C.. OUTT
     UOUTT=CG(8)(1:2)//CG(1)(1:2)//'OUTT'//'.OUT'
     VOUTT=CG(8)(1:2)//CG(2)(1:2)//'OUTT'//'.OUT'
     WOUTT=CG(8)(1:2)//CG(3)(1:2)//'OUTT'//'.OUT'
     KEOUTT=CG(8)(1:2)//CG(4)(1:2)//'OUTT'//'.OUT'
     EPOUTT=CG(8)(1:2)//CG(5)(1:2)//'OUTT'//'.OUT'
     TOUTT=CG(8)(1:2)//CG(6)(1:2)//'OUTT'//'.OUT'
     POUTT=CG(8)(1:2)//CG(7)(1:2)//'OUTT'//'.OUT'


C.. MAIN OUTLETS
C.. ============
C.. For X-Y face write out the velocities
C.. ====================================
C.. At end of the run write the velocity components from the last slab
C.. to files
      OPEN(UNIT=66,FILE=UOUTB,FORM='UNFORMATTED',STATUS='NEW')
      OPEN(UNIT=67,FILE=VOUTB,FORM='UNFORMATTED',STATUS='NEW')
      OPEN(UNIT=68,FILE=WOUTB,FORM='UNFORMATTED',STATUS='NEW')
     OPEN(UNIT=69,FILE=KEOUTB,FORM='UNFORMATTED',STATUS='NEW')
     OPEN(UNIT=70,FILE=EPOUTB,FORM='UNFORMATTED',STATUS='NEW')
      OPEN(UNIT=76,FILE=TOUTB,FORM='UNFORMATTED',STATUS='NEW')
      OPEN(UNIT=124,FILE=POUTB,FORM='UNFORMATTED',STATUS='NEW')

C.. Find the zero location indices of each variable on the last slab.
C.. Need nz-1 for w1 as at nz w1 has been set to zero (re:staggered grid)

      L0U1OUTB=L0F(ANYZ(U1,NZ))
      L0V1OUTB=L0F(ANYZ(V1,NZ))
      L0W1OUTB=L0F(ANYZ(W1,NZ-1))
      L0KEOUTB=L0F(ANYZ(KE,NZ))
      L0EPOUTB=L0F(ANYZ(EP,NZ))
      L0TOUTB =L0F(ANYZ(14,NZ))
      L0P1OUTB=L0F(ANYZ(P1,NZ))
```

```
      WRITE(*,*)'VELOCITIES FROM LAST SLAB BEING WRITTEN TO FILES'
      WRITE(*,64)'UOUTB','VOUTB','WOUTB','KEOUTB','EPOUTB','TOUTB'
      DO 1111 IX=1,NX
        DO 1112 IY=1,NY/2
           I=IY+(IX-1)*NY
           WRITE(66) (F(L0U1OUTB+I))
           WRITE(67) (F(L0V1OUTB+I))
           WRITE(68) (F(L0W1OUTB+I))
           WRITE(69) (F(L0KEOUTB+I))
           WRITE(70) (F(L0EPOUTB+I))
           WRITE(76) (F(L0TOUTB+I))
           WRITE(124)(F(L0P1OUTB+I))

C.. Display the velocities that have been written to files
           WRITE(*,65) (F(L0U1OUTB+I)),(F(L0V1OUTB+I)),
     +       (F(L0W1OUTB+I)),(F(L0KEOUTB+I)),(F(L0EPOUTB+I)),
     +       (F(L0TOUTB+I))
 1112    CONTINUE
 1111 CONTINUE

 64   FORMAT(1X,6(A8))
 65   FORMAT(1X,6(F8.4))
      CLOSE(66)
      CLOSE(67)
      CLOSE(68)
      CLOSE(69)
      CLOSE(70)
      CLOSE(76)
      CLOSE(124)

C.. For Y-Z face write out the velocities
C.. ====================================
      OPEN(UNIT=71,FILE=UOUTT,FORM='UNFORMATTED',STATUS='NEW')
      OPEN(UNIT=72,FILE=VOUTT,FORM='UNFORMATTED',STATUS='NEW')
      OPEN(UNIT=73,FILE=WOUTT,FORM='UNFORMATTED',STATUS='NEW')
      OPEN(UNIT=74,FILE=KEOUTT,FORM='UNFORMATTED',STATUS='NEW')
      OPEN(UNIT=75,FILE=EPOUTT,FORM='UNFORMATTED',STATUS='NEW')
      OPEN(UNIT=77,FILE=TOUTT,FORM='UNFORMATTED',STATUS='NEW')
      OPEN(UNIT=125,FILE=POUTT,FORM='UNFORMATTED',STATUS='NEW')

      WRITE(*,*)'VELOCITIES FROM Y-Z FACE BEING WRITTEN TO FILES'

C.. Need to find L0F for each variable and each slab
      DO 1113 K=1,NZ
        L0U1OUTT=L0F(ANYZ(U1,K))
        L0V1OUTT=L0F(ANYZ(V1,K))
        L0W1OUTT=L0F(ANYZ(W1,K))
        L0KEOUTT=L0F(ANYZ(KE,K))
```

```
      L0EPOUTT=L0F(ANYZ(EP,K))
      L0TOUTT =L0F(ANYZ(14,K))
      L0P1OUTT=L0F(ANYZ(P1,K))

C.. Need to get it to read the nx-1 for u1 but nx for v1 and w1 -
C.. something to do with the staggered grid and the u1 being set to 0

        WRITE(*,*)'GUOUTT: '
        DO 1122 IX=NX-1,NX-1
          DO 1123 IY=NY/2+1,NY
            I=IY+(IX-1)*NY
            WRITE(71) (F(L0U1OUTT+I))
            WRITE(*,*)  (F(L0U1OUTT+I))
1123        CONTINUE
1122      CONTINUE

        WRITE(*,*)'GVOUTT: ','GWOUTT: ','GKET: ',
     +'GEPT: ','  TEM1:  '
        DO 1124 IX=NX,NX
          DO 1125 IY=NY/2+1,NY
            I=IY+(IX-1)*NY
              WRITE(72) (F(L0V1OUTT+I))
              WRITE(73) (F(L0W1OUTT+I))
              WRITE(74) (F(L0KEOUTT+I))
              WRITE(75) (F(L0EPOUTT+I))
              WRITE(77) (F(L0TOUTT+I))
              WRITE(125)(F(L0P1OUTT+I))
              WRITE(*,822) (F(L0V1OUTT+I)),(F(L0W1OUTT+I)),
     +(F(L0KEOUTT+I)),(F(L0EPOUTT+I)),(F(L0TOUTT+I))
1125        CONTINUE
1124      CONTINUE

1113 CONTINUE

      CLOSE(71)
      CLOSE(72)
      CLOSE(73)
      CLOSE(74)
      CLOSE(75)
      CLOSE(77)
      CLOSE(125)
 822    FORMAT(1X,5(F8.4))
 823  FORMAT(1X,F8.4)

      OPEN(UNIT=126,FILE='AREA.OUT',FORM='FORMATTED')

      DO 1555 I=1,NGX
        DO 1556 J=1,NGY
          WRITE(126,*) GAREA(I,J)
```

```
1556   CONTINUE
1555 CONTINUE
     CLOSE(126)
C
     RETURN
C*****************************************************************
C
C--- GROUP 20. Preliminary print-out
C
  20 CONTINUE
     RETURN
C*****************************************************************
C* Make changes to data for GROUPS 21 and 22 only in GROUP 19.
C*****************************************************************
C
C--- GROUP 23. Field print-out and plot control
  23 CONTINUE
     RETURN
C*****************************************************************
C
C--- GROUP 24. Dumps for restarts
C
  24 CONTINUE
     END
```

APPENDIX 6 - Q1 FILE FOR PLAIN JUNCTION, CCM SOLVER

```
TALK=T;RUN( 1, 1);VDU=X11-TERM
 IRUNN  =      1 ;LIBREF =      0
**************************************************************
 Group 1. Run Title
TEXT(TRIANGULAR JUNCTION (45deg) J11, CCM )
**************************************************************
 Group 2. Transience
STEADY  =   T
**************************************************************
 Groups 3, 4, 5  Grid Information
  * Overall number of cells, RSET(M,NX,NY,NZ,tolerance)
RSET(M,15,20,15)
  * Set overall domain extent:
  *       xulast  yvlast  zwlast   name
XSI= 1.500E-02;YSI= 1.800E-02;ZSI= 1.500E-02;RSET(D,CHAM   )
**************************************************************
 Group 6. Body-Fitted coordinates
BFC=T
  * Set points
XPO= 7.0000E-03;YPO= 0.0000E+00;ZPO= 0.0000E+00;GSET(P,P1  )
XPO= 8.0000E-03;YPO= 0.0000E+00;ZPO= 0.0000E+00;GSET(P,P2  )
XPO= 0.0000E+00;YPO= 9.0000E-03;ZPO= 0.0000E+00;GSET(P,P3  )
XPO= 1.5000E-02;YPO= 9.0000E-03;ZPO= 0.0000E+00;GSET(P,P4  )
XPO= 0.0000E+00;YPO= 9.0000E-03;ZPO= 1.5000E-02;GSET(P,P5  )
XPO= 0.0000E+00;YPO= 1.8000E-02;ZPO= 7.0000E-03;GSET(P,P6  )
XPO= 0.0000E+00;YPO= 1.8000E-02;ZPO= 8.0000E-03;GSET(P,P7  )
  * Set lines/arcs
GSET(L,L1,P1,P2,15,1.0)
GSET(L,L2,P2,P4,10,1.0)
GSET(L,L3,P4,P3,15,1.0)
GSET(L,L4,P3,P1,10,1.0)
GSET(L,L5,P3,P5,15,1.0)
GSET(L,L6,P5,P7,10,1.0)
GSET(L,L7,P7,P6,15,1.0)
GSET(L,L8,P6,P3,10,1.0)
  * Set frames
GSET(F,F1,P1,-,P2,-,P4,-,P3,-)
GSET(F,F2,P3,-,P5,-,P7,-,P6,-)
  * Match a grid mesh
GSET(M,F1,+I+J,1,1,1,TRANS)
GSET(M,F2,+K+J,1,11,1,TRANS)
  * Copy/Transfer/Block grid planes
GSET(C,K16,F,K1,1,15,1,10,+,0,0,1.5000E-02,INC,1)
GSET(C,I16,F,I1,11,20,1,15,+,1.5000E-02,0,0,INC,1)
  *********
NONORT  =   f
  * X-cyclic boundaries switched
```

```
*************************************************************
 Group 7. Variables: STOREd,SOLVEd,NAMEd
ONEPHS =  T
  * Non-default variable names
NAME(14) =TEM1
NAME(16) =UC1  ; NAME(17) =VC1
NAME(18) =WC1  ; NAME(46) =ENUT
NAME(47) =WCRT ; NAME(48) =VCRT
NAME(49) =VPOR ; NAME(50) =UCRT
  * Solved variables list
SOLVE(P1  ,U1  ,V1  ,W1  ,KE  ,EP  ,UC1 ,VC1 )
SOLVE(WC1 ,TEM1)
  * Stored variables list
STORE(UCRT,VPOR,VCRT,WCRT,ENUT)
  * Additional solver options
SOLUTN(P1  ,Y,Y,Y,N,N,Y)
SOLUTN(U1  ,Y,Y,N,Y,N,Y)
SOLUTN(V1  ,Y,Y,N,Y,N,Y)
SOLUTN(W1  ,Y,Y,N,Y,N,Y)
  ** note last argument = y for uc's + ke + ep
SOLUTN(KE  ,Y,Y,Y,N,N,y)
SOLUTN(EP  ,Y,Y,Y,N,N,y)
SOLUTN(ENUT,Y,N,N,N,N,Y)
SOLUTN(UC1 ,Y,Y,Y,N,N,y)
SOLUTN(VC1 ,Y,Y,Y,N,N,y)
SOLUTN(WC1 ,Y,Y,Y,N,N,y)
SOLUTN(WCRT,Y,N,Y,N,N,N)
SOLUTN(VCRT,Y,N,Y,N,N,N)
SOLUTN(UCRT,Y,N,Y,N,N,N)
SOLUTN(TEM1,Y,Y,Y,N,N,y)
*************************************************************
 Group 8. Terms & Devices
TERMS (P1  ,Y,Y,Y,N,Y,N)
TERMS (U1  ,N,N,N,N,N,N)
TERMS (V1  ,N,N,N,N,N,N)
TERMS (W1  ,N,N,N,N,N,N)
TERMS (KE  ,N,Y,Y,Y,Y,N)
TERMS (EP  ,N,Y,Y,Y,Y,N)
TERMS (UC1 ,N,Y,Y,N,Y,Y)
TERMS (VC1 ,N,Y,Y,N,Y,Y)
TERMS (WC1 ,N,Y,Y,N,Y,Y)
TERMS (TEM1,y,Y,Y,N,Y,N)
HUNIT = 1/1005
NEWENT =  T
UCONV  =  T
UDIFF  =  T
USOLVE =  T
*************************************************************
 Group 9. Properties
```

```
RHO1    = 3.400E+00
EL1     = GRND4
ENUL    = 2.760E-06 ;ENUT   = GRND3
PRT   (EP  ) =  1.314E+00
************************************************************
 Group 10.Inter-Phase Transfer Processes
************************************************************
 Group 11.Initialise Var/Porosity Fields
    NAMFI = CHAM
    restrt(all)
    RESTRT(P1,U1,V1,W1,KE,EP,ENUT,WC1,VC1,UC1,WCRT,VCRT,UCRT)
FIINIT(TEM1) = 1.000E-05
FIINIT(P1  ) =  1.000E-10 ;FIINIT(U1  ) =  1.000E-10
FIINIT(V1  ) =  1.000E-10 ;FIINIT(W1  ) =  1.000E-10
FIINIT(KE  ) =  1.300E-03 ;FIINIT(EP  ) =  5.100E-03
FIINIT(ENUT) =  1.000E-10
FIINIT(WC1 ) =  1.000E-05 ;FIINIT(VC1 ) =  1.000E-05
FIINIT(UC1 ) =  1.000E-05 ;FIINIT(WCRT) =  1.000E-10
FIINIT(VCRT) =  1.000E-10 ;FIINIT(UCRT) =  1.000E-10
 No PATCHes used for this Group
RSTGRD  =   F
INIADD  =   T
************************************************************
 Group 12. Convection and diffusion adjustments
************************************************************
 Group 13. Boundary & Special Sources

PATCH (KESOURCE,PHASEM,1,15,1,20,1,15,1,1)
COVAL (KESOURCE,KE  , GRND4   , GRND4   )
COVAL (KESOURCE,EP  , GRND4   , GRND4   )

INLET (INB    ,LOW   ,#1,#1,#1,#1,#1,#1,#1,#1)
VALUE (INB    ,P1  , rho1*3.6)
VALUE (INB    ,KE  , 1.3E-03)
VALUE (INB    ,EP  , 5.1E-03)
VALUE (INB    ,UC1 , 0.0)
VALUE (INB    ,VC1 , 0.0)
VALUE (INB    ,WC1 , 3.600E+00)

INLET (INT    ,WEST  ,#1,#1,#2,#2,#1,#1,#1,#1)
VALUE (INT    ,P1  , rho1*3.6)
VALUE (INT    ,KE  , 1.3E-03)
VALUE (INT    ,EP  , 5.1E-03)
VALUE (INT    ,UC1 , 3.600E+00)
VALUE (INT    ,VC1 , 0.0)
VALUE (INT    , WC1 , 0.0)

OUTLET(OUTB   ,HIGH  ,#1,#1,#1,#1,#1,#1,#1,#1)
VALUE (OUTB   ,P1  , 0.000E+00)
```

```
OUTLET(OUTT   ,EAST  ,#1,#1,#2,#2,#1,#1,#1,#1)
VALUE (OUTT   ,P1    , 0.000E+00)


PATCH (WALL1  ,WWALL ,#1,#1,#1,#1,#1,#1,#1,#1)
COVAL (WALL1  ,UC1   , GRND2   , 0.000E+00)
COVAL (WALL1  ,Vc1   , GRND2   , 0.000E+00)
COVAL (WALL1  ,Wc1   , GRND2   , 0.000E+00)
COVAL (WALL1  ,KE    , GRND2   , GRND2   )
COVAL (WALL1  ,EP    , GRND2   , GRND2   )
COVAL (WALL1  ,TEM1, GRND2   , 50)

PATCH (WALL2  ,EWALL ,#1,#1,#1,#1,#1,#1,#1,#1)
COVAL (WALL2  ,Uc1   , GRND2   , 0.000E+00)
COVAL (WALL2  ,Vc1   , GRND2   , 0.000E+00)
COVAL (WALL2  ,Wc1   , GRND2   , 0.000E+00)
COVAL (WALL2  ,KE    , GRND2   , GRND2   )
COVAL (WALL2  ,EP    , GRND2   , GRND2   )
COVAL (WALL2  ,TEM1, GRND2   , 50)

PATCH (WALL3  ,LWALL ,#1,#1,#2,#2,#1,#1,#1,#1)
COVAL (WALL3  ,Uc1   , GRND2   , 0.000E+00)
COVAL (WALL3  ,Vc1   , GRND2   , 0.000E+00)
COVAL (WALL3  ,Wc1   , GRND2   , 0.000E+00)
COVAL (WALL3  ,KE    , GRND2   , GRND2   )
COVAL (WALL3  ,EP    , GRND2   , GRND2   )
COVAL (WALL3  ,TEM1, GRND2   , 50)

PATCH (WALL4  ,HWALL ,#1,#1,#2,#2,#1,#1,#1,#1)
COVAL (WALL4  ,Uc1   , GRND2   , 0.000E+00)
COVAL (WALL4  ,Vc1   , GRND2   , 0.000E+00)
COVAL (WALL4  ,Wc1   , GRND2   , 0.000E+00)
COVAL (WALL4  ,KE    , GRND2   , GRND2   )
COVAL (WALL4  ,EP    , GRND2   , GRND2   )
COVAL (WALL4  ,TEM1, GRND2   , 50)

  ** note the ordering of the Bc's
  ** This is because the values in the corner get overwritten
  ** at overlapping patches

PATCH (TOP    ,NWALL ,#1,#1,#2,#2,#1,#1,#1,#1)
COVAL (TOP    ,Uc1   , GRND2   , 0.000E+00)
COVAL (TOP    ,Vc1   , GRND2   , 0.000E+00)
COVAL (TOP    ,Wc1   , GRND2   , 0.000E+00)
COVAL (TOP    ,KE    , GRND2   , GRND2   )
COVAL (TOP    ,EP    , GRND2   , GRND2   )
COVAL (TOP    ,TEM1, GRND2   , 50)
```

```
PATCH (BOT    ,SWALL ,#1,#1,#1,#1,#1,#1,#1,#1)
COVAL (BOT    ,Uc1  , GRND2   , 0.000E+00)
COVAL (BOT    ,Vc1  , GRND2   , 0.000E+00)
COVAL (BOT    ,Wc1  , GRND2   , 0.000E+00)
COVAL (BOT    ,KE   , GRND2   , GRND2   )
COVAL (BOT    ,EP   , GRND2   , GRND2   )
COVAL (BOT    ,TEM1, GRND2   , 50)

BFCA   = 3.400E+00
************************************************************
 Group 14. Downstream Pressure For PARAB
************************************************************
 Group 15. Terminate Sweeps
LSWEEP  =   1000
SELREF  =    T
RESFAC  = 1.000E-05
************************************************************
 Group 16. Terminate Iterations
LITER (P1  ) =    20 ;LITER (U1  ) =   1
LITER (V1  ) =     1 ;LITER (W1  ) =   1
LITER (KE  ) =    20 ;LITER (EP  ) =  20
LITER (WC1 ) =    20 ;LITER (VC1 ) =  20
LITER (UC1 ) =  20
ENDIT (P1  ) = 1.000E-05 ;ENDIT (U1  ) = 1.000E-03
ENDIT (V1  ) = 1.000E-03 ;ENDIT (W1  ) = 1.000E-03
ENDIT (KE  ) = 1.000E-03 ;ENDIT (EP  ) = 1.000E-03
ENDIT (UC1 ) = 1.000E-05 ;ENDIT (VC1 ) = 1.000E-05
ENDIT (WC1 ) = 1.000E-05
ENDIT (TEM1) = 1.000E-03
************************************************************
 Group 17. Relaxation
RELAX(P1  ,LINRLX, 3.000E-01)
RELAX(Uc1  ,FALSDT, 2.778E-03)
RELAX(Vc1  ,FALSDT, 2.778E-03)
RELAX(Wc1  ,FALSDT, 2.778E-03)
RELAX(ke   ,FALSDT, 2.778E-04)
RELAX(ep   ,FALSDT, 2.778E-04)
RELAX(TEM1 ,linrlx, 2.000E-01)
     RELAX(KE  ,LINRLX, 0.3)
     RELAX(EP  ,LINRLX, 0.3)
KELIN  =      1
************************************************************
 Group 18. Limits
************************************************************
 Group 19. EARTH Calls To GROUND Station
GENK   =   T
LSG4   =   T
CSG3   =LCRU
NSAVE=J1FI
```

```
NAMXYZ=J1XY
CG(1)=U1
CG(2)=V1
CG(3)=W1
CG(4)=KE
CG(5)=EP
CG(6)=T1
CG(7)=P1
CG(8)=J1
CG(9)=J0
RG(1) = 1000
************************************************************
 Group 20. Preliminary Printout
ECHO   =   T
************************************************************
 Group 21. Print-out of Variables
WALPRN = T
OUTPUT(P1,y,N,N,Y,Y,Y);OUTPUT(U1,N,N,N,Y,Y,Y)
OUTPUT(V1,N,N,N,Y,Y,Y);OUTPUT(W1,N,N,N,Y,Y,Y)
OUTPUT(KE,N,N,N,Y,Y,Y);OUTPUT(EP,N,N,N,Y,Y,Y)
OUTPUT(TEM1,Y,N,N,Y,Y,Y)
OUTPUT(ENUT,N,N,N,N,N,N);OUTPUT(VCRT,N,N,N,N,N,N)
OUTPUT(UCRT,n,N,N,N,N,N)
OUTPUT(WCRT,n,N,N,N,N,N)
OUTPUT(WC1 ,Y,N,N,Y,Y,Y)
************************************************************
 Group 22. Monitor Print-Out
IXMON  =     7 ;IYMON  =     5 ;IZMON  =    14
TSTSWP  =  12345
************************************************************
 Group 23.Field Print-Out & Plot Control
NPRINT  =   1000
NUMCLS  =     10
NXPRIN  =      1
IXPRF   =      1 ;IXPRL  =      1
NYPRIN  =      1
IYPRF   =      1 ;IYPRL  =     10
NZPRIN  =      1
IZPRF   =      1 ;IZPRL  =     15
ITABL   =      1
  No PATCHes used for this Group
************************************************************
 Group 24. Dumps For Restarts
************************************************************
 MENSAV(S,RELX,DEF,1.0000E-03,3.6000E+00,10)
 MENSAV(S,PHSPROP,DEF,200,273,3.4000E+00,1.0000E-05)
 MENSAV(S,FLPRP,DEF,LAMINAR,CONSTANT,AIR-CONSTANT)
STOP
```

APPENDIX 7 - ADDITIONAL GROUND CODING FOR SLOTS

```
C FILE NAME GROUND.FTN----------011093
C GROUND STATION TO READ INPUT AND WRITE OUTPUT FROM
TRIANGULAR JUNCTION
C FOR VARIABLES P1,U1,V1,W1,KE,EP,TEM1
C Also reads and writes data for slots called INB2, OUTB2, INT2, OUTT2
C
      SUBROUTINE GROUND
      INCLUDE 'lp2/d_includ/satear'
      INCLUDE 'lp2/d_includ/grdloc'
      INCLUDE 'lp2/d_includ/grdear'
      INCLUDE 'lp2/d_includ/grdbfc'
CXXXXXXXXXXXXXXXXXXXXXXXXXXXXXXXXXXXXXXXX USER
SECTION STARTS:
C
C 1   Set dimensions of data-for-GROUND arrays here. WARNING: the
C     corresponding arrays in the MAIN program of the satellite
C     and EARTH must have the same dimensions.
      PARAMETER (NLG=100, NIG=200, NRG=200, NCG=100)
      PARAMETER (NGX = 50, NGY = 50)
      PARAMETER (MX = 13, MY = 2, MZ = 13)
C

COMMON/LGRND/LG(NLG)/IGRND/IG(NIG)/RGRND/RG(NRG)/CGRND/CG(
NCG)
      LOGICAL LG
      CHARACTER*4 CG
C
C 2   User dimensions own arrays here, for example:
C     DIMENSION GUH(10,10),GUC(10,10),GUX(10,10),GUZ(10)

      DIMENSION GUINB(NGX,NGY),GVINB(NGX,NGY),GWINB(NGX,NGY),

+GUINT(NGX,NGY),GVINT(NGX,NGY),GWINT(NGX,NGY),GKEB(NGX,NG
Y),

+GEPB(NGX,NGY),GKET(NGX,NGY),GEPT(NGX,NGY),GTINB(NGX,NGY),
     +GTINT(NGX,NGY),
     +GUINB2(NGX*NGY),GVINB2(NGX*NGY),GWINB2(NGX*NGY),
     +GKEB2(NGX*NGY),GEPB2(NGX*NGY),GTINB2(NGX*NGY),
     +GUINT2(NGX*NGY),GVINT2(NGX*NGY),GWINT2(NGX*NGY),
     +GKET2(NGX*NGY),GEPT2(NGX*NGY),GTINT2(NGX*NGY),
     +GVCRTB(NGX,NGY),GVCRTT(NGX,NGY)


C 3   User places his data statements here, for example:
C     DATA NXDIM,NYDIM/10,10/
C
```

```
C 4  Insert own coding below as desired, guided by GREX examples.
C    Note that the satellite-to-GREX special data in the labelled
C    COMMONs /RSG/, /ISG/, /LSG/ and /CSG/ can be included and
C    used below but the user must check GREX for any conflicting
C    uses. The same comment applies to the EARTH-spare working
C    arrays EASP1, EASP2,....EASP20. In addition to the EASPs,
C    there are 10 GRound-earth SPare arrays, GRSP1,...,GRSP10,
C    supplied solely for the user, which are not used by GREX. If
C    the call to GREX has been deactivated then all of the arrays
C    may be used without reservation.
C
c*************************************************************************
****
c
    IXL=IABS(IXL)
    IF(IGR.EQ.13) GO TO 13
    IF(IGR.EQ.19) GO TO 19
    GO TO (1,2,3,4,5,6,25,8,9,10,11,12,13,14,25,25,25,25,19,20,25,
   125,23,24),IGR
  25 CONTINUE
    RETURN
C************************************************************************
C
C--- GROUP 1. Run title and other preliminaries
C
   1 GO TO (1001,1002),ISC
 1001 CONTINUE
C
C    User may here change message transmitted to the VDU screen
     IF(IGR.EQ.1.AND.ISC.EQ.1.AND..NOT.NULLPR)
    1  CALL WRYT40('GROUND file is GROUND.F   of:   011093 ')
       CALL WRYT40('THIS IS A PRIVATE VERSION OF GROUND    ')
       CALL WRYT40('WRITES/READS U1,V1,W1,KE,EP,TEM1       ')
       CALL WRYT40('NEW PACKING-READS/WRITES DATA FOR SLOTS ')
C
     RETURN
 1002 CONTINUE
     RETURN
C************************************************************************

Ground coding deleted

C************************************************************************
C------------------ SECTION 13 ------------------ value = GRND1
C.. For the patch named INB2 ie the bottom inlet slot
c.. ================================================================

     IF(NPATCH.EQ.'INB2') THEN
```

```
C.. Define PSI - the angle of normal to cell into cell, approx 38deg
     PSI = 0.663225136

C.. Define the angle of e2 to the horizontal, approx 125deg
     ANGE2 = 2.181661565

C.. Find the zero location index of VAL
     L0VAL=L0F(VAL)

C.. Initialise COUNT to zero
     COUNT = 0.0

C.. For P1 set VAL = DENSITY * velocity
C.. Ignore W1 as has no effect on velocity through slot
          IF(INDVAR.EQ.P1) THEN
            DO 1182 IY=1,MY
          DIFF = IZSTEP - (NZ-MZ)/2 - 1
                  COUNT = IY + DIFF * MY
                  F(L0VAL+IY) = RHO1*(SQRT(GUINB2(COUNT)**2
     +           +GVINB2(COUNT)**2))
     +           *COS(ATAN2(GVINB2(COUNT),GUINB2(COUNT))-PSI)
     +           *COS(PSI)
     1182       CONTINUE

          ELSEIF (INDVAR.EQ.U1) THEN
             DO 1184 IY=1,MY
           DIFF = IZSTEP - (NZ-MZ)/2 - 1
                  COUNT = IY + DIFF * MY
                  F(L0VAL+IY) =
     +          (SQRT(GUINB2(COUNT)**2+GVINB2(COUNT)**2))
     +          *COS(ATAN2(GVINB2(COUNT),GUINB2(COUNT)))
     1184       CONTINUE

          ELSEIF (INDVAR.EQ.V1) THEN
            DO 1186 IY=1,MY
          DIFF = IZSTEP - (NZ-MZ)/2 - 1
                  COUNT = IY + DIFF * MY
                  F(L0VAL+IY) =
     +          (SQRT(GVINB2(COUNT)**2+GUINB2(COUNT)**2))
     +          *COS(ANGE2-ATAN2(GVINB2(COUNT),GUINB2(COUNT)))
     1186       CONTINUE

          ELSEIF (INDVAR.EQ.W1) THEN
            DO 1188 IY=1,MY
          DIFF = IZSTEP - (NZ-MZ)/2 - 1
                  COUNT = IY + DIFF * MY
                  F(L0VAL+IY) = GWINB2(COUNT)
     1188       CONTINUE
```

```
      ELSEIF (INDVAR.EQ.KE) THEN
        DO 1190 IY=1,MY
      DIFF = IZSTEP - (NZ-MZ)/2 - 1
             COUNT = IY + DIFF * MY
             F(L0VAL+IY) = GKEB2(COUNT)
1190    CONTINUE

      ELSEIF (INDVAR.EQ.EP) THEN
        DO 1192 IY=1,MY
      DIFF = IZSTEP - (NZ-MZ)/2 - 1
             COUNT = IY + DIFF * MY
             F(L0VAL+IY) = GEPB2(COUNT)
1192    CONTINUE

      ELSEIF (INDVAR.EQ.14) THEN
        DO 1194 IY=1,MY
      DIFF = IZSTEP - (NZ-MZ)/2 - 1
             COUNT = IY + DIFF * MY
             F(L0VAL+IY) = GTINB2(COUNT)
1194    CONTINUE

      ENDIF
    ENDIF


C.. For the patch named INT2 ie the top inlet slot
C.. ==========================================

    IF(NPATCH.EQ.'INT2') THEN

C..  Define PSI - the angle of the normal into the cell approx -38deg
    PSI = -0.663225115

C.. Define the angle e2 approx 52deg
    ANGE2 = 0.907571211

C.. Find zero location index of VAL
    L0VAL=L0F(VAL)

C.. Initialise COUNT to zero
    COUNT=0.0

C.. For P1 set VAL = DENSITY * VELOCITY
C.. Ignore U1 as no effect on velocity through slot
    IF(INDVAR.EQ.P1) THEN
      DO 1167 IX=(NX-MX)/2+1,NX-(NX-MX)/2
       DO 1168 IY=NY-MY+1,NY
         I=IY+(IX-1)*NY
            COUNT=COUNT+1
```

```
            F(L0VAL+I) = RHO1*(SQRT(GVINT2(COUNT)**2
     +      +GWINT2(COUNT)**2))
     +      *COS(ATAN2(GVINT2(COUNT),GWINT2(COUNT))-PSI)
     +      *COS(PSI)
1168        CONTINUE
1167    CONTINUE

C.. U velocity
      ELSEIF (INDVAR.EQ.U1) THEN
         DO 1169  IX=(NX-MX)/2+1,NX-(NX-MX)/2
          DO 1170  IY=(NY-MY)+1,NY
                I=IY+(IX-1)*NY
                COUNT=COUNT+1
            F(L0VAL+I) = GUINT2(COUNT)
1170      CONTINUE
1169    CONTINUE

c.. V velocity
      ELSEIF (INDVAR.EQ.V1) THEN
       DO 1171 IX=(NX-MX)/2+1,NX-(NX-MX)/2
          Do 1172  IY=NY-MY+1,NY
                I=IY+(IX-1)*NY
                COUNT=COUNT+1
            F(L0VAL+I) =
     +      (SQRT(GVINT2(COUNT)**2+GWINT2(COUNT)**2))
     +      *COS(ANGE2-ATAN2(GVINT2(COUNT),GWINT2(COUNT)))
1172      CONTINUE
1171    CONTINUE

C.. W velocity
      ELSEIF (INDVAR.EQ.W1) THEN
       DO 1173 IX=(NX-MX)/2+1,NX-(NX-MX)/2
          Do 1174  IY=NY-MY+1,NY
                I=IY+(IX-1)*NY
                COUNT=COUNT+1
            F(L0VAL+I) =
     +      (SQRT(GWINT2(COUNT)**2+GVINT2(COUNT)**2))
     +      *COS(ATAN2(GVINT2(COUNT),GWINT2(COUNT)))
1174      CONTINUE
1173    CONTINUE

C.. turbulence ke
      ELSEIF (INDVAR.EQ.KE) THEN
       DO 1175 IX=(NX-MX)/2+1,NX-(NX-MX)/2
          Do 1176  IY=NY-MY+1,NY
                I=IY+(IX-1)*NY
                COUNT=COUNT+1
            F(L0VAL+I) = GKET2(COUNT)
1176      CONTINUE
```

```
1175   CONTINUE

C.. turbulence ep
    ELSEIF (INDVAR.EQ.EP) THEN
     DO 1177 IX=(NX-MX)/2+1,NX-(NX-MX)/2
        Do 1178  IY=NY-MY+1,NY
              I=IY+(IX-1)*NY
              COUNT=COUNT+1
          F(L0VAL+I) = GEPT2(COUNT)
1178    CONTINUE
1177   CONTINUE

C.. Temperature
    ELSEIF (INDVAR.EQ.14) THEN
     DO 1179 IX=(NX-MX)/2+1,NX-(NX-MX)/2
        Do 1180  IY=NY-MY+1,NY
              I=IY+(IX-1)*NY
              COUNT=COUNT+1
          F(L0VAL+I) = GTINT2(COUNT)
1180    CONTINUE
1179   CONTINUE

    ENDIF
    ENDIF

    RETURN
 1313 CONTINUE
C------------------- SECTION 14 ------------------- value = GRND2
    RETURN
 1314 CONTINUE

C*****************************************************************
C* Make changes to data for GROUPS 15, 16, 17, 18  GROUP 19.
C*****************************************************************
C
C--- GROUP 19. Special calls to GROUND from EARTH
C
  19 GO TO (191,192,193,194,195,196,197,198,199,1910),ISC
 191 CONTINUE
C   * ------------------- SECTION 1 ---- Start of time step.



C.. Do the same thing for the inlet slot velocities

     OPEN(UNIT=102,FILE='uinb2.in',FORM='UNFORMATTED')
     OPEN(UNIT=103,FILE='vinb2.in',FORM='UNFORMATTED')
     OPEN(UNIT=104,FILE='winb2.in',FORM='UNFORMATTED')
     OPEN(UNIT=105,FILE='keinb2.in',FORM='UNFORMATTED')
```

```
      OPEN(UNIT=106,FILE='epinb2.in',FORM='UNFORMATTED')
      OPEN(UNIT=107,FILE='tinb2.in',FORM='UNFORMATTED')
      OPEN(UNIT=108,FILE='uint2.in',FORM='UNFORMATTED')
      OPEN(UNIT=109,FILE='vint2.in',FORM='UNFORMATTED')
      OPEN(UNIT=110,FILE='wint2.in',FORM='UNFORMATTED')
      OPEN(UNIT=111,FILE='keint2.in',FORM='UNFORMATTED')
      OPEN(UNIT=112,FILE='epint2.in',FORM='UNFORMATTED')
      OPEN(UNIT=113,FILE='tint2.in',FORM='UNFORMATTED')


      DO 1163 P=1,MZ*MY
         READ(102) GUINB2(P)
         READ(103) GVINB2(P)
         READ(104) GWINB2(P)
         READ(105) GKEB2(P)
        READ(106) GEPB2(P)
        READ(107) GTINB2(P)
1163  CONTINUE

      DO 1164 P=1,MX*MY
         READ(108) GUINT2(P)
         READ(109) GVINT2(P)
         READ(110) GWINT2(P)
         READ(111) GKET2(P)
         READ(112) GEPT2(P)
         READ(113) GTINT2(P)
1164  CONTINUE

C.. Check what is in the arrays

      WRITE(*,*) 'INITIAL VELOCITIES READ INTO ARRAYS ARE:'

      WRITE(*,79)'GUINB2:','GVINB2:','GWINB2:','GKEINB2:','GEPINB2:',
     +'GTINB2:'
      DO 1165 P=1,MZ*MY
         WRITE(*,80) GUINB2(P),GVINB2(P),GWINB2(P),GKEB2(P),
     +GEPB2(P),GTINB2(P)
1165 CONTINUE

      WRITE(*,79)'GUINT2:','GVINT2:','GWINT2:','GKET2:','GEPT2:',
     +'GTINT2:'
      DO 1166 P=1,MX*MY
         WRITE(*,80) GUINT2(P),GVINT2(P),GWINT2(P),GKET2(P),
     +     GEPT2(P),GTINT2(P)
1166 CONTINUE

      CLOSE(102)
      CLOSE(103)
      CLOSE(104)
```

```
      CLOSE(105)
      CLOSE(106)
      CLOSE(107)
      CLOSE(108)
      CLOSE(109)
      CLOSE(110)
      CLOSE(111)
      CLOSE(112)
      CLOSE(113)


      RETURN
  192 CONTINUE
C     * ------------------ SECTION 8 ---- Finish of time step.

C.. SLOT OUTLETS
C.. ============
C.. Bottom half of junction - OUTB2 = y-z face
C.. ==========================================

      OPEN(UNIT=90, FILE='uoutb2.out',FORM='UNFORMATTED')
      OPEN(UNIT=91, FILE='voutb2.out',FORM='UNFORMATTED')
      OPEN(UNIT=92, FILE='woutb2.out',FORM='UNFORMATTED')
      OPEN(UNIT=93, FILE='keoutb2.out',FORM='UNFORMATTED')
      OPEN(UNIT=94, FILE='epoutb2.out',FORM='UNFORMATTED')
      OPEN(UNIT=95, FILE='toutb2.out',FORM='UNFORMATTED')

      WRITE(*,*)'VELOCITIES FROM BOTTOM SLOT BEING WRITTEN TO
FILES'

C.. Find L0F for each variable and each slab.  Need to get cartesian
C.. components of veloctiy for calculating angles and Q, velocity vector
      DO 1156 K=(NZ-MZ)/2+1,NZ-((NZ-MZ)/2)
         L0U1OUTB2=L0F(ANYZ(50,K))
         L0V1OUTB2=L0F(ANYZ(48,K))
         L0W1OUTB2=L0F(ANYZ(47,K))
         L0KEOUTB2=L0F(ANYZ(KE,K))
         L0EPOUTB2=L0F(ANYZ(EP,K))
         L0TOUTB2 =L0F(ANYZ(14,K))

C.. For u1 get velocities at nx-1 position (set to 0 at nx)
C       WRITE(*,*) 'GUOUTB2: '
C       DO 1157 IX=NX-1,NX-1
C             DO 1158 IY=(NY/2-MY)+1,NY/2
C                   I=IY+(IX-1)*NY
C                   WRITE(90) (F(L0U1OUTB2+I))
C                   WRITE(*,*) (F(L0U1OUTB2+I))
C1158         CONTINUE
C1157         CONTINUE
```

```
C.. For all other variables use nx
     WRITE(*,*) 'GUOUTB2','GVOUTB2:   ','GWOUTB2: ','GKEB2: ',
    +'GEPB2:   ','GTOUTB2:  '
        DO 1159 IX=NX,NX
                DO 1160 IY=(NY/2-MY)+1,NY/2
                        I=IY+(IX-1)*NY
                        WRITE(90) (F(L0U1OUTB2+I))
                        WRITE(91) (F(L0V1OUTB2+I))
                        WRITE(92) (F(L0W1OUTB2+I))
                        WRITE(93) (F(L0KEOUTB2+I))
                        WRITE(94) (F(L0EPOUTB2+I))
                        WRITE(95) (F(L0TOUTB2+I))
                WRITE(*,65) (F(L0U1OUTB2+I)), (F(L0V1OUTB2+I)),
     +          (F(L0W1OUTB2+I)),(F(L0KEOUTB2+I)),(F(L0EPOUTB2+I)),
     +       (F(L0TOUTB2+I))
1160            CONTINUE
1159    CONTINUE

1156  CONTINUE

      CLOSE(90)
      CLOSE(91)
      CLOSE(92)
      CLOSE(93)
      CLOSE(94)
      CLOSE(95)


C.. Top half of junction - OUTT2 = x-y face
C.. ========================================
      OPEN(UNIT=96, FILE='uoutt2.out',FORM='UNFORMATTED')
      OPEN(UNIT=97, FILE='voutt2.out',FORM='UNFORMATTED')
      OPEN(UNIT=98, FILE='woutt2.out',FORM='UNFORMATTED')
      OPEN(UNIT=99, FILE='keoutt2.out',FORM='UNFORMATTED')
      OPEN(UNIT=100,FILE='epoutt2.out',FORM='UNFORMATTED')
      OPEN(UNIT=101,FILE='toutt2.out',FORM='UNFORMATTED')

C.. Find zero location indicies of each variable on last slab
C.. Get w1 from nz-1 - set to 0 at nz
      L0U1OUTT2=L0F(ANYZ(50,NZ))
      L0V1OUTT2=L0F(ANYZ(48,NZ))
      L0W1OUTT2=L0F(ANYZ(47,NZ))
      L0KEOUTT2=L0F(ANYZ(KE,NZ))
      L0EPOUTT2=L0F(ANYZ(EP,NZ))
      L0TOUTT2 =L0F(ANYZ(14,NZ))

      WRITE(*,*)'VELOCITIES FROM TOP SLOT BEING WRITTEN TO FILES'
```

```
      WRITE(*,64) 'GUOUTT2: ','GVOUTT2: ','GWOUTT2: ','GKET2: ',
     +'GEPT2: ','GTOUTT2: '
      DO 1161 IX=(NX-MX)/2+1,NX-(NX-MX)/2
         DO 1162 IY=NY/2+1,NY/2+MY
                I=IY+(IX-1)*NY
                WRITE(96) (F(L0U1OUTT2+I))
                WRITE(97) (F(L0V1OUTT2+I))
                WRITE(98) (F(L0W1OUTT2+I))
                WRITE(99) (F(L0KEOUTT2+I))
                WRITE(100)(F(L0EPOUTT2+I))
                WRITE(101)(F(L0TOUTT2+I))
          WRITE(*,65) (F(L0U1OUTT2+I)),(F(L0V1OUTT2+I)),
     +  (F(L0W1OUTT2+I)),(F(L0KEOUTT2+I)),(F(L0EPOUTT2+I)),
     +  (F(L0TOUTT2+I))
1162    CONTINUE
1161  CONTINUE

       CLOSE(96)
       CLOSE(97)
       CLOSE(98)
       CLOSE(99)
       CLOSE(100)
       CLOSE(101)

 823   FORMAT(1X,F8.4)
       RETURN
C*************************************************************
C
C--- GROUP 20. Preliminary print-out
C
  20 CONTINUE
     RETURN
C*************************************************************
C* Make changes to data for GROUPS 21 and 22 only in GROUP 19.
C*************************************************************
C
C--- GROUP 23. Field print-out and plot control
   23 CONTINUE
      RETURN
C*************************************************************
C
C--- GROUP 24. Dumps for restarts
C
   24 CONTINUE
      END
```